

12-17-2004

## Simulation of Coal Gasification Process Inside a Two-Stage Gasifier

Armin Silaen  
*University of New Orleans*

Follow this and additional works at: <https://scholarworks.uno.edu/td>

---

### Recommended Citation

Silaen, Armin, "Simulation of Coal Gasification Process Inside a Two-Stage Gasifier" (2004). *University of New Orleans Theses and Dissertations*. 198.  
<https://scholarworks.uno.edu/td/198>

This Thesis is protected by copyright and/or related rights. It has been brought to you by ScholarWorks@UNO with permission from the rights-holder(s). You are free to use this Thesis in any way that is permitted by the copyright and related rights legislation that applies to your use. For other uses you need to obtain permission from the rights-holder(s) directly, unless additional rights are indicated by a Creative Commons license in the record and/or on the work itself.

This Thesis has been accepted for inclusion in University of New Orleans Theses and Dissertations by an authorized administrator of ScholarWorks@UNO. For more information, please contact [scholarworks@uno.edu](mailto:scholarworks@uno.edu).

SIMULATION OF  
COAL GASIFICATION PROCESS INSIDE  
A TWO-STAGE GASIFIER

A Thesis

Submitted to the Graduate Faculty of the  
University of New Orleans  
in Partial fulfillment of the  
requirement for the degree of

Master of Science  
in  
The Department of Mechanical Engineering

by

Armin K. Silaen

B.S. University of New Orleans, 2002

December 2004

## **ACKNOWLEDGEMENTS**

I would like to express my sincere gratitude to my advisor, Dr. Ting Wang, for his support, guidance, and patience during the entire period of this study. His willingness to give his time, insight, wisdom, and interest for this study made this work a success.

I would also like to thank Dr. Carsie A. Hall and Dr. Martin J. Guillot for taking the time to serve on my thesis defense committee.

I acknowledge all Energy Conversion & Conservation Center (ECCC) personnel. Special thanks to Dr. Xianchang Li and Mr. Raja Saripalli for their help and advice.

I thank my friends for their friendship and support. Finally, I am grateful for my mother and late father, to whom I dedicate this work, and my siblings for their unconditional love, support, encouragement, and sacrifice.

## TABLE OF CONTENTS

LIST OF FIGURES .....	v
LIST OF TABLES .....	viii
NOMENCLATURE .....	ix
ABSTRACT.....	xi
CHAPTER	
1. INTRODUCTION .....	1
1.1 Background .....	1
1.2 Literature .....	2
1.2.1. Basic Gasification Reactions .....	2
1.2.2. Gasification Methods .....	3
1.3 Research and Development (R&D) in Gasification Industry .....	17
1.4 Objectives.....	18
2. COMPUTATIONAL MODEL.....	19
2.1 Assumptions.....	21
2.2 Governing Equations .....	21
2.3 Turbulence Model.....	23
2.4 Radiation Model.....	28
2.5 Combustion Model.....	29
2.6 Boundary Conditions .....	33
3. COMPUTATIONAL PROCESS .....	36
3.1 Solution Methodology .....	36
3.2 Computational Grid .....	37
3.3 Numerical Procedure.....	37
3.4 Gas temperature and species fractions for three different grids.....	44
4. RESULTS AND DISCUSSIONS.....	46
4.1 Baseline Case .....	47
4.2 Effects of Coal Mixture (Slurry vs. Powder) .....	57
4.3 Effects of Wall Cooling (Case 3) .....	61
4.4 Effects of Coal Distribution (Cases 4 and 8) .....	62

4.5	Effects of Oxidant (Air-blown, Case 5).....	65
4.6	Effects of Injector Angle (Cases 6 and 7).....	67
5.	CONCLUSIONS.....	78
REFERENCES	.....	82
APPENDICES	.....	83
A.	Application of FLUENT code.....	84
B.	Geometry Generation and Meshing .....	109
VITA	.....	116

## LIST OF FIGURES

Figure 1.1	Schematic of a KRW fluidized-bed gasifier (US Department of Energy/1996). .....	6
Figure 1.2	Schematic of a Lurgy dry ash moving-bed gasifier. ....	8
Figure 1.3	Schematic of Texaco entrained-flow gasifier (US Department of Energy, 2000(a)). ....	11
Figure 1.4	Schematic of a Shell entrained-flow gasifier (From Shell commercial Brochure). ....	13
Figure 1.5	Schematic of E-Gas entrained-flow gasifier (US Department of Energy, 2000(c)). ....	14
Figure 2.1	Schematic of a two-stage entrained-flow gasifier configuration. ....	20
Figure 2.2	Boundary conditions for the baseline case of the generic two-stage entrained-flow gasifier. ....	34
Figure 3.1	Basic program structure of FLUENT code. ....	39
Figure 3.2	Meshed geometry for the REI gasifier. ....	40
Figure 3.3	Overview of the segregated solution method. ....	41
Figure 4.1	Axial distributions of the gas temperature and the gas mole fraction at the center vertical plane in the oxygen-blown gasifier with coal-slurry fuel (Case 1). ....	51
Figure 4.2	Distributions of the gas temperature and the gas mole fraction at different horizontal planes in the oxygen-blown gasifier with coal-slurry fuel (Case 1). ....	52
Figure 4.3	Distribution of gas temperature and gas mole fraction at lower inlet level for oxygen-blown gasifier with coal-slurry fuel (Case 1). ....	53
Figure 4.4	Distribution of gas temperature and gas mole fraction at upper inlet level for oxygen-blown gasifier with coal-slurry fuel (Case 1). ....	54

Figure 4.5	Mass-weighted average of gas temperature and mole fraction along the gasifier height for oxygen-blown gasifier with coal-slurry fuel (Case 1).....	55
Figure 4.6	Midplane axial distributions of the gas temperature and the gas mole fraction in the oxygen-blown gasifier with coal powder fuel (Case 2).....	56
Figure 4.7	Mass-weighted average gas temperature and mole fraction along the gasifier height for oxygen-blown gasifier with coal powder fuel (Case 2). .	59
Figure 4.8	Mass-weighted average gas temperature and mole fraction along the gasifier height for gasifier with wall cooling (Case 3). .....	62
Figure 4.9	Mass-weighted average gas temperature and mole fraction along the gasifier height for Case 4 with 50-50 equal coal distribution between two stages (Case 4). .....	64
Figure 4.10	Mass-weighted average gas temperature and mole fraction along the gasifier height for gasifier with one-stage coal injection (Case 8). .....	64
Figure 4.11	Mass-weighted average gas temperature and mole fraction along the gasifier height for air-blown gasifier (Case 5). .....	66
Figure 4.12	Lower injector configurations of (a) Case 6 and (b) Case 7. ....	68
Figure 4.13	Velocity vectors on the center vertical plane for gasifier with the first stage injectors position horizontally (Case 1). .....	69
Figure 4.14	Velocity vectors on the center vertical plane for gasifier with the first stage injectors tilted 30° downward (Case 6). .....	70
Figure 4.15	Velocity vectors on the center vertical plane for gasifier with the first stage injectors tilted 30° upward (Case 7). .....	71
Figure 4.16	Flow path lines for gasifier with the first stage injectors horizontal (Case 1). .....	73
Figure 4.17	Flow path lines for gasifier with the first stage injectors tilted 30° downward (Case 6). .....	74
Figure 4.18	Flow path lines for gasifier with the first stage injectors tilted 30° upward (Case 7). .....	75
Figure 4.19	Mass-weighted average gas temperature and mole fraction along the gasifier height for gasifier with the first stage injectors tilted 30° downward (Case 6). .....	76

Figure 4.20 Mass-weighted average gas temperature and mole fraction along the  
gasifier height for gasifier with the first stage injectors tilted 30°  
upward (Case 7). .....77

## LIST OF TABLES

Table 2.1	Parameters and operating conditions for simulated cases.....	35
Table 3.1	Gas temperature and species fractions for three different grids.....	45
Table 4.1	Parameters and operating conditions for simulated cases.....	48
Table 4.2	Summary of simulation results .....	49

## NOMENCLATURE

$a$	local speed of sound (m/s)
$c$	concentration (mass/volume, moles/volume)
$c_p$	heat capacity at constant pressure (J/kg-K)
$c_v$	heat capacity at constant volume (J/kg-K)
$D$	mass diffusion coefficient ( $\text{m}^2/\text{s}$ )
$D_H$	hydraulic diameter (m)
$D_{ij}$	mass diffusion coefficient ( $\text{m}^2/\text{s}$ )
$D_t$	turbulent diffusivity ( $\text{m}^2/\text{s}$ )
$E$	total energy (J)
$g$	gravitational acceleration ( $\text{m}/\text{s}^2$ )
$G$	incident radiation
Gr	Grashof number ( $L^3 \cdot \rho^2 \cdot g \cdot \beta \cdot \Delta T / \mu^2$ )
$H$	total enthalpy ( $\text{W}/\text{m}^2\text{-K}$ )
$h$	species enthalpy ( $\text{W}/\text{m}^2\text{-K}$ )
$J$	mass flux; diffusion flux ( $\text{kg}/\text{m}^2\text{-s}$ )
$k$	turbulence kinetic energy ( $\text{m}^2/\text{s}^2$ )
$k$	thermal conductivity ( $\text{W}/\text{m-K}$ )
$m$	mass (kg)
$M_w$	molecular weight (kg/kgmol)
$M$	Mach number
$p$	pressure (atm)
Pr	Prandtl number ( $\nu/a$ )
$q$	heat flux
$q_r$	radiation heat flux
$R$	universal gas constant
$S$	source term

$Sc$	Schmidt number ( $n/D$ )
$t$	time (s)
$T$	temperature (K)
$U$	mean velocity (m/s)
$X$	mole fraction (dimensionless)
$Y$	mass fraction (dimensionless)
$x, y, z$	coordinates

#### Greek letter

$b$	coefficient of thermal expansion ( $K^{-1}$ )
$e$	turbulence dissipation ( $m^2/s^3$ )
$e_w$	wall emissivity
$k$	von Karman constant
$m$	dynamics viscosity (kg/m-s)
$m_k$	turbulent viscosity (kg/m-s)
$\nu$	kinematic viscosity ( $m^2/s$ )
$\nu'$	stoichiometric coefficient of reactant
$\nu''$	stoichiometric coefficient of product
$\rho$	density ( $kg/m^3$ )
$r_w$	wall reflectivity
$s$	Stefan-Boltzmann constant
$s_s$	scattering coefficient
$t$	stress tensor ( $kg/m-s^2$ )

#### Subscript

$i$	reactant i
$j$	product j
$r$	reaction r

## ABSTRACT

Gasification is a very efficient method of producing clean synthetic gas (syngas) which can be used as fuel for electric generation or chemical building block for petrochemical industries. This study performs detailed simulations of coal gasification process inside a generic two-stage entrained-flow gasifier to produce syngas carbon monoxide and hydrogen. The simulations are conducted using the commercial Computational Fluid Dynamics (CFD) solver FLUENT. The 3-D Navier-Stokes equations and seven species transport equations are solved with eddy-breakup combustion model. Simulations are conducted to investigate the effects of coal mixture (slurry or dry), oxidant (oxygen-blown or air-blown), wall cooling, coal distribution between the two stages, and the feedstock injection angles on the performance of the gasifier in producing CO and H<sub>2</sub>. The result indicates that coal-slurry feed is preferred over coal-powder feed to produce hydrogen. On the other hand, coal-powder feed is preferred over coal-slurry feed to produce carbon monoxide. The air-blown operation yields poor fuel conversion efficiency and lowest syngas heating value. The two-stage design gives the flexibility to adjust parameters to achieve desired performance. The horizontal injection design gives better performance compared to upward and downward injection designs.

## CHAPTER ONE

### INTRODUCTION

#### 1.1 Background

Gasification is the process of converting various carbon-based feedstocks to clean synthetic gas (syngas), which is primarily a mixture of hydrogen ( $H_2$ ) and carbon-monoxide (CO). This conversion is achieved through the reaction of the feedstock with oxygen and steam at high temperature and pressure with only less than 30% of the required oxygen for complete combustion being provided. The syngas produced can be used as a fuel, usually as a fuel for boilers or gas turbines to generate electricity, or can be used to make a synthetic natural gas hydrogen gas or other chemical products. The gasification technology is applicable to any type of carbon-based feedstock, such as coal, natural gas, heavy refinery residues, petroleum coke, biomass, and municipal wastes.

The gas produced from coal gasification can be used for syngas or as a source for methanol and hydrogen, which are used in the manufacturing process of ammonia or hydrogenation applications in refineries. Another usage of syngas, which is gaining more popularity recently, is using syngas as fuel in electricity generation by employing the Integrated Gasification Combined Cycle (IGCC). The syngas produced in the gasifier is cleaned and used as a fuel for gas turbines. The gas is burned with compressed air in the combustor of the gas turbine. The high pressure and hot gases produced in the combustor then expand through the gas turbine to drive the air compressor and an electric generator.

The hot exhaust gases from the gas turbine are sent to a boiler that heats water producing steam that expands through a steam turbine to drive another electric generator.

IGCC plants can achieve efficiencies of about 50% and low emissions, compared to 43-45% efficiencies and high emissions for regular or critical pulverized coal combustion power plants. Gasification integrated in IGCC is considered a clean and efficient alternative to coal combustion for power generation. The high-pressure and high-temperature syngas from the gasifier can especially take advantage of the new generation of advanced turbine systems (ATS), which require high compression ratio and high turbine inlet temperature to produce up to 60% combined cycle efficiency. Furthermore, the syngas stream can also be tapped to produce methanol and hydrogen.

## 1.2 Literature Survey

### 1.2.1 Basic Gasification Reactions

Coal gasification reactions occur when coal is heated with limited oxygen and usually steam in a gasification reaction chamber. The main global reactions in a gasification process are as follows:

Heterogeneous (solid and gas) phase



(Gasification, Boudouard reaction)



(Gasification)

Homogenous gas phase



(Watershift)

Reactions given in R1.1 and R1.4 are two exothermic reactions that provide the complete energy for the gasification. Based on these global reactions, approximately 22% of the stoichiometric oxygen is required to provide sufficient energy for gasification reactions. In real applications, 25~30% of the stoichiometric oxygen is provided to ensure high-efficient carbon conversion.

Partial combustion occurs when the coal mixes with oxygen (R1.1). The energy released from (R1.1) also heats up any coal that has not burned. When the coal is heated without oxygen, it undergoes pyrolysis during which phenols and hydrocarbon gases are released. At the same time, char gasification (R1.2) takes place and releases CO. If a significant amount of steam exists, gasification (R1.3) and water shift reaction (R1.5) occur and release H<sub>2</sub>.

### 1.2.2 Gasification Methods

The formation of volatile components from coal was observed in the 17<sup>th</sup> century. Murdoch used partial gasification to produce coal gas (town's gas) for gas lighting in 1797, which led to a major industry in many countries. In the mid-19<sup>th</sup> century, Siemens introduced the complete gasification, where coke produced by the coal devolatilization

step is also gasified.. Oxygen gasification, where pure oxygen is used, was introduced around 1925 as a means of producing a high-calorific-value town's gas.

As technology progressed, the next phase was the development of gasification to meet the needs of the petroleum industry. The goal was to produce synthetic gas or substitute natural gas for

- synthesis of gasoline,
- hydrogen for refinery purposes,
- synthetic, sulfur-free, diesel fuel, and
- chemical feedstocks for methanol and ammonia were emphasised.

The next development was the power generation using gas turbines. The current preferred choice of fuel for gas turbines is natural gas. However, this may not be the most economic choice as future natural gas prices rise. . On the other hand, coal has a reserve of more than 250 years and the cost of coal is expected to be low for many years to come. The use of syngas produced from coal gasification reactions as a fuel for gas turbines has led to the interest and development of coal gasification technology.

Commercial gasifiers have been extensively studied and can be classified based on flow speeds, feedstock feeding direction, and oxidant feeds. Based on the flow speeds, gasifiers are classified as:

- a. Fluidized-bed gasifier
- b. Moving-bed gasifier
- c. Entrained-flow gasifier

Based on the direction of feedstock feeding, gasifiers are divided into:

- a. Co-current: the coal and the oxidant move in the same direction.

- b. Counter-current: the coal and the oxidant move in opposite directions.
- c. Updraft: the oxidant is supplied from the bottom, and syngas is extracted on the top of the gasifier.
- d. Downdraft: the oxidant is supplied from the top, and syngas is extracted from the bottom.

Based on the oxidant feed, gasifiers are categorized into:

- a. Oxygen blown
- b. Air blown

Each type of gasifier, in terms of the flow speed, is discussed briefly below.

#### a) Fluidized-Bed Gasifier

The flow speed in a fluidized-bed gasifier is about 0.9 m/s. Figure 1.1 shows the schematic of a fluidized-bed gasifier. Due to the low flow speed, a fluidized-bed gasifier has long residence time (several minutes). Coal particles with diameters less than 5 mm are thoroughly mixed with steam and oxygen at the lower part of the reactor. The syngas formed from the gasification reaction leaves the reactor from the top. The fluidized-bed gasifier is operated at a constant low temperature, which is below the ash fusion temperature to avoid agglomeration and clinker formation in the fluidized bed. The advantage that the fluidized-bed gasifier has over the moving-bed gasifier is the small temperature difference between the fuel particles and the oxidant due to the thorough mixing, which results in higher efficiency. Fluidized-bed gasifiers have mid-size capacity with an operating temperature of 870-1038°C (1600-1900°F). This small range of operating temperature is the biggest drawback to fluidized-bed gasifiers. The operating temperature needs to be kept lower than the melting point of ash but high

enough to avoid formation of tar. Currently, there are 3 types of high-pressure fluidized-bed gasifier (Kellogg KRW, HT Winkler and U Gas) and one type of low-pressure fluidized-bed gasifier (Winkler) available commercially.

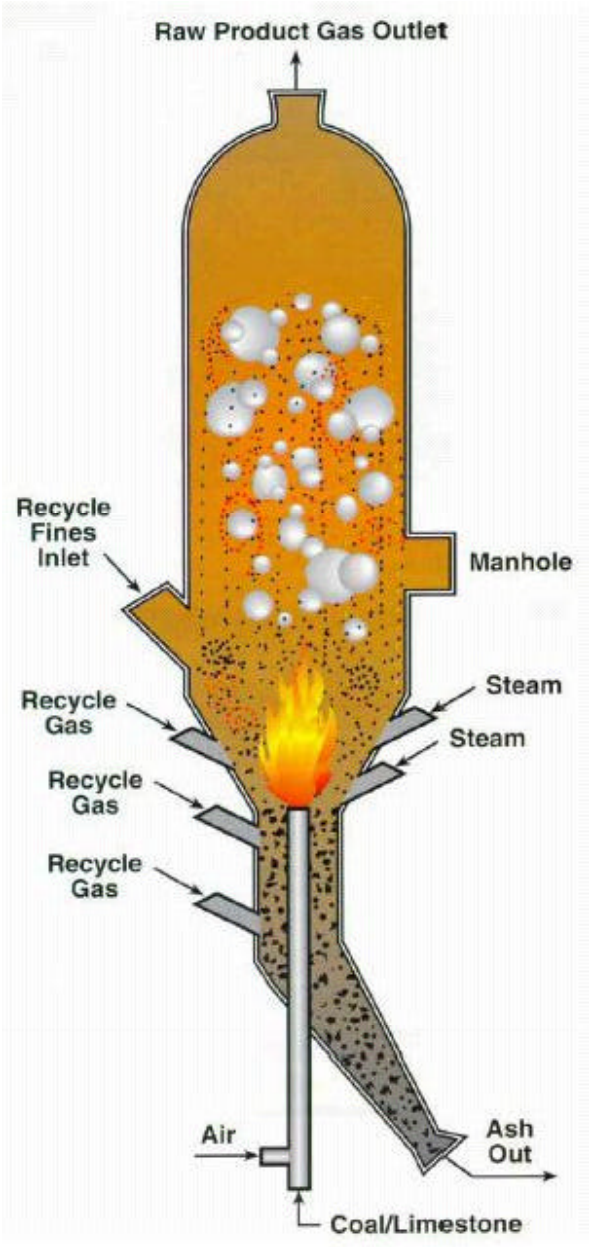


Figure 1.1 Schematic of a KRW fluidized-bed gasifier (US Department of Energy, 1996).

## b) Moving-Bed Gasifier

In a typical moving-bed gasifier, coal is fed into the reactor from the top while steam and oxygen are fed at the bottom. Steam and oxygen react with coal as they move up the reactor to form syngas, which then exits from the top. Compared to other types of gasifiers, the moving-bed gasifier produces the highest heating value fuel gas and requires the least amount of oxygen. However, a non-uniform mixing and temperature distribution is a disadvantage; therefore, very high temperature to maintain the equilibrium of the gasification reaction is required. Due to the countercurrent operation, there is a significant temperature drop in the reactor and a significant temperature difference of coal and of gas. This means coal particles and gasses do not mix thoroughly and results in low efficiency. A moving-bed gasifier can be operated either as dry-ash bed or slagging bed, depending on temperature and the steam/oxygen ratio injected into the gasifier. The operating temperature for a slagging bed ranges from 430°C to 1540°C (800-2800°F). The temperature in the reactor must be higher than the ash melting temperature before quenching is applied. The by-products, tar and liquid volatile, flow down to the slagging area and decompose. Slagging bed is usually used with fine coal particles, and dry-ash bed is usually used for coarse coal particles. The design operating temperature for a dry ash bed ranges from 430°C to 1095°C (800-2000°F), which is below the ash melting temperature.

Figure 1.2 shows the schematic of a Lurgi dry ash moving-bed gasifier. A Lurgi gasifier is a high-pressure and dry-fed moving-bed gasifier. Coal with a diameter between ¼” to 2” (6~50 mm) is fed from the top of the gasifier through a lock hopper. Steam and oxygen enter at the bottom and react with the coal as the gasses move up the

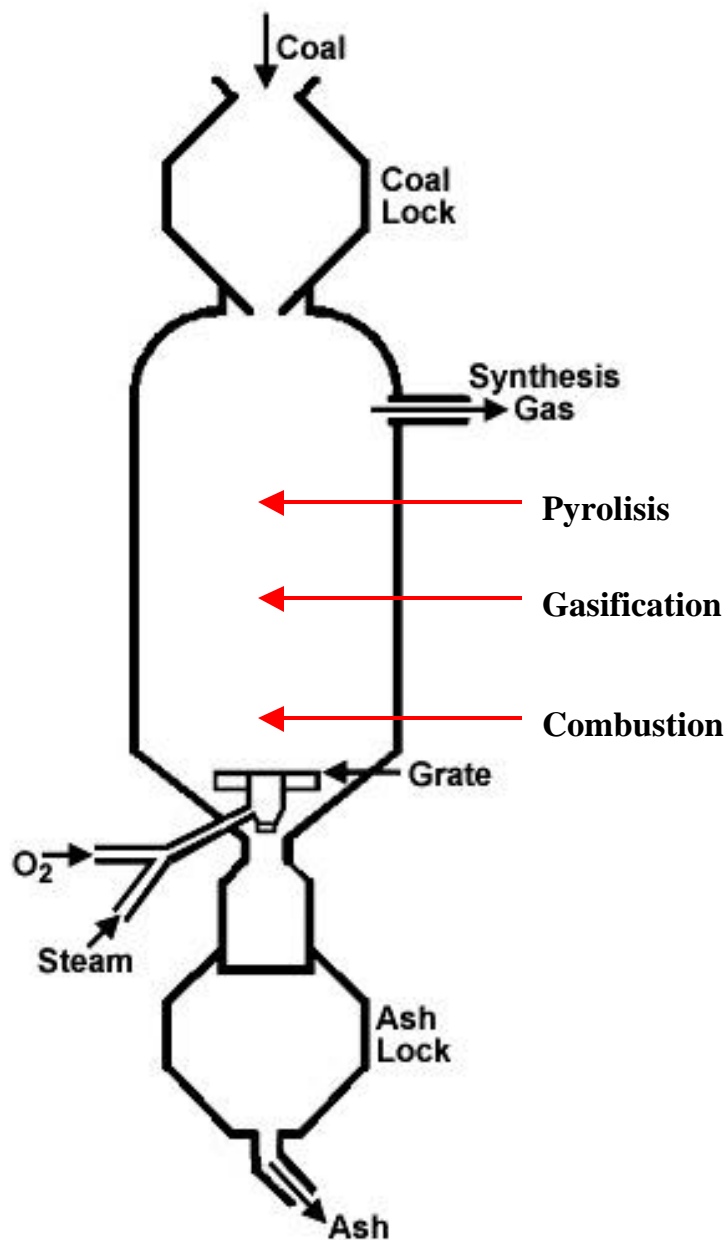


Figure 1.2 Schematic of a Lurgi dry ash moving-bed gasifier.

gasifier. The temperature in the combustion region (bottom part) is around 2000°F, and the temperature of raw syngas leaving the gasifier from the top is approximately 500-1000°F. The raw syngas is cooled with recycled water to condensed tar. Steam needs to

be injected into the bottom of the gasifier to keep the temperature lower than the melting point of ash.

Among different types of gasifiers, moving-bed gasifier has the longest history and is the most widely used commercially. Some examples of moving-bed gasifier are high-pressure Lurgi dry ash gasifier, British Gas Lurgi (BGL) slagging gasifier, and low-pressure Wellman Balusha gasifier. Lurgi's are the predominant gasifiers used by the South African Coal, Oil, and Gas Corporation (SASOL) to produce a variety of chemicals and syngas from coal. Although Lurgi is widely used, relatively low capacity and the inability to handle fine coal powders limit its application. On the other hand, BGL, co-developed by British Gas and Lurgi, is well fitted to anthracite, and there are commercial applications showing success.

#### c) Entrained-Bed Gasifier

The flow speed in an entrained-bed gasifier is the highest among all gasifiers, and the flow resident time is about 3~5 seconds. Very fine coal particles with diameters less than 0.13 mm are injected into the reactor together with steam and oxygen. Coal particles mix and react thoroughly with steam and oxygen in the gasifier, and the syngas produced exits through the outlet. The operating temperature is high, ranging between 930-1650°C, making efficiency very high. Because the temperature is above the melting point of ash, most of the ash forms slag and is discharged from the bottom of the gasifier. The temperature distribution is pretty uniform, and there is nearly no temperature difference between gas and syngas. The entrained-bed gasifier produces a better mixing of fuel and oxidant resulting in a higher efficiency compared to moving-bed and

fluidized-bed gasifiers. This makes it widely used in power generation plant. However, an entrained-bed gasifier does have disadvantages as it requires the highest amount of  $O_2$  and produces the lowest heating values gas. Entrained-flow gasifiers predominantly used in commercial applications are Texaco<sup>\*</sup>, E-Gas<sup>\*\*</sup>, Shell, Prenflo, and GSP. The first three gasifiers are briefly described below.

Figure 1.3 shows a schematic of a Texaco gasifier. The Texaco gasifier is a single-stage, high-pressure, oxygen-blown, downward firing entrained gasifier. Coal-water slurry and oxygen enters the hot gasifier from the top. The mass fraction of coal in the coal-water slurry is 60-70%, and the oxidant is 95% pure oxygen. At a temperature of about  $1500^{\circ}C$  ( $2700^{\circ}F$ ), gasification occurs rapidly. The coal slurry reacts with oxygen to produce syngas and molten ash. The hot syngas flows downward into a radiant syngas cooler or a water quench section where high-pressure steam is produced. The syngas passes over the surface of a pool of water at the bottom of the radiant syngas cooler and exits the reactor. The slag drops into the water pool and cools down. It is then fed from the radiant syngas cooler sump to a lock hopper. The black water flowing out with the slag is separated and recycled after processing in a dewatering system.

The Shell gasifier is a high-pressure, dry-fed, oxygen-blown, downdraft entrained-flow gasifiers. Figure 1.4 illustrates a schematic of the Shell gasifier. Pulverized, dried coal is fed into the high-pressure vessel with transport gas through a lock hopper system. The transport gas is usually nitrogen. Steam and oxygen enter into

---

\* Texaco: Texaco Inc merged with Chevron Corp to form ChevronTexaco in 2001. The ChevronTexaco gasification division was purchased by General Electric in 2004.

\*\* E-Gas Technology: Was originally Dow which then evolved into Destec. Destec was later purchased by NGC in 1997 but changed its name to Dynegy a year later. Then Global Energy, Inc. acquired Dynegy's gasification unit in 2000 and marketed it under the name E-Gas Technology. Global Energy, Inc. sold the technology to ConocoPhillips in July 2003.

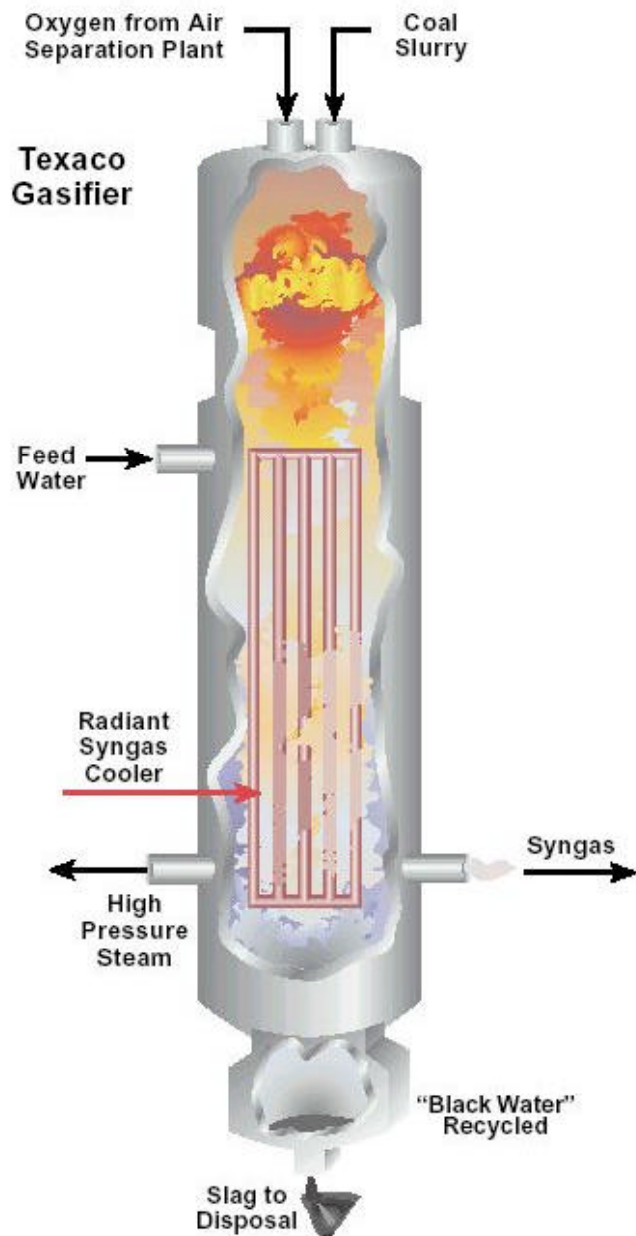


Figure 1.3 Schematic of Texaco entrained-flow gasifier (US Department of Energy, 2000(a)).

the gasifier together with dry coal particles. At about 1370°C (2500°F), reaction of coal and oxygen occurs with the main products of H<sub>2</sub>, CO, and a small amount of CO<sub>2</sub>. Because of the high temperature, no hydrocarbon volatile will be produced. At this high

temperature, the ash is converted into molten slag that flows down the refractory wall into a water bath at the bottom of the vessel and then discharged with the water through a lock hopper. When the raw syngas at the temperature of 1370-1650°C (2500-3000°F) leaves the vessel, it contains a small amount of unburned carbon as well as about half of the molten ash. To prevent the molten ash from sticking to the wall, the raw syngas is partially cooled down to around 870°C (1600°F) by quenching it with cooled recycle product gas. The raw syngas goes through a further cooling process in the syngas cooler unit for further clean up.

The E-Gas gasifier is a two-stage, high-pressure, oxygen-blown, slurry-fed, upflow, slagging entrained gasifier. Figure 1.5 shows the E-Gas gasifier. Its two-stage operation and the large combustion chamber make it unique. Feed coal is mixed with water in coal mills and becomes slurry. The water fraction in the slurry depends upon the water content of the coal, which generally ranges from 50% to 70% by weight. About 80% of the slurry and all the oxygen are fed to the first stage of the gasifier. The first stage is located at the bottom part of the gasifier, a horizontal cylinder with one burner at each end. One is used for fresh coal slurry and the other is for recycled unburned charcoal. Gasification and oxidation take place rapidly increasing the temperature to about 1316-1427°C (2400-2600°F). The coal ash melts and forms molten slag, which flows down and out of the vessel through a tap hole. The molten ash is quenched in water and removed.

The hot syngas from the first stage flows up to the second stage consisting of a vertical cylinder perpendicular to the first stage cylinder. The remaining 20% of the coal slurry is injected into the second stage. The endothermic gasification and devolatilization

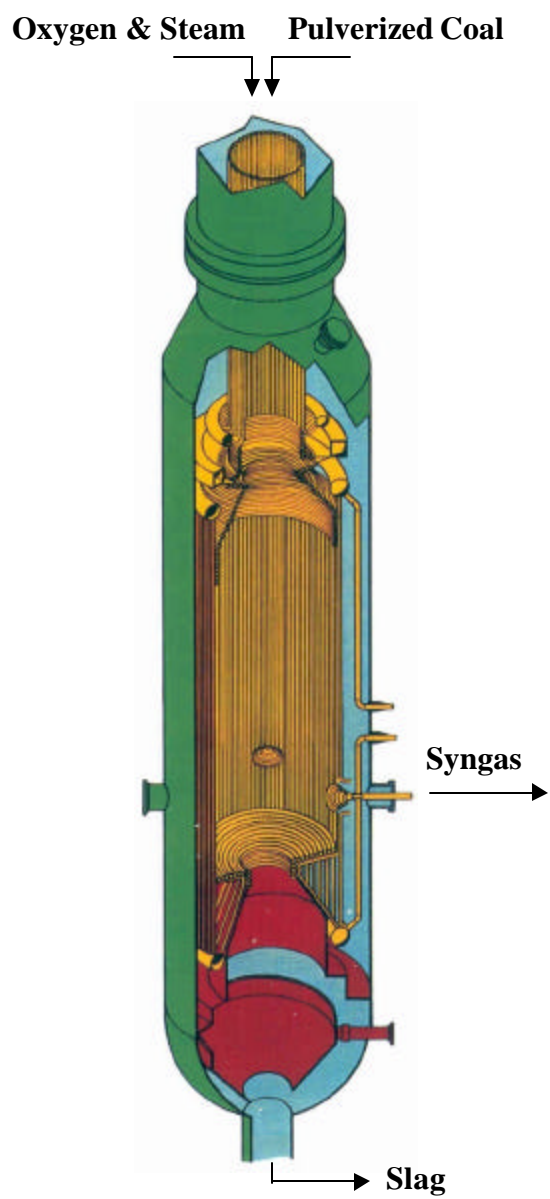


Figure 1.4 Schematic of a Shell entrained-flow gasifier (From Shell commercial brochure).

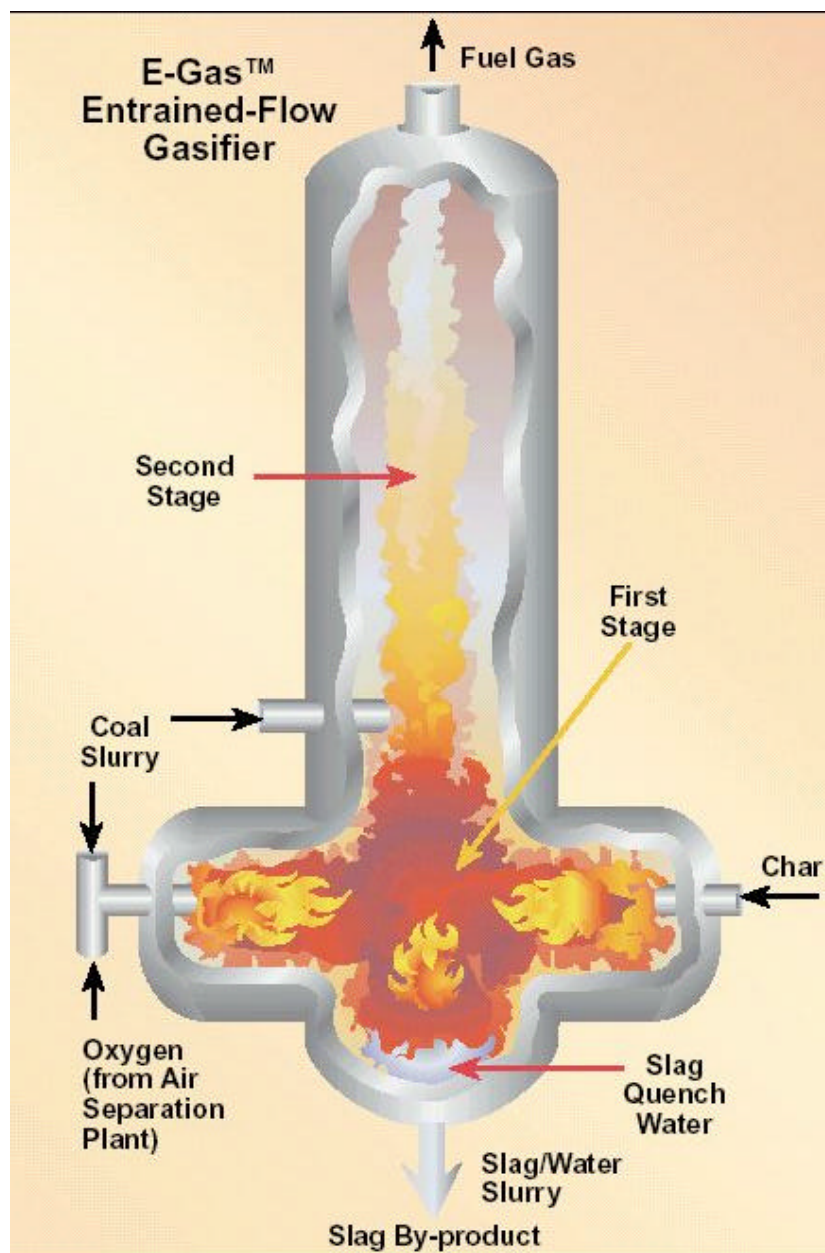


Figure 1.5 Schematic of E-Gas entrained-flow gasifier (US Department of Energy, 2000(c)).

occur in this stage and reduce the temperature to 1035°C (1900°F). The amount of char produced in the second stage is relatively small because only 20% of the coal slurry is fed to the second stage. The char is recycled down to the first stage and gasified. The syngas leaves the vessel from the top.

Chen et al. [Chen et al., 1999] developed a comprehensive three-dimensional simulation model for entrained coal gasifiers. Chen et al. applied an extended coal gas mixture fraction model with the Multi Solids Progress Variables (MSPV) method to simulate the gasification reaction and reactant mixing process. Four mixture fractions were employed to separately track the variable coal off-gas from the coal devolatilization, char-O<sub>2</sub>, char-CO<sub>2</sub>, and char-H<sub>2</sub>O reactions. Chen et al. performed a series of numerical simulations for a 200 tpd two-stage air blown entrained flow gasifier developed for an IGCC process under various operation conditions (heterogeneous reaction rate, coal type, particle size, and air/coal partitioning to the two stages). The predicted gas temperature profile and the exit gas composition were in general agreement with the measured data.

The model predicts a combustion zone, a gasification zone and a devolatilization zone in the two-stage gasifier. The results show that coal devolatilization and char oxidation were responsible for most of the carbon conversion (up to 80%) in the two-stage air blown entrained flow gasifier. The predicted carbon conversion was independent of devolatilization rate, sensitive to the chemical kinetics of heterogeneous reactions on the char surface, and less sensitive to a change in coal particle size. Chen et al. found that the increasing air ratio leads to increased CO<sub>2</sub> and decreased CO and H<sub>2</sub> concentrations and there exists a best air ratio for each coal type depending on the volatile matter content and the element composition/heating value of the coal. The

carbon conversion and the heating value of the product gas were found to be nearly independent of air/coal partitioning between the combustor and the reductor, and also the feed rate of recycle char.

Bockelie et al. [Bockelie et al., 2002(b)] of Reaction Engineering International developed a CFD modeling capability for entrained flow gasifiers that focus on two gasifier configurations: single-stage down fired system and two-stage with multiple feed inlets. The model was constructed using GLACIER, an REI in-house comprehensive coal combustion and gasification tool. The basic combustion flow field was established by employing full equilibrium chemistry. Gas properties were determined through local mixing calculations and are assumed to fluctuate randomly according to a statistical probability density function (PDF) which is characteristic of the turbulence. Gas-phase reactions were assumed to be limited by mixing rates for major species as opposed to chemical kinetic rates. Gaseous reactions were calculated assuming local instantaneous equilibrium. The particle reaction processes include coal devolatilization, char oxidation, particle energy, particle liquid vaporization and gas-particle interchange. The model also includes a flowing slag model.

Chen et al. predicted that increasing the average coal particle size decreases the carbon conversion, which results in an increase in the exit gas temperature and lower heating value. They also predicted that dry feed yields more CO mole fraction than wet feed does due to injecting less moisture into the system. Chen et al.'s study of the effect of system pressure shows that an increase in the system pressure increases the average residence time due to the reduced average gas velocity which further results in increased particle residence time and increased carbon conversion.

### 1.3 Research and Development (R&D) in Gasification Industry

To achieve wider acceptance of gasification technology, reliability has been identified as the most important technical limitation. . The following are technologies that need R&D and improvement (US Department of Energy 2000(b)).

- a. Feed Injectors - Gasifier users claim that short injector life is a major problem in the reliability of the gasification system. A typical injector nozzle generally lasts from two to six months only. Improvement of the injectors would involve (1) a comprehensive study to determine the cause of the failure of gasifier feed injectors, (2) development of new injector material that can increase the injector life while reducing the manufacturing and refurbishing costs, (3) development of reliable and cost effective orifice injectors and multiple-fuel injectors that can adjust to load and feedstock changes, and (4) use CFD to study the combustion and thermal flow behavior surrounding the injectors.
- b. Refractory Liners - Gasifiers users want new refractory liner materials that have an expected useful life of at least three years with 50 % t reduction costs. The current refractory liners deteriorate in only 6-18 months of operation. Additional R&D on water-cooled refractories needs to be conducted. CFD calculations of flow patterns and temperature are important for providing accurate boundary conditions for refractory analysis.
- c. Ash/Slag Removal – A comprehensive study needs to be conducted to achieve a better understanding of the properties and characteristics of the molten slag and better knowledge of flux (compound used to lower ash fusion temperatures)

effectiveness for solid feedstock units, and new fluxing agents that reduce the ash fusion temperature to 1200°C (2000°F) or less need to be developed.

- d. Gasification Modeling – More accurate modeling of the gasification process in 3-D is required by developing gasifier comprehensive CFD technology in conjunction with improved reaction rates.

#### **1.4 Objectives**

Coal gasification is a very complicated process. There are many parameters that affect the efficiency of syngas production in coal gasifiers, such as fuel type (coal powder or coal-slurry), oxidant type (pure oxygen or air), and the distribution of fuel. To help industry resolving concerns and improve gasifiers' efficiency and reliability, this research will study gasification/thermal flow interactions and investigate the effects these different input parameters have on the performance of entrained-bed coal gasifiers by modeling the gasification process and employing the Computational Fluid Dynamics (CFD) technology. The specific goals are:

1. Incorporate the gasification models into a commercial CFD code
2. Simulate a two-stage entrained-bed coal gasifier
3. Investigate the effects of the following parameters:
  - a. Slurry vs. dry coal feed
  - b. Different arrangement of coal feeding ratio between the first and the second stages
  - c. Effects of wall cooling
  - d. Different fuel injection angles.

## **CHAPTER TWO**

### **COMPUTATIONAL MODEL**

This research studies a two-stage entrained gasifiers. The geometry of the gasifier used in the simulation is shown in Fig 2.1. The geometry and the operating conditions are based on papers by Bockelie et al. [Bockelie et al., 2002] and by Chen et al. [Chen et al., 1999]. The gasifier is divided into two regions: a combustion region (combustor) in the first or the lower stage and a reduction region (reductor) in the second or the upper stage. The gasifier has three levels of injectors that are positioned symmetrically with two levels in the first stage, and the other is in the second stage of the gasifier. To create swirling inside the gasifier, the lower injectors are placed similar to a tangential firing system. The upper injectors are aimed directly at the center of the reductor. All oxidant and a fraction of the coal-slurry mixture are injected through the lower injectors, and the remaining coal-slurry mixture is injected through the upper injectors. Neither paper by Bockelie et al. [Bockelie et al., 2002] nor Chen et al. [Chen et al., 1999] gives gasifier dimension details; therefore, some engineering judgments were made to determine the part sizes.

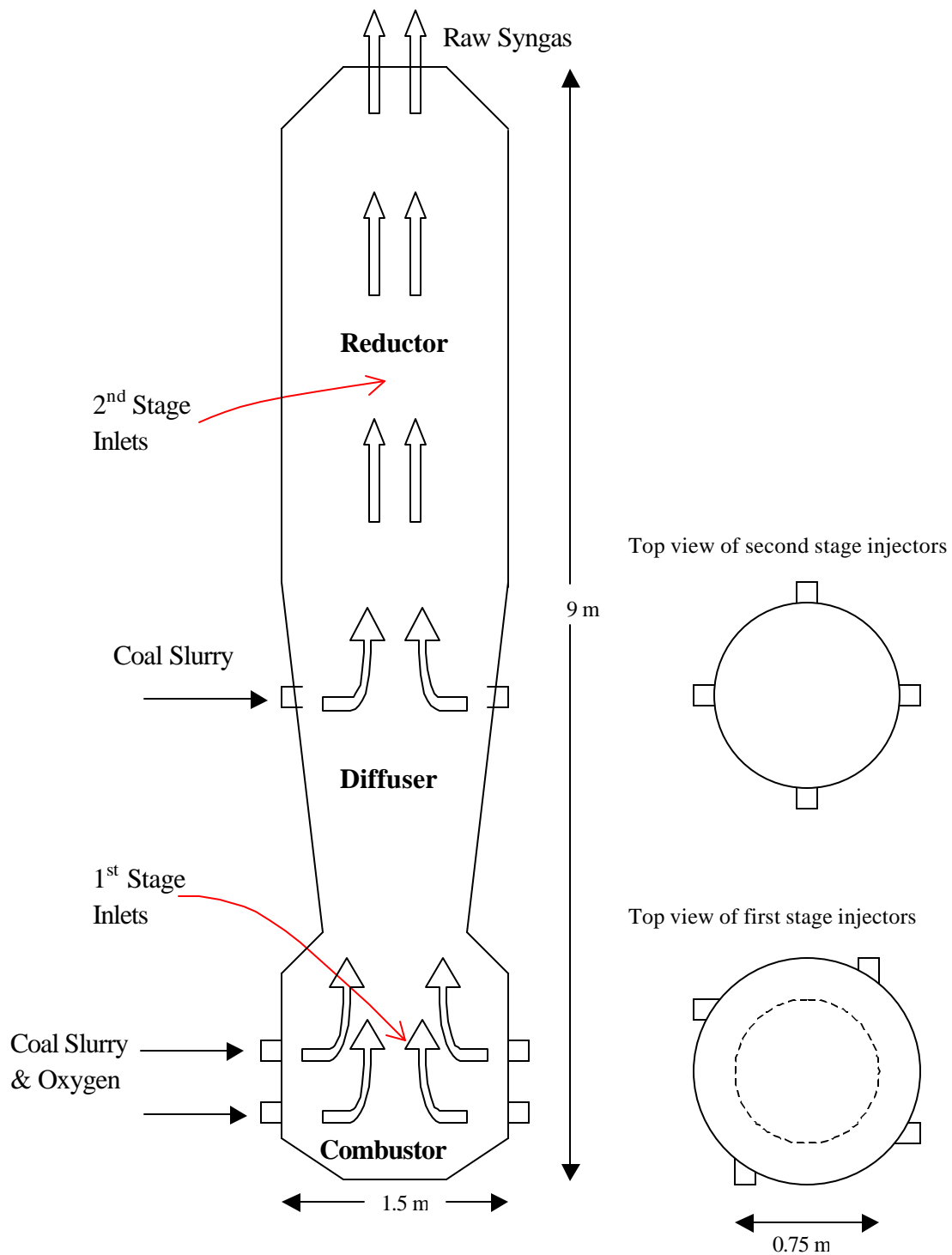


Figure 2.1 Schematic of a two-stage entrained flow gasifier configuration.

## 2.1 Physical Characteristics of the Problem and Assumptions Made

The physical characteristics of the problem are as follow:

1. Three-dimensional
2. Bouyancy force considered
3. Varying fluid properties
4. Impermeable walls

The following are the general assumptions made in this study:

1. The flow is steady.
2. No-slip condition (zero velocity) is imposed on wall surfaces.
3. Chemical reaction is faster than the time scale of the turbulence eddies.

## 2.2 Governing Equations

The equations for conservation of mass, conservation of momentum, and energy equation are given as:

$$\nabla \cdot (\mathbf{r}\bar{v}) = S_m \quad (2.1)$$

$$\nabla \cdot (\mathbf{r}\bar{v}\bar{v}) = -\nabla p + \nabla \cdot \left( \bar{\mathbf{t}} \right) + \mathbf{r}\bar{g} + \bar{F} \quad (2.2)$$

$$\nabla \cdot (\bar{v}(\mathbf{r}E + p)) = \nabla \cdot \left( \mathbf{I}_{eff} \nabla T - \sum_j h_j \bar{J}_j + \left( \bar{\mathbf{t}}_{eff} \cdot \bar{v} \right) \right) + S_h. \quad (2.3)$$

where  $\mathbf{I}_{eff}$  is the effective conductivity ( $\mathbf{I} + \mathbf{I}_t$ , where  $\mathbf{I}_t$  is the turbulence conductivity) and  $\bar{J}_j$  is the diffusion of species  $j$ .

The stress tensor  $\bar{\mathbf{t}}$  is given by

$$\bar{\mathbf{t}} = \mathbf{m} \left[ (\nabla \bar{\mathbf{v}} + \nabla \bar{\mathbf{v}}^T) - \frac{2}{3} \nabla \cdot \bar{\mathbf{v}} \mathbf{I} \right]. \quad (2.4)$$

where  $\mathbf{m}$  is the molecular dynamic viscosity,  $\mathbf{I}$  is the unit tensor, and the second term on the right-hand side is the effect of volume dilatation. The first three terms on the right-hand side of equation (2.3) represent heat transfer due to conduction, species diffusion, and viscous dissipation.  $S_h$  is a source term including the enthalpy formation from the chemical reaction of the species. The energy  $E$  is defined as

$$E = h - \frac{p}{\mathbf{r}} + \frac{v^2}{2} \quad (2.5)$$

where  $h$  is the sensible enthalpy and for incompressible flow and is given as

$$h = \sum_j Y_j h_j + \frac{p}{\mathbf{r}}. \quad (2.6)$$

$Y_j$  is the mass fraction of species  $j$  and

$$h = \int_{T_{ref}}^T c_{p,j} dT \quad (2.7)$$

where  $T_{ref}$  is 298.15 K.

### 2.3 Turbulence Model

The velocity field in turbulent flows always fluctuates. As a result, the transported quantities such as momentum, energy, and species concentration fluctuate as well. The fluctuations can be small scale and high frequency, which is computationally expensive to be directly simulated. To overcome this, a modified set of equations that are

computationally less expensive to solve can be obtained by replacing the instantaneous governing equations with their time-averaged, ensemble-averaged, or otherwise manipulated to remove the small time scales. However, the modifications of the instantaneous governing equations introduce new unknown variables. Many turbulence models have been developed to determine these new unknown variables in terms of known variables. General turbulence models widely available are:

- a. Spalart-Allmaras
- b.  $k$ - $\epsilon$  models:
  - Standard  $k$ - $\epsilon$  model
  - RNG  $k$ - $\epsilon$  model
  - Realizable  $k$ - $\epsilon$  model
- c.  $k$ - $\omega$  model
  - Standard  $k$ - $\omega$  model
  - Shear-stress transport (SST)  $k$ - $\omega$  model
- d. Reynolds Stress
- e. Large Eddy Simulation

The standard  $k$ - $\epsilon$  turbulence model, which is the simplest two-equation turbulence model, is used in this simulation due to its suitability for a wide range of wall-bound and free-shear flows. The standard  $k$ - $\epsilon$  turbulence is based on the model transport equations for the turbulence kinetic energy,  $k$ , and its dissipation rate,  $\epsilon$ . The model transport equation for  $k$  is derived from the exact equation; however, the model transport equation for  $\epsilon$  is obtained using physical reasoning and bears little resemblance to its mathematically exact counterpart.

The standard  $k$ - $\mathbf{e}$  turbulence model is robust, economic for computation, and accurate for a wide range of turbulent flows. The turbulence kinetic energy,  $k$ , and its rate of dissipations,  $\mathbf{e}$ , are calculated from the following equations

$$\frac{\partial}{\partial x_i}(\mathbf{r}k u_i) = \frac{\partial}{\partial x_j} \left[ \left( \mathbf{m} + \frac{\mathbf{m}_t}{\mathbf{s}_k} \right) \frac{\partial k}{\partial x_j} \right] + G_k + G_b - \mathbf{r}\mathbf{e} - Y_M + S_k \quad (2.8)$$

and

$$\frac{\partial}{\partial x_i}(\mathbf{r}\mathbf{e} u_i) = \frac{\partial}{\partial x_j} \left[ \left( \mathbf{m} + \frac{\mathbf{m}_t}{\mathbf{s}_e} \right) \frac{\partial \mathbf{e}}{\partial x_j} \right] + C_{1e} \frac{\mathbf{e}}{k} (G_k + C_{3e} G_b) - C_{2e} \mathbf{r} \frac{\mathbf{e}^2}{k} + S_e. \quad (2.9)$$

In equations (2.8) and (2.9),  $G_k$  represents the generation of turbulence kinetic energy due to the mean velocity gradients and is defined as

$$G_k = -\overline{\mathbf{r} u_i u_j} \frac{\partial u_j}{\partial x_i}. \quad (2.10)$$

$G_b$  represents the generation of turbulence kinetic energy due to buoyancy and is calculated as

$$G_b = \mathbf{b} g_i \frac{\mathbf{m}_t}{\text{Pr}_t} \frac{\partial T}{\partial x_i}. \quad (2.11)$$

$\text{Pr}_t$  is the turbulent Prandtl number and  $g_i$  is the component of the gravitational vector in the  $i$ -th direction. For standard  $k$ - $e$  model the value for  $\text{Pr}_t$  is set 0.85 in this study. The coefficient of thermal expansion,  $\mathbf{b}$ , is given as

$$\mathbf{b} = -\frac{1}{\mathbf{r}} \left( \frac{\partial \mathbf{r}}{\partial T} \right)_p. \quad (2.12)$$

$Y_M$  represents the contribution of the fluctuating dilatation in compressible turbulence to the overall dissipation rate, and is defined as

$$Y_M = 2 \mathbf{r} \mathbf{e} M_t^2 \quad (2.13)$$

where  $M_t$  is the turbulent Mach number which is defined as

$$M = \sqrt{\frac{k}{a^2}} \quad (2.14)$$

where  $a$  ( $\equiv \sqrt{gRT}$ ) is the speed of sound.

The turbulent viscosity,  $\mathbf{m}_k$ , is calculated from equation

$$\mathbf{m}_k = rC_m \frac{k^2}{e} . \quad (2.15)$$

The values of constants  $C_{1e}$ ,  $C_{2e}$ ,  $C_m$ ,  $\mathbf{s}_k$ , and  $\mathbf{s}_e$  used are

$$C_{1e} = 1.44, C_{2e} = 1.92, C_m = 0.09, \mathbf{s}_k = 1.0, \mathbf{s}_e = 1.3.$$

The turbulence models are valid for the turbulent core flows, i.e. the flow in the regions somewhat far from walls. The flow very near the walls is affected by the presence of the walls. Viscous damping reduces the tangential velocity fluctuations and the kinematic blocking reduces the normal fluctuations. The solution in the near-wall region can be very important because the solution variables have large gradients in this region.

However, the solution in the boundary layer is not important in this study. Therefore, the viscous sublayer, where the solution variables change most rapidly, does not need to be solved. Instead, wall functions, which are a collection of semi-empirical formulas and functions, are employed to connect the viscosity-affected region between the wall and the fully-turbulent region. The wall functions consist of:

- laws-of-the-wall for mean velocity and temperature (or other scalars)
- formulas for near-wall turbulent quantities

There are two types of wall function: (a) standard wall function and (b) non-equilibrium wall function. The former is employed in this study. The wall function for the momentum is expressed as

$$U^+ = \frac{1}{k} \ln(Ey^+) \quad (2.16)$$

where

$$U^+ \equiv \frac{U_P C_m^{1/4} k_P^{1/2}}{t_v / r} \quad (2.17)$$

$$y^+ \equiv \frac{r C_m^{1/4} k_P^{1/2} y_P}{m} \quad (2.18)$$

and

$k$  = von Karman constant (= 0.42)

$E$  = empirical constant (= 9.793)

$U_P$  = mean velocity of fluid at point P

$k_P$  = turbulence kinetic energy at point P

$y_P$  = distance from point P to the wall

$m$  = dynamic viscosity of the fluid.

The wall function for the temperature is given as

$$T^+ \equiv \frac{(T_w - T_P) r c_p C_m^{1/4} k_P^{1/2}}{\dot{q}} = \begin{cases} \text{Pr } y^+, y^+ \langle y_T^+ \\ \text{Pr}_t \left[ \frac{1}{k} \ln(Ey^+) + P \right], y^+ \rangle y_T^+ \end{cases} \quad (2.19)$$

where  $P$  is given as

$$P = 9.24 \left[ \left( \frac{\text{Pr}}{\text{Pr}_T} \right)^{3/4} - 1 \right] \left[ 1 + 0.28 e^{-0.007 \text{Pr}/\text{Pr}_T} \right] \quad (2.20)$$

and

$r$  = density of the fluid

$c_p$  = specific heat of fluid

$q$  = wall heat flux

$T_P$  = temperature at cell adjacent to the wall

$T_W$  = temperature at the wall

$Pr$  = molecular Prandtl number

$Pr_t$  = turbulent Prandtl number (0.85 at the wall)

$A = 26$  (Van Driest constant)

$k = 0.4187$  (von Karman constant)

$E = 9.793$  (wall function constant)

$U_c$  = mean velocity magnitude at  $y^+ = y^+_T$

$y^+_T$  = non-dimensional thermal sublayer thickness.

The species transport is assumed to behave analogously to the heat transfer. The equation is expressed as

$$Y^+ \equiv \frac{(Y_{i,w} - Y_i) r c_p C_m^{1/4} k_p^{1/2}}{J_{i,w}} = \begin{cases} Sc y^+, & y^+ < y^+_c \\ Sc_t \left[ \frac{1}{k} \ln(E y^+) + P_c \right], & y^+ > y^+_c \end{cases} \quad (2.21)$$

where  $Y_i$  is the local mass fraction of species  $i$ ,  $Sc$  and  $Sc_t$  are the Schmidt numbers, and

$J_{i,w}$  is the diffusion flux of species  $i$  at the wall. The turbulent Schmidt number,  $Sc_t$ , is

given as  $\frac{\mu}{rD}$ , where  $\mu$  is the viscosity and  $D$  is the diffusivity. The  $P_c$  and  $y^+_c$  are

calculated in a similar way as  $P$  and  $y^+_T$ , with the difference being that the Prandtl

numbers are replaced by the corresponding Schmidt numbers.

In the  $k$ - $\epsilon$  model, the  $k$  equation is solved in the whole domain, including the wall-adjacent cells. The boundary condition for  $k$  imposed at the wall is

$$\frac{\partial k}{\partial n} = 0 \quad (2.22)$$

where  $n$  is the local coordinate normal to the wall. The production of kinetic energy,  $G_k$ , and its dissipation rate,  $\epsilon$ , at the wall-adjacent cells, which are the source terms in  $k$  equation, are computed on the basis of equilibrium hypothesis with the assumption that the production of  $k$  and its dissipation rate assumed to be equal in the wall-adjacent control volume. The production of  $k$  and  $\epsilon$  is computed as

$$G_k \approx \mathbf{t}_w \frac{\partial U}{\partial y} = \mathbf{t}_w \frac{\mathbf{t}_w}{\mathbf{kr} C_m^{1/4} k_p^{1/4} y_P} \quad (2.23)$$

and

$$\epsilon_P = \mathbf{t}_w \frac{C_m^{3/4} k_p^{3/2}}{k y_P}. \quad (2.24)$$

## 2.4 Radiation Model

The P-1 radiation model is used to calculate the flux of the radiation at the inside walls of the gasifier. The P-1 radiation model is the simplest case of the more general P-N radiation model that is based on the expansion of the radiation intensity  $I$ . The P-1 model requires only a little CPU demand and can easily be applied to various complicated geometries. It is suitable for applications where the optical thickness  $aL$  is large where  $a$  is the absorption coefficient and  $L$  is the length scale of the domain.

The heat sources or sinks due to radiation is calculated using the equation

$$-\nabla q_r = aG - 4aG\mathbf{s}T^4 \quad (2.25)$$

where

$$q_r = -\frac{1}{3(a + \mathbf{s}_s) - C\mathbf{s}_s} \nabla G \quad (2.26)$$

and  $q_r$  is the radiation heat flux,  $a$  is the absorption coefficient,  $\mathbf{s}_s$  is the scattering coefficient,  $G$  is the incident radiation,  $C$  is the linear-anisotropic phase function coefficient, and  $\mathbf{s}$  is the Stefan-Boltzmann constant.

The flux of the radiation,  $q_{r,w}$ , at walls caused by incident radiation  $G_w$  is given as

$$q_{r,w} = -\frac{4\mathbf{p}\mathbf{e}_w \frac{\mathbf{s}T_w^4}{\mathbf{p}} - (1 - \mathbf{r}_w)G_w}{2(1 + \mathbf{r}_w)} \quad (2.27)$$

where  $\mathbf{e}_w$  is the emissivity and is defined as

$$\mathbf{e}_w = 1 - \mathbf{r}_w \quad (2.28)$$

and  $\mathbf{r}_w$  is the wall reflectivity.

## 2.5 Combustion Model

The global reaction mechanism is modeled to involve the following chemical species: C, O<sub>2</sub>, N<sub>2</sub>, CO, CO<sub>2</sub>, H<sub>2</sub>O and H<sub>2</sub> (see reactions R1.1 through R1.5 in Chapter 1). All of the species are assumed to mix in the molecular level. The chemical reactions inside the gasifier are modeled by calculating the transport and mixing of the chemical species by solving the conservation equations describing convection, diffusion, and reaction of each component species. The general form of the transport equation for each species is defined as

$$\frac{\partial}{\partial t}(\mathbf{r}Y_i) + \nabla \cdot (\mathbf{r}\bar{v}Y_i) = -\nabla \cdot \bar{\mathbf{J}}_i + R_i. \quad (2.29)$$

$R_i$  is the net rate of production of species  $i$  by chemical reaction.  $\bar{\mathbf{J}}_i$  is the diffusion flux of species  $i$ , which arises due to concentration gradients. Mass diffusion for laminar flows is given as

$$\bar{\mathbf{J}}_i = -\mathbf{r}D_{i,m} \nabla Y_i \quad (2.30)$$

For turbulent flows, mass diffusion flux is given as

$$\bar{\mathbf{J}}_i = -\left( \mathbf{r}D_{i,m} + \frac{\mathbf{m}_i}{Sc_t} \right) \nabla Y_i \quad (2.30)$$

where  $Sc_t$  is the turbulent Schmidt number.

So, the transport equations for each chemical species are

$$\frac{\partial}{\partial t}(\mathbf{r}Y_C) + \nabla \cdot (\mathbf{r}\bar{v}Y_C) = -\nabla \cdot \bar{\mathbf{J}}_C + R_C \quad (2.32a)$$

$$\frac{\partial}{\partial t}(\mathbf{r}Y_{O_2}) + \nabla \cdot (\mathbf{r}\bar{v}Y_{O_2}) = -\nabla \cdot \bar{\mathbf{J}}_{O_2} + R_{O_2} \quad (2.32b)$$

$$\frac{\partial}{\partial t}(\mathbf{r}Y_{N_2}) + \nabla \cdot (\mathbf{r}\bar{v}Y_{N_2}) = -\nabla \cdot \bar{\mathbf{J}}_{N_2} + R_{N_2} \quad (2.32c)$$

$$\frac{\partial}{\partial t}(\mathbf{r}Y_{CO}) + \nabla \cdot (\mathbf{r}\bar{v}Y_{CO}) = -\nabla \cdot \bar{\mathbf{J}}_{CO} + R_{CO} \quad (2.32d)$$

$$\frac{\partial}{\partial t}(\mathbf{r}Y_{CO_2}) + \nabla \cdot (\mathbf{r}\bar{v}Y_{CO_2}) = -\nabla \cdot \bar{\mathbf{J}}_{CO_2} + R_{CO_2} \quad (2.32e)$$

$$\frac{\partial}{\partial t}(\mathbf{r}Y_{H_2O}) + \nabla \cdot (\mathbf{r}\bar{v}Y_{H_2O}) = -\nabla \cdot \bar{\mathbf{J}}_{H_2O} + R_{H_2O} \quad (2.32f)$$

$$\frac{\partial}{\partial t}(\mathbf{r}Y_{H_2}) + \nabla \cdot (\mathbf{r}\bar{v}Y_{H_2}) = -\nabla \cdot \bar{\mathbf{J}}_{H_2} + R_{H_2}. \quad (2.32g)$$

The reaction equations that need to be solved are given below.



There are three approaches to solving these reactions.

- (a) Eddy-dissipation model: The assumption in this model is that the chemical reaction is faster than the time scale of the turbulence eddies. Thus, the reaction rate is determined by the turbulence mixing of the species. The reaction is assumed to occur instantaneously when the reactants meet.
- (b) Equilibrium model: The rate of chemical reaction is governed by the rate of mixing of gaseous oxidant and reactant. The reactions are fast compare to the time scale of turbulence. The gaseous properties become functions of the turbulent mixing rate and can be calculated using equilibrium considerations [Fletcher, 1983].
- (c) Reaction rate model: The rate of chemical reaction is computed using an expression that takes into account temperature and pressure and ignores the effects of the turbulent eddies.

In this study, the eddy-dissipation model is used. The sources term  $R_i$  in equation (2.29) is calculated using the eddy-dissipation model based on the work of Magnussen and Hjertager [Magnusses et al., 1976]. The net rate of production or destruction of

species  $i$  as the result of reaction  $r$ ,  $R_{i,r}$ , is given by the smaller of the two expressions below.

$$R_{i,r} = \mathbf{n}'_{i,r} M_{i,r} A r \frac{e}{k} \min \left( \frac{Y_R}{\mathbf{n}'_{R,r} M_{w,R}} \right) \quad (2.38)$$

and

$$R_{i,r} = \mathbf{n}'_{i,r} M_{i,r} B r \frac{e}{k} \left( \frac{\sum_P Y_P}{\sum_j^N \mathbf{n}''_{j,r} M_{w,j}} \right) \quad (2.39)$$

where,

$Y_P$  is the mass fraction of any product species,  $P$

$Y_R$  is the mass fraction of a particular reactant,  $R$

$A$  is an empirical constant equal to 4.0

$B$  is an empirical constant equal to 0.5

$\mathbf{v}'_{i,r}$  is the stoichiometric coefficient of reactant  $i$  in reaction  $r$

$\mathbf{v}''_{j,r}$  is stoichiometric coefficient of product  $j$  in reaction  $r$ .

In equations (2.12) and (2.13), the chemical reaction rate is governed by large-eddy mixing time scale,  $k/e$ . The smaller of the two expressions (2.12) and (2.13) is used because it is the limiting value that determines the reaction rate.

The procedure to solve the reactions is as follows.

1. The net local production or destruction of species  $i$  in each reaction is calculated by solving equations (2.12) and (2.13).
2. The smaller of these values is substituted into the corresponding species transport equation (2.10) to calculate the local species mass fraction,  $Y_i$ .

3.  $Y_i$  is then used in equation (2.11) to calculate the net enthalpy production of each reaction equation.
4. The net enthalpy production becomes the source term in energy equation (2.3) that affects the temperature distribution. In an endothermic process, the net enthalpy production is negative, which becomes a sink term in the energy equation.

## 2.6 Boundary Conditions

Figure 2.3 shows the boundary conditions for the baseline case of the generic two-stage entrained-flow gasifier. Boundary conditions for all the cases simulated in this study are summarized in Table 2.1.

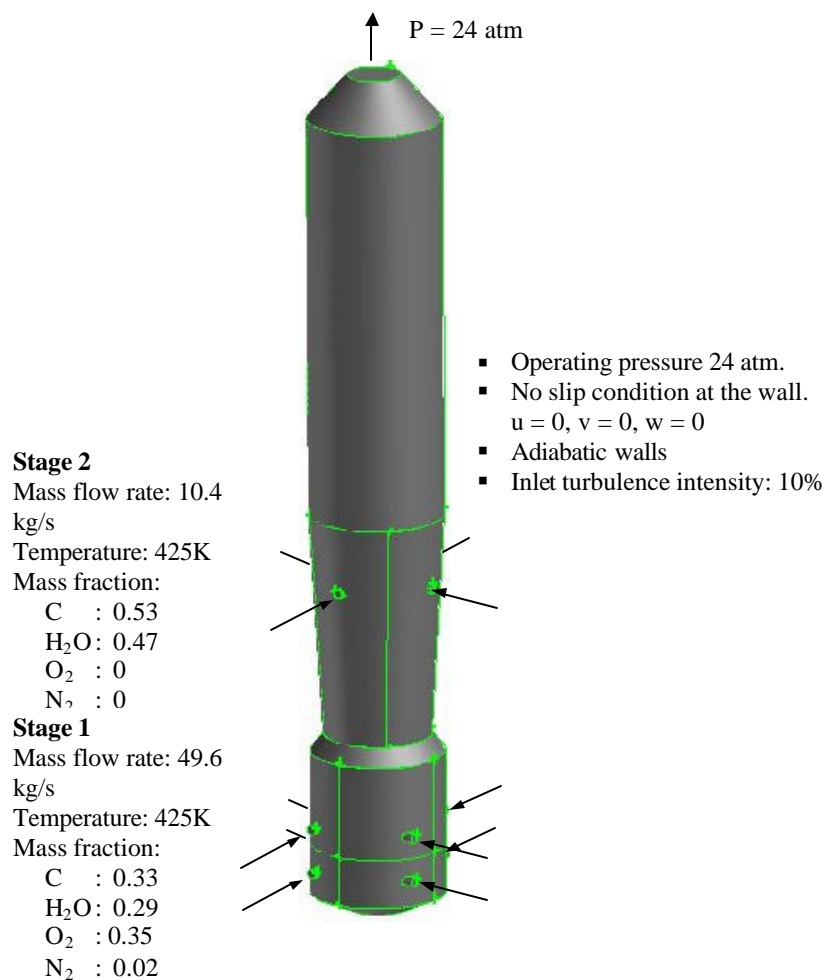


Figure 2.2 Boundary conditions for the baseline case of the generic two-stage entrained-flow gasifier.

Table 2.1 Parameters and operating conditions for simulated cases

<i>Parameters</i>	<i>Cases 1, 6 and 7*</i>			<i>Case 2</i>			<i>Case 3</i>		
Fuel	Coal slurry			Coal <b>powder</b>			Coal powder		
Oxidant	Oxygen			Oxygen			Oxygen		
Stage	<u>1</u>	<u>2</u>	<u>Total</u>	<u>1</u>	<u>2</u>	<u>Total</u>	<u>1</u>	<u>2</u>	<u>Total</u>
Fuel distribution	75%	25%		75%	25%		75%	25%	
Oxidant distribution	100%	0%		100%	0%		100%	0%	
Total mass flow rate, kg/s	49.6	10.4	60	51.4	8.6	60	51.4	8.6	60
Coal mass flow rate, kg/s	16.4	5.5	21.9	23.1	7.7	30.8	23.1	7.7	30.8
Mass fraction at inlet	(kmole/s)			(kmole/s)			(kmole/s)		
C	0.33	0.53	1.82	0.45	0.89	2.57	0.45	0.89	2.57
H <sub>2</sub> O	0.29	0.47	1.07	0.06	0.11	0.22	0.06	0.11	0.22
O <sub>2</sub>	0.35	0	0.54	0.47	0	0.75	0.47	0	0.75
N <sub>2</sub>	0.02	0	0.04	0.02	0	0.04	0.02	0	0.04
Wall temperature, K	Adia.	Adia.		Adia.	Adia.		<b>1800</b>	<b>1600</b>	

<i>Parameters</i>	<i>Case 4</i>			<i>Case 5</i>			<i>Case 8</i>		
Fuel	Coal slurry			Coal slurry			Coal slurry		
Oxidant	Oxygen			<b>Air</b>			Oxygen		
Stage	<u>1</u>	<u>2</u>	<u>Total</u>	<u>1</u>	<u>2</u>	<u>Total</u>	<u>1</u>	<u>2</u>	<u>Total</u>
Fuel distribution	<b>50%</b>	<b>50%</b>		75%	25%		<b>100%</b>	<b>0%</b>	
Oxidant distribution	100%	0%		100%	0%		100%	0%	
Total mass flow rate, kg/s	39.3	20.7	60	55	5	60	60	0	60
Coal mass flow rate, kg/s	11.0	11.0	22.0	7.7	2.7	10.4	22.2	0.0	22.2
Mass fraction at inlet	(kmole/s)			(kmole/s)			(kmole/s)		
C	0.28	0.53	1.83	0.14	0.53	0.86	0.37	0	1.85
H <sub>2</sub> O	0.25	0.47	1.09	0.13	0.47	0.53	0.32	0	1.07
O <sub>2</sub>	0.45	0	0.55	0.15	0	0.26	0.29	0	0.54
N <sub>2</sub>	0.02	0	0.03	0.58	0	1.14	0.02	0	0.04
Wall temperature, K	Adia.	Adia.		Adia.	Adia.		Adia.	Adia.	

\* In Cases 6 & 7, the injectors in Stage 1 are modified to tilt 30 degrees downward (Case 6) and 30 degrees upward (Case 7).

## **CHAPTER THREE**

### **COMPUTATIONAL PROCESS**

#### **3.1 Solution Methodology**

The major steps taken in performing the computational simulation are given as follows:

1. Preprocessing:

The preprocessing phase starts with the geometry generation. This phase includes geometry generation, mesh generation, fluid properties specifications, physical model selection, and boundary condition specifications.

2. Processing:

In the processing phase, the equations and models set up in the preprocessing phase are solved using the CFD code. The progress of the calculation to achieve a converged result is observed. Sometimes adjustments on under-relaxation factors need to be made to help reach the convergence.

3. Postprocessing:

The postprocessing phase includes the analysis and interpretation of the results. The results can be presented in the form of x-y plots, contour plots, velocity vector plots, streamline plots, and animations.

The preprocessing tool used in this study is GAMBIT, which provides one interface to build and mesh the geometry. The CFD solver is the commercial CFD code FLUENT Version 6.1.22. FLUENT is a finite-volume-based CFD solver written in C language, and has the ability to solve fluid flow, heat transfer and chemical reactions in complex geometries and supports both structured and unstructured mesh. Figure 3.1 illustrates the basic program structure that can be used to support CFD simulation in FLUENT.

### **3.2 Computational Grid**

The geometry is generated and meshed in GAMBIT. Three-dimensional hexahedral mesh is used for meshing the gasifier (Figure 3.2). A total of 95,185 grids are employed. After the model has been meshed, it is exported to FLUENT.

### **3.3 Numerical Procedure**

The procedure for performing the simulation in FLUENT is outlined below.

1. Create and mesh the geometry model using GAMBIT
2. Import geometry into FLUENT
3. Define the solver model
4. Define the turbulence model
5. Define the species model
6. Define the materials and the chemical reactions
7. Define the boundary conditions
8. Initialize the calculations

9. Iterate/calculate until convergence is achieved.

10. Postprocess the results

FLUENT offers two solution methods: (a) segregated solution and (b) coupled solution. Segregated solution solves the governing equations of continuity, momentum, energy, and species transport sequentially (segregated from one another). On the other hand, coupled solution solves the governing equations of continuity, momentum, energy, and species transport simultaneously. The equations for scalars such as turbulence and radiation are solved using the previously updated values from the momentum equations. Segregated solution is chosen for this study. The detailed steps of segregated solution are given below.

- (i) Fluid properties are updated based on the current solution or the initialized solution.
- (ii) The momentum equations are solved using the current values of pressure and face mass fluxes to get the updated velocity field.
- (iii) Equation for the pressure correction is calculated from the continuity equation and the linearized momentum equations since the velocity field obtained in step (ii) may not satisfy the continuity equation.
- (iv) The pressure correction equations obtained from step (iii) are solved to correct the pressure and velocity fields, and face mass such that the continuity equation is satisfied.
- (v) The equations for scalars such as turbulence, energy, radiation, and species are solved using the updated values of the other variables.

(vi) The equation is checked for convergence.

These steps are repeated until the convergence criteria are met. Figure 3.3 shows the flow chart of the above steps.

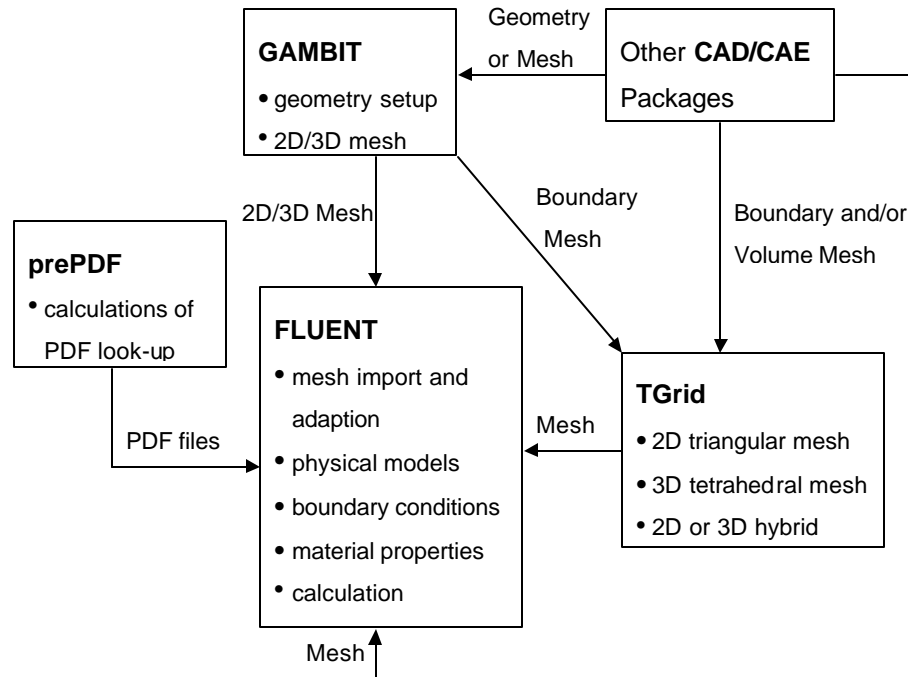


Figure 3.1 Basic program structure of FLUENT code.

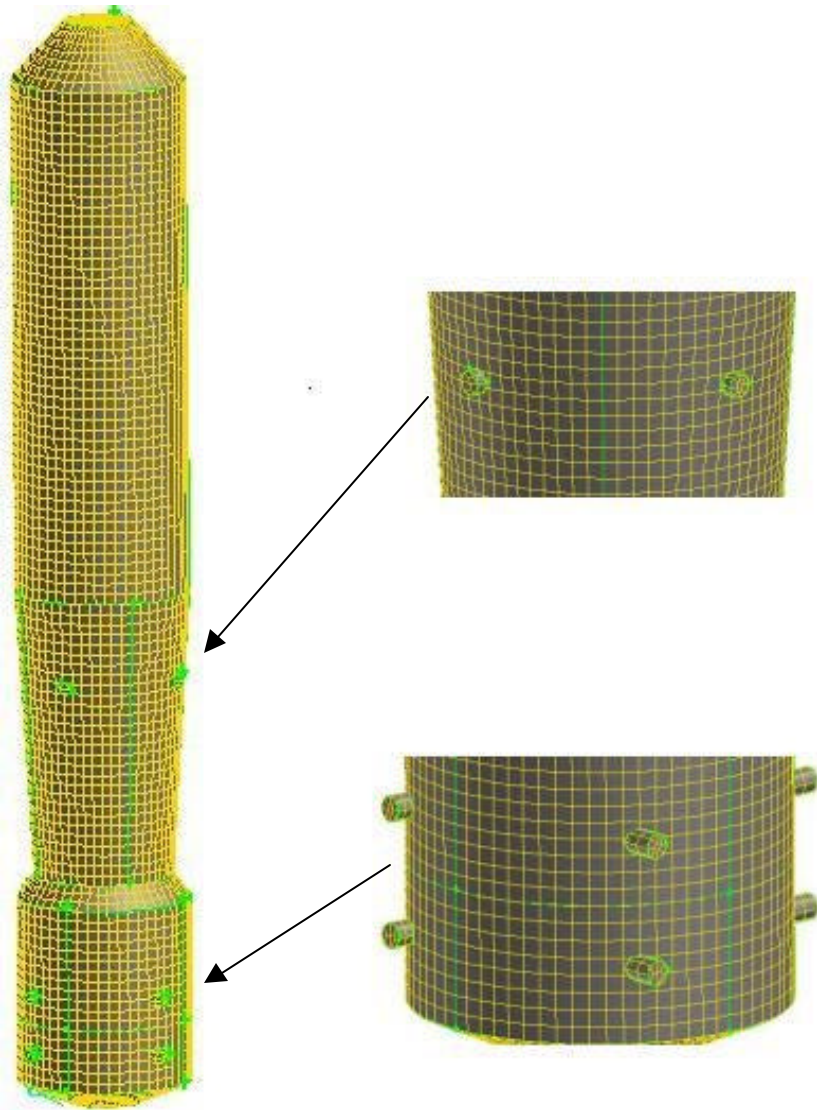


Figure 3.2 Meshed geometry for the generic gasifier.

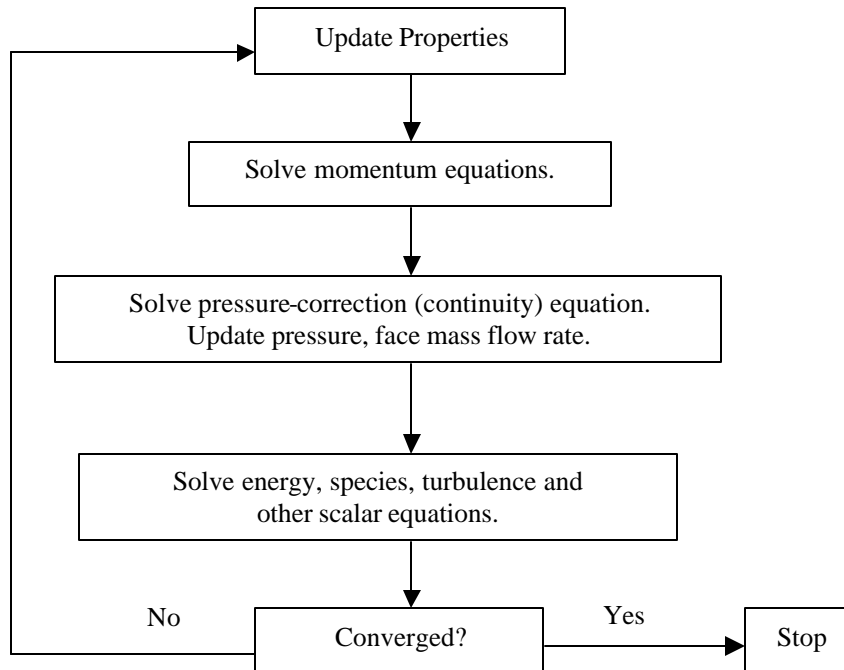


Figure 3.3 Overview of the Segregated Solution Method.

The non-linear governing equations can be linearized implicitly or explicitly with respect to the dependent variables. If linearized implicitly, the unknown value in each cell is computed using a relation that includes both existing and unknown values from neighboring cells. If linearized explicitly, the unknown value in each cell is computed using a relation that includes only existing values. In the segregated solution, the linearization is implicit. Therefore, each unknown will appear in more than one equation in the linear system, and these equations must be solved simultaneously to give the unknown quantities.

FLUENT uses a control-volume-based technique to convert the governing equations to algebraic equations, which are then solved mathematically. The discretization of the governing equations yields discrete equations that conserve each

quantity on a control-volume basis. There are several discretization schemes available in FLUENT: (a) First Order, (b) Second Order, (c) Power Law, and (d) QUICK.

The first order discretization scheme is applied for the momentum, the turbulence kinetic energy, the turbulence kinetic dissipation, the energy, and all the species.

FLUENT provides three algorithms for pressure-velocity coupling in the segregated solver: (a) SIMPLE, (b) SIMPLEC, and (c) PISO. The SIMPLE algorithm [Patankar et. al, 1980] is used in this study.

The built-in standard  $k$ - $\epsilon$  turbulence model is used, and the model constants are as follow:  $C_m = 0.09$ ,  $C_{1\epsilon} = 1.44$ ,  $C_{2\epsilon} = 1.92$ ,  $\sigma_k = 1.0$ ,  $\sigma_\epsilon = 1.3$ .

FLUENT offers several species model:

- Species transport: laminar finite-rate, eddy-dissipation, or eddy-dissipation-concept (EDC)
- Non-premixed combustion
- Premixed combustion
- Partially premixed combustion
- Composition PDF combustion

The species model and transport model with volumetric reaction are chosen to simulate the diffusion and production/destruction of the chemical species. The eddy-dissipation model is utilized to calculate the net production and destruction of the species. Eddy-dissipation model assumes that chemical kinetics are fast compared to the mixing rate of the reactants by the turbulent fluctuations.

A mixture material that consists of seven chemical species (C, O<sub>2</sub>, N<sub>2</sub>, CO, CO<sub>2</sub>, H<sub>2</sub>O and H<sub>2</sub>) is defined. All the species, including C, are defined as fluid species and are assumed to mix at the molecular level. The specific heat of the species is temperature dependant and is defined as a piecewise-polynomial function of temperature. The chemical reactions (R1.1) through (R1.5) in Chapter 1 are then defined in the reaction window.

The types of boundary conditions on the surface geometry have been assigned in GAMBIT. There are three types of boundary conditions for the model.

- a. Mass flow rate inlet --- All the inlet surfaces are defined as mass flow rate inlets. The mass flow rate, temperature of the mixture, and the mass fractions of all species in the mixture are specified according to the values given in the Table 2.1 in Chapter Two.
- b. Pressure outlet --- The outlet surface is assigned as a pressure outlet boundary. The pressure, temperature, and species mass fractions of the gas mixture outside the computational domain are specified. This information does not affect the calculations inside the computational domain but will be used if backflow occurs at the outlet.
- c. Walls --- The outside surfaces are defined as wall boundary. The walls are stationary with no-slip condition imposed (zero velocity) on the surface. For adiabatic case, the heat flux on the wall is set to 0 (zero). For constant wall temperature, the wall temperature is set to a certain constant value as specified in Table 2.1.

The complete inlet and boundary conditions for all the cases conducted in this study are listed in Table 2.1.

Before FLUENT can begin solving governing equations, flow field guessed initial values, used as the initial values of the solution, have to be provided. Once the initial values have been provided, the iteration is performed until a converged result is obtained. An example of the step-by-step procedure for performing the baseline case is given in Appendix A.

### **3.4 Grid Independence Study**

A grid independence study was conducted using three different grids: coarse grid (35,168 grids), medium grid (95,182 grids), and fine grid (160,170 grids). Parameters and operating conditions for Case 1 given in Table 2.1 were used in this grid independence study. The calculations were performed by a personal computer with Pentium 4, 2.8 GHz CPU. Table 3.1 shows the mass-weighted average temperature and species mole fractions of the exit gas for all grids. It can be seen that the exit gas temperature for the coarse grid is the highest at 763 K followed by fine grid at 723 K and medium grid 717 K. The temperatures for the medium and fine grids only differ by 8 K, which is less than 1.5%. The differences in the species mole fractions for the medium and fine grids are less than 2 percentage points, which are small and acceptable to this study. Therefore, to ensure obtaining good results with reasonable computational time, the medium grid is used for this study.

## CHAPTER FOUR

### RESULTS AND DISCUSSIONS

The objective of this study is to investigate the effects of different parameters on the performance of a two-stage entrained coal gasifier. The following different operating conditions and parameters are simulated:

1. Coal mixture: coal slurry or coal powder
2. Oxidant: oxygen-blown or air-blown
3. Various first and second stage mass flow rates
4. Various feedstock injection angles

The operating conditions and the model parameters used in the simulations for various cases are summarized in Table 4.1 and is a duplicate of Table 2.1. The simulation results on the gas temperature, carbon fuel conversion, and mole fractions of species at the gasifier outlet are listed in Table 4.2. The values in Table 4.2 are the mass-weighted average values at the gasifier exit.

The oxygen or air provided for all simulations is based on the theoretical energy needed to produce all gasification processes for a complete carbon conversion. The theoretical energy needed to complete reactions is calculated from the endothermic reaction (R1.2 and R1.3). This results in an overall oxygen over carbon mole ratio ( $O_2:C$ ) of approximately 0.3. Similar to the simulation conducted by Bockelie et al., [Bockelie et al., 2002(b)], Illinois #6 coal with a composition of 79% char, 11%  $H_2O$ , and 10% ash is

used. However, for the simplicity of this study, the coal is assumed to contain no ash, resulting in 89% char and 11% H<sub>2</sub>O. The oxidant of the oxygen-blown cases consists of 95% O<sub>2</sub> and 5% N<sub>2</sub> by weight. For the air-blown cases, the air consists of 21% O<sub>2</sub> and 79% N<sub>2</sub> by weight. The simulated coal-slurry mixture contains 60% coal and 40% H<sub>2</sub>O by weight.

#### 4.1 Baseline Case

The baseline case (Case 1) is oxygen-blown with 2 stages, coal slurry input (75%-25% split) and adiabatic wall. The distributions of gas temperature and gas composition in the gasifier for Case 1 are illustrated in Figures 4.1 and 4.2. The planes in Figure 4.1 are the vertical midplanes, if the gasifier is sliced vertically through the upper inlets. The lower inlets are not shown on the plane because they are positioned tangential to the gasifier cylinder. Figure 4.3 shows the gas temperature and composition on a horizontal plane at the lower level injector in the combustor region.

In Figure 4.1, the temperature distribution in stage 1 (or the combustor at the bottom of the gasifier) is almost uniform at about 1600 K. The char immediately burns to produce CO, according to reaction  $C + 0.5O_2 \rightarrow CO$  (R1.1), as it enters the gasifier in stage 1 as shown in Figure 4.3 in a cross-sectional view. The strong temperature gradient field near each injector in Figure 4.3 clearly indicates the flame propagation direction is a cyclic flow induced by the 45-degree tangential injections and skewed in a clockwise direction. . Due to a fast char reaction with oxygen, the mole fraction of CO immediately increases as the gas enters the vessel. The CO mole fraction quickly increases from 0 to 0.42. This reaction releases energy and raises the gas temperature to around 1600 K.

Table 4.1 Parameters and operating conditions for simulated cases

<i>Parameters</i>	<i>Cases 1, 6 and 7*</i>			<i>Case 2</i>			<i>Case 3</i>		
Fuel	Coal slurry			Coal <b>powder</b>			Coal powder		
Oxidant	Oxygen			Oxygen			Oxygen		
Stage	<u>1</u>	<u>2</u>	<u>Total</u>	<u>1</u>	<u>2</u>	<u>Total</u>	<u>1</u>	<u>2</u>	<u>Total</u>
Fuel distribution	75%	25%		75%	25%		75%	25%	
Oxidant distribution	100%	0%		100%	0%		100%	0%	
Total mass flow rate, kg/s	49.6	10.4	60	51.4	8.6	60	51.4	8.6	60
Coal mass flow rate, kg/s	16.4	5.5	21.9	23.1	7.7	30.8	23.1	7.7	30.8
Mass fraction at inlet	(kmole/s)			(kmole/s)			(kmole/s)		
C	0.33	0.53	1.82	0.45	0.89	2.57	0.45	0.89	2.57
H <sub>2</sub> O	0.29	0.47	1.07	0.06	0.11	0.22	0.06	0.11	0.22
O <sub>2</sub>	0.35	0	0.54	0.47	0	0.75	0.47	0	0.75
N <sub>2</sub>	0.02	0	0.04	0.02	0	0.04	0.02	0	0.04
Wall temperature, K	Adia.	Adia.		Adia.	Adia.		<b>1800</b>	<b>1600</b>	

<i>Parameters</i>	<i>Case 4</i>			<i>Case 5</i>			<i>Case 8</i>		
Fuel	Coal slurry			Coal slurry			Coal slurry		
Oxidant	Oxygen			<b>Air</b>			Oxygen		
Stage	<u>1</u>	<u>2</u>	<u>Total</u>	<u>1</u>	<u>2</u>	<u>Total</u>	<u>1</u>	<u>2</u>	<u>Total</u>
Fuel distribution	<b>50%</b>	<b>50%</b>		75%	25%		<b>100%</b>	<b>0%</b>	
Oxidant distribution	100%	0%		100%	0%		100%	0%	
Total mass flow rate, kg/s	39.3	20.7	60	55	5	60	60	0	60
Coal mass flow rate, kg/s	11.0	11.0	22.0	7.7	2.7	10.4	22.2	0.0	22.2
Mass fraction at inlet	(kmole/s)			(kmole/s)			(kmole/s)		
C	0.28	0.53	1.83	0.14	0.53	0.86	0.37	0	1.85
H <sub>2</sub> O	0.25	0.47	1.09	0.13	0.47	0.53	0.32	0	1.07
O <sub>2</sub>	0.45	0	0.55	0.15	0	0.26	0.29	0	0.54
N <sub>2</sub>	0.02	0	0.03	0.58	0	1.14	0.02	0	0.04
Wall temperature, K	Adia.	Adia.		Adia.	Adia.		Adia.	Adia.	

\* In Cases 6 & 7, the injectors in Stage 1 are modified to tilt 30 degrees downward (Case 6) and 30 degrees upward (Case 7).

Table 4.2 Summary of simulation results

<i>Parameters</i>	<i>Case 1</i>		<i>Case 2</i>		<i>Case 3</i>		<i>Case 4</i>	
Exit temperature, K	717		2077		1853		1045	
Carbon fuel conversion efficiency, %	86%		74%		74%		65%	
Fuel conversion efficiency, %	79%		91%		91%		61%	
Components at exit:								
	Mole fraction	Mole no. (kmole)						
CO	53.0%	1.57	73.1%	1.91	72.6%	1.90	40.7%	1.20
H <sub>2</sub>	36.0%	1.07	8.9%	0.23	8.6%	0.22	39.7%	1.17
CO <sub>2</sub>	9.8%	0.29	0.0%	0.00	0.0%	0.00	18.6%	0.55
H <sub>2</sub> O	0.0%	0.00	0.0%	0.00	0.0%	0.00	0.0%	0.00
N <sub>2</sub>	1.2%	0.04	1.4%	0.04	1.4%	0.04	0.0%	0.00
C	0.0%	0.00	16.5%	0.43	17.4%	0.45	0.0%	0.00
HHV of syngas (MJ/kg)	12.5		10.1		10.0		11.3	

<i>Parameters</i>	<i>Case 5</i>		<i>Case 6</i>		<i>Case 7</i>		<i>Case 8</i>	
Exit temperature, K	813		740		728		734	
Carbon fuel conversion efficiency, %	48%		69%		79%		82%	
Fuel conversion efficiency, %	46%		65%		73%		76%	
Components at exit:								
	Mole fraction	Mole no. (kmole)						
CO	16.0%	0.42	42.0%	1.26	47.0%	1.45	50.1%	1.51
H <sub>2</sub>	27.1%	0.70	41.0%	1.23	36.7%	1.13	37.6%	1.13
CO <sub>2</sub>	13.4%	0.35	16.0%	0.48	11.9%	0.37	10.8%	0.33
H <sub>2</sub> O	0.0%	0.00	0.0%	0.00	0.0%	0.00	0.0%	0.00
N <sub>2</sub>	43.5%	1.13	1.2%	0.03	1.2%	0.04	1.4%	0.04
C	0.0%	0.00	0.0%	0.00	0.0%	0.00	0.0%	0.00
HHV of syngas (MJ/kg)	5.3		11.9		12.3		12.5	

A large fraction of CO, produced from reaction (R1.1), reacts with some O<sub>2</sub> to yield CO<sub>2</sub> as described in reaction  $\text{CO} + 0.5\text{O}_2 \rightarrow \text{CO}_2$  (R1.4) in Chapter 1. These two oxidation reactions release all the energy needed for all other endothermic reactions under a controlled condition with limited oxidations. The H<sub>2</sub>O distribution shows that water vapor reacts with char as soon as it enters the gasifier and produces CO and H<sub>2</sub> as described by the gasification reaction  $\text{C} + \text{H}_2\text{O} \rightarrow \text{CO} + \text{H}_2$  (R1.3) in Chapter 1.

The conversion of coal to syngas is further boosted in the second stage by injection the remaining 25% of the feedstock. The gasification reactions  $C + CO_2 \rightarrow 2CO$  (R1.2) and  $C + H_2O \rightarrow CO + H_2$  (R1.3) are dominant in the second stage. The  $CO_2$  produced in the combustor flows up to the second stage and reacts with the fresh coal injected into the second stage to yield CO. This is indicated by an increase in CO mole fraction and a decrease in  $CO_2$  mole fraction in Figure 4.1. Gasification of char with  $CO_2$  (R1.2) is an efficient process to consume  $CO_2$  to obtain CO. Unfortunately, not all  $CO_2$  from the first stage reacts with the char in the second stage. A fraction of the char reacts with the water vapor to form more CO and  $H_2$  via gasification reaction R1.3. The watershift reaction plays a minor role in the second stage because the mole fraction increase of  $H_2$  is negligible in the second stage. As a result of these endothermic reactions (R1.2) and (R1.3), the gas temperature decreases to 717 K.

To make analysis easier, a mass-flow-weighted average of each gas component is calculated across the cross-section area along the height of the gasifiers as shown in Figure 4.5. The CO concentration is clearly seen to quickly increase from 41.5% to 53% near the second injection location. The dips in Figure 4.5 occur at the injector levels, at the heights of 0.5 m and 1.0 m for the first stage injectors and height of 3.75 m for the second stage injectors, and are caused by the inclusion of the new fuels. The component, exit gas, and mole fractions are shown in Table 4.2 as 53% CO, 36%  $H_2$ , 9.8%  $CO_2$  and 1.2%  $N_2$ . The high  $H_2$  production is due to the moisture in the slurry.

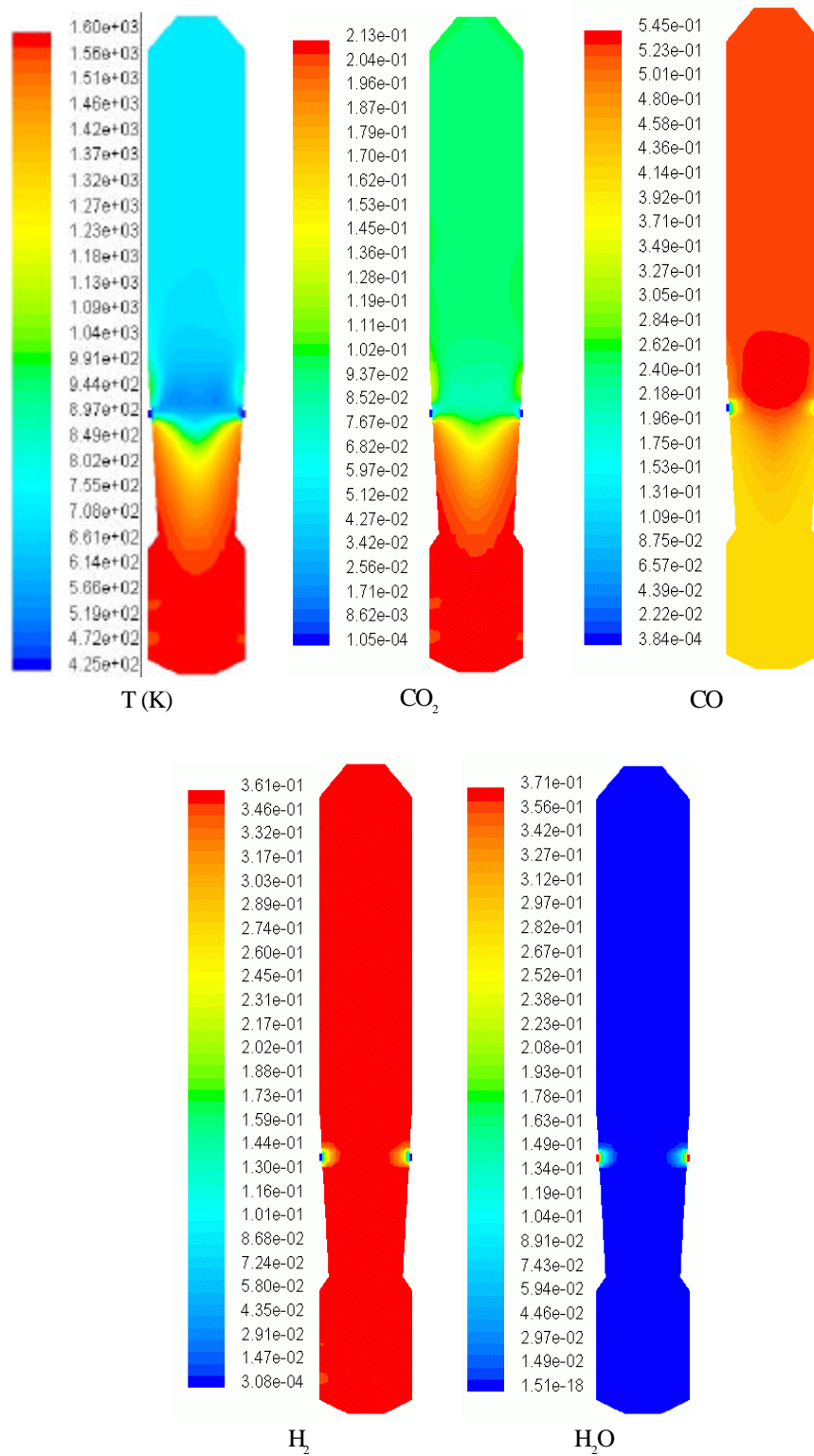


Figure 4.1 Midplane axial distribution of the gas temperature and the gas mole fraction at the center vertical plane in the oxygen-blown gasifier with coal-slurry fuel (Case 1).

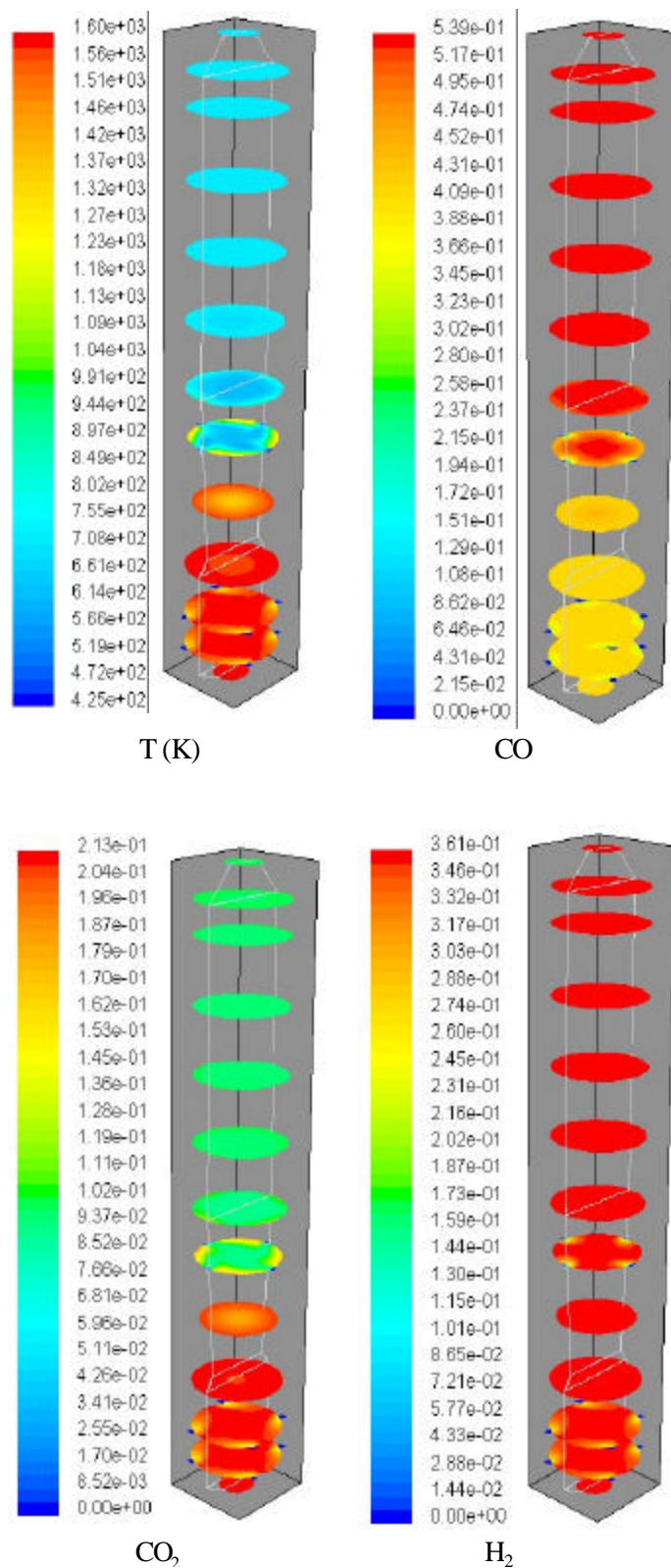


Figure 4.2 Distribution of the gas temperature and the gas mole fraction at different horizontal planes in the oxygen-blown gasifier with coal-slurry fuel (Case 1).

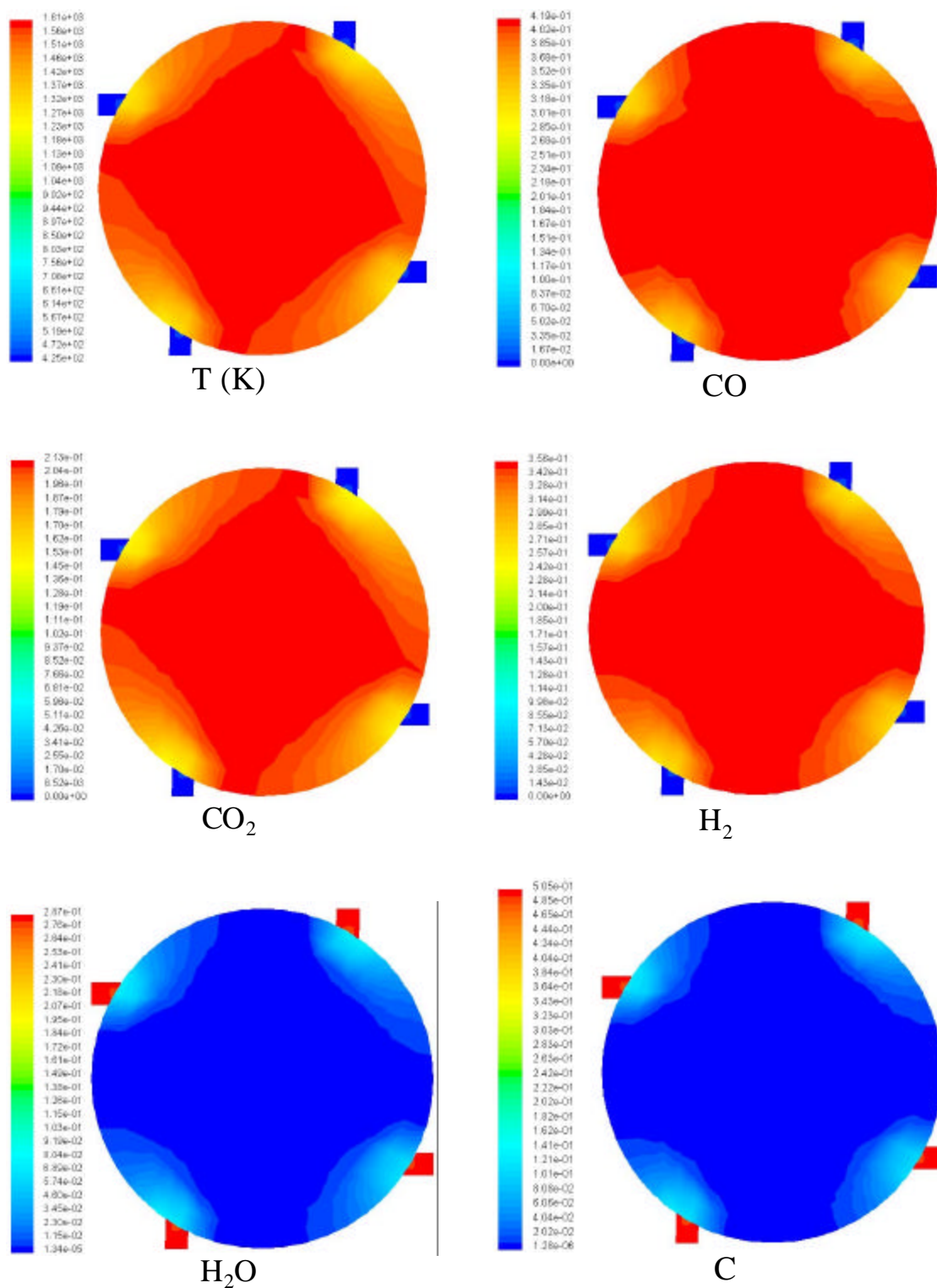


Figure 4.3 Distribution of gas temperature and gas mole fraction at lower inlet level for oxygen-blown gasifier with coal-slurry fuel (Case 1).

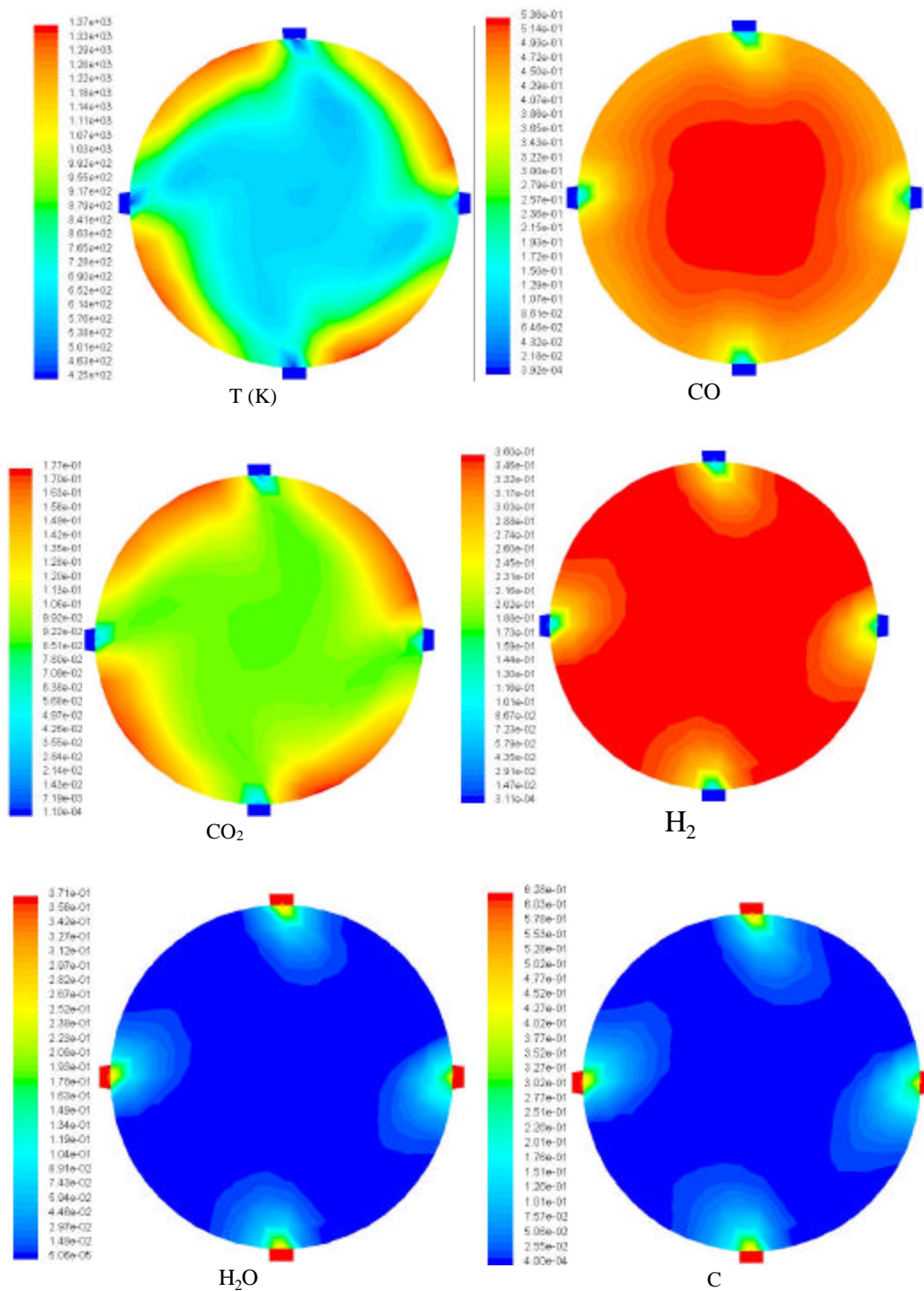


Figure 4.4 Distribution of gas temperature and gas mole fraction at upper inlet level for oxygen-blown gasifier with coal-slurry fuel (Case 1).

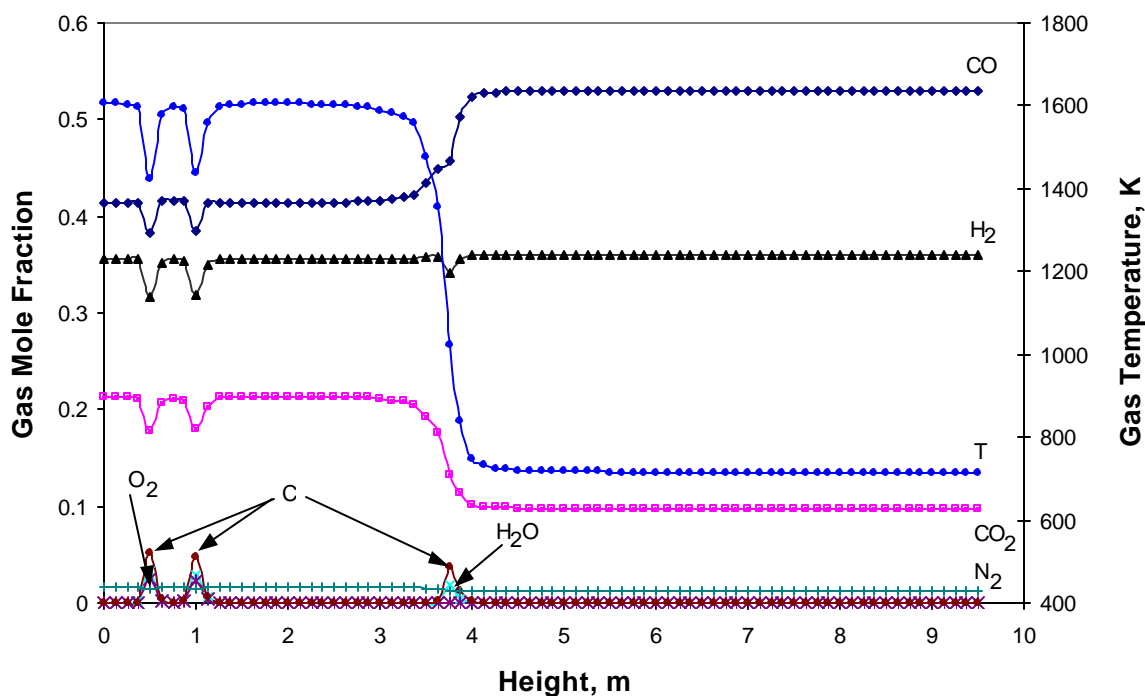


Figure 4.5 Mass-weighted average of gas temperature and mole fraction along the gasifier height for oxygen-blown gasifier with coal-slurry fuel (Case 1).

As listed in Table 4.2, 100% of the carbon has reacted once the gas exits the gasifier. This is due to the eddy-dissipation model used in this study. In the eddy-dissipation model, the chemical reactions are assumed to be faster than the turbulence time scale; so for the size of this gasifier, the residence time is sufficient for all the reactions to be completed when the flow exits the gasifier. Bockelie et al. [Bockelie et al., 2002] simulated a gasifier that operates under similar conditions as in Case 1. The CO and H<sub>2</sub> concentrations predicted by Bockelie et al. is lower than the values predicted in this study because they used a devolatilization model and the kinetics of char gasification which imposes slower reaction rates to control the reaction process.

The efficiency of the gasifier is considered by three indicators in this study:

- The carbon conversion efficiency
- The carbon fuel conversion efficiency
- The fuel conversion efficiency

The carbon conversion efficiency is defined as

$$\text{Carbon conversion efficiency} \equiv 1 - \frac{\text{carbon at the exit}}{\text{raw carbon} + \text{recycled carbon}} \quad (4.1)$$

Although the carbon conversion efficiency is 100% in Case 1, not all carbon is converted to useful fuel. In this study, the term **carbon fuel conversion efficiency** is defined as the percentage of carbon converted into useful fuel and CO and written as,

$$\text{Carbon fuel conversion efficiency} \equiv \frac{[CO]}{[\text{raw carbon}]} \quad (4.2)$$

So, the useful carbon conversion of Case 1 is not 100% even though 100% of carbon reacts but rather 86% because some of the C reacts to produce CO<sub>2</sub>, which is not a useful fuel, in the final product.

Another term, **fuel conversion efficiency**, is defined as the ratio of the total mass of the useful syngas produced (H<sub>2</sub> and CO) to the total mass of the raw carbon, water, and oxygen injected in the process. The fuel conversion efficiency is written as,

$$\text{Fuel conversion efficiency} \equiv \frac{H_2 + CO}{\text{raw carbon} + H_2O + O_2} \quad (4.3)$$

The fuel conversion efficiency in Case 1, as given in Table 4.2, is 79%. The heating value of the syngas is 12.55 MJ/kg.

## 4.2 Effects of Coal Mixture (Slurry vs. Powder)

Simulation for Case 2 was conducted to study the effects of using coal powder as fuel. The overall mole ratio of  $O_2:C$  (0.3) and the total inlet mass flow rate (60 kg/s) remain the same as in Case 1. However, the ratio  $C:H_2O$  changes and results in the change of the mass flow rates and the mass fractions of each species at each inlet as listed in Table 4.1. Pictured in Figures 4.6 and 4.7 are the predicted mass-weighted average of gas temperature and compositions obtained from the simulation of using coal powder.

The maximum temperature predicted, which occurs in the combustor, is around 3000 K. It is much higher compared to the maximum temperature 1600 K predicted for the gasifier using slurry (Case 1). The gasifier using coal slurry has a higher water mass fraction, which absorbs some of the heat released for the char combustion in its reaction with some of the remaining char through the gasification reaction (R1.3). The latent heat absorbed to vaporize the water lowers the gas temperature.

From Figures 4.6 and 4.7, the mole fraction of  $CO_2$  in the combustor is almost a third of the case using coal-slurry (Case 1). This suggests that only a small fraction of CO produced from the incomplete combustion (R1.1) reacts with  $O_2$  to form  $CO_2$  (R1.4). Unlike the calculation in the coal slurry simulation, all  $CO_2$  from combustor reacts with the fresh coal injected in the second stage to form CO. As a result, the coal power simulation yields a much higher CO compared with the coal-slurry feed in Case 1 (1.91 kmole vs. 1.57 kmole as listed in Table 4.2). This is expected because Case 2 has more carbon input than Case 1. On the other hand, the  $H_2$  production of Case 2 using coal powder is approximately a quarter of the  $H_2$  production with coal slurry (0.23 kmole vs. 1.01 kmole) due to the lesser amount of water

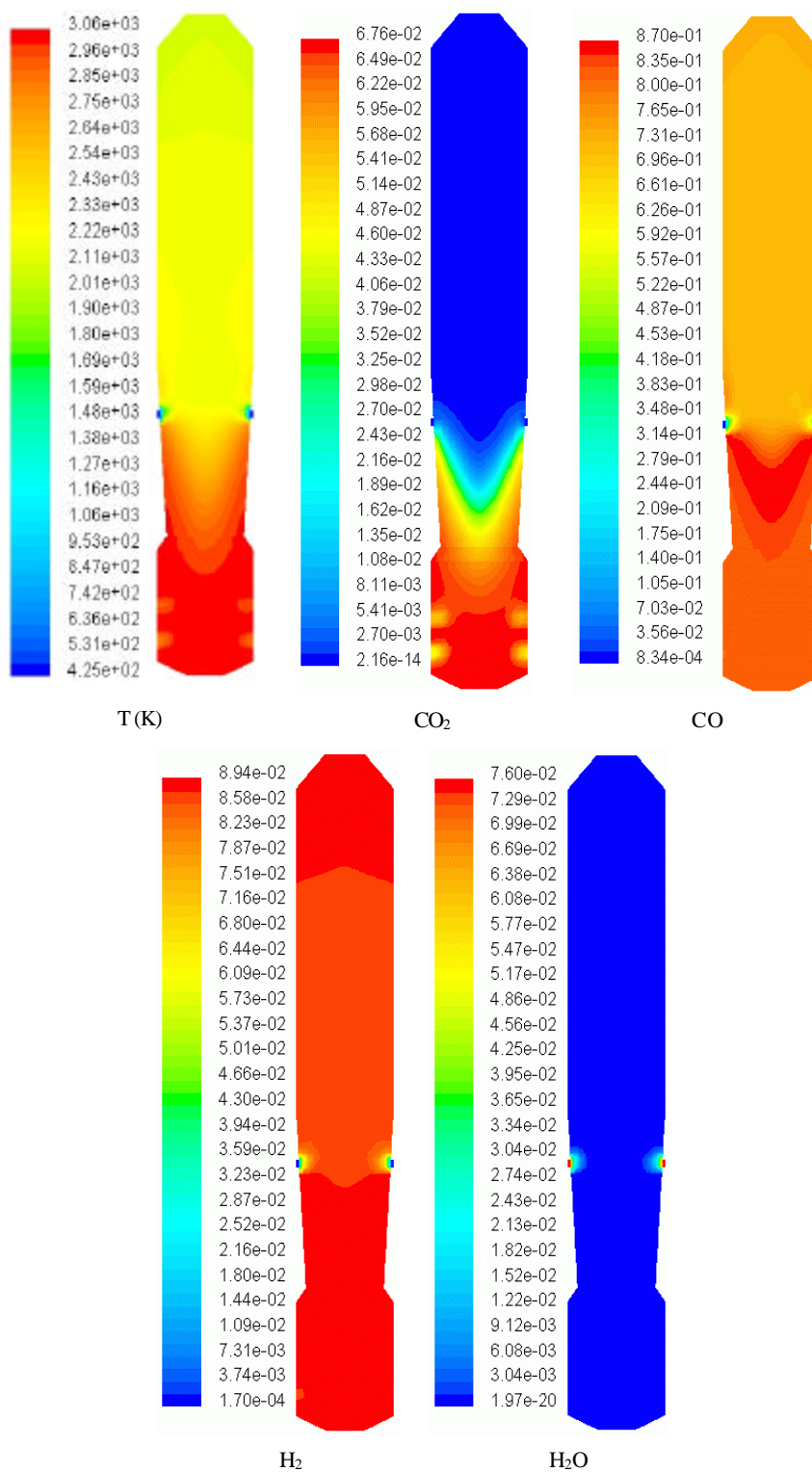


Figure 4.6 Midplane axial distribution of the gas temperature and the gas mole fraction in the oxygen-blown gasifier with coal powder fuel (Case 2).

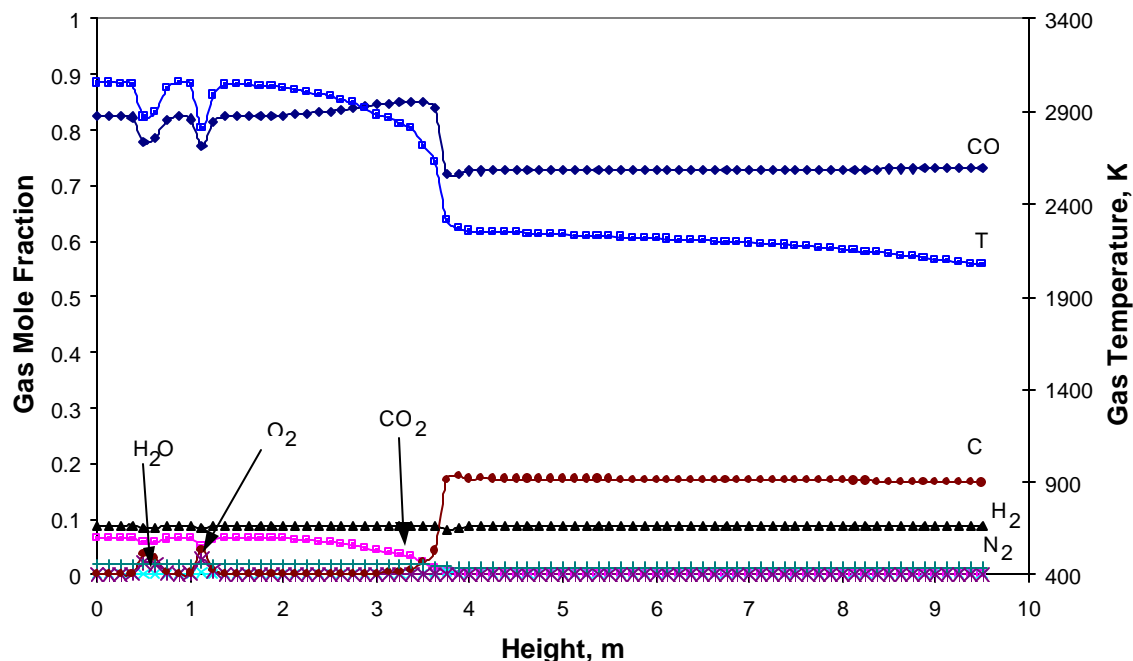


Figure 4.7 Mass-weighted average gas temperature and mole fraction along the gasifier height for oxygen-blown gasifier with coal powder fuel (Case 2).

reacting with C and CO to produce  $H_2$  in the gasification (R1.3) and watershift (R1.5) reactions.

Figure 4.7 indicates that there is some unburned C in the exit gas. As mentioned earlier, the raw carbon in the fresh coal injected in the second stage reacts with the  $CO_2$  produced in the first stage and the  $H_2O$  contained in the coal. The amount of C available is more than needed to consume all the available  $CO_2$  and  $H_2O$  through the gasification reactions (R1.2) and (R1.3). As a result, 0.43 kmoles of unburned C exits the vessel. A similar situation where the C reacts with  $CO_2$  and  $H_2O$  in the second stage also occurs in the slurry-fed simulation. However, due to the higher moisture injected and the higher  $CO_2$  from stage 1 in Case 1, all of the carbon injected in the stage 2 reacts with both  $CO_2$  and  $H_2O$ . The carbon fuel conversion of the coal-powder-fed case (74%) is lower than

that of the coal-slurry-fed case (86%). The other 26% of the carbon in the coal-powder-fed case remains as C; however, the other 14% of the carbon in the coal-slurry-fed case reacts and produces CO<sub>2</sub> as the end product. Case 2 shows that dry fed produces more CO but less H<sub>2</sub> and less carbon fuel conversion. The heating value of the syngas in Case 2 is 10.1 MJ/kg.

Table 4.2 shows that the fuel conversion efficiency in Case 2 is 91%, which is 12 percentage points higher than in Case 1. The fuel conversion efficiency is defined as the ratio of the total mass of the useful syngas produced (H<sub>2</sub> and CO) to the total mass of raw carbon, water, and oxygen injected in the process. Of the total mass of raw carbon, water and oxygen injected in the process, only a small fraction is not converted into H<sub>2</sub> or CO. In this case, some of the raw carbon remains unburned and exits in the gasifier. On the other hand, at the end of the process, a bigger fraction of the total mass of raw carbon, water and oxygen in Case 2 is converted into H<sub>2</sub> or CO instead of CO<sub>2</sub>. Therefore, the fuel conversion efficiency of Case 2 is higher than Case 1 even though the carbon fuel conversion efficiency in Case 2 is lower than in Case 1.

Due to no CO<sub>2</sub> forming in Case 2, all the CO<sub>2</sub> produced in reaction  $\text{CO} + 0.5\text{O}_2 \rightarrow \text{CO}_2$  (R1.4) is consumed by carbon via gasification process  $\text{C} + \text{CO}_2 \rightarrow 2\text{CO}$  (R1.2). In real application when the finite reaction rate occurs, reaction (R1.2) may not be quick enough to consume all the CO<sub>2</sub>. The unreacted carbon at the exit suggests that less coal be fed into the gasifier in coal powder application, and recycling of charcoal is important for coal-powder-fed operation. Moreover, in the slurry-fed operation (Case 1), the conversion of H<sub>2</sub>O to H<sub>2</sub> is 100% efficient (1.07 kmoles of H<sub>2</sub>O to 1.07 kmoles of H<sub>2</sub>). The oxygen in H<sub>2</sub>O becomes CO<sub>2</sub>, and this reduces the fuel conversion efficiency.

### 4.3 Effects of Wall Cooling (Case 3)

Wall temperature control by employing wall cooling is very important for any gasifier that operates with a slagging mode. Although this study does not simulate slagging, wall cooling is simulated as Case 3 to provide qualitative information of wall cooling's effect on the gasification process. Case 3 is an oxygen-blown, dry feed gasifier with the wall temperature of the combustor and the reductor set to 1800 K and 1600 K, respectively, and assuming the wall is cooled by water-cooled tubes or any other cooling means. The mass-weighted average gas temperature and gas compositions at different heights are plotted in Figure 4.8.

As expected, the overall gas temperature is lower than Case 2 due to the wall cooling. The exit gas temperature drops from 2077 K to 1853 K when compared to Case 2, which has a temperature drop of approximately 220 K. The constant wall temperature did not have a big effect on the gas flow and the reaction. The overall species distribution is very similar to the result in Case 2. The cool wall temperature only affects the region very near the wall. The gas far from the wall does not experience any effect from the cooled wall.

The carbon fuel conversion efficiency and the fuel conversion efficiency for Case 3 are the same as in Case 2, i.e. 74% and 91%, respectively. The heating value in Case 3 is roughly the same as in Case 1, i.e. 10.0 MJ/kg. Table 4.2 shows very small decreases of CO and H<sub>2</sub> mole numbers at the exit for Case 3 compared to Case 2. The effect of wall cooling insignificantly affects the gas composition in this study.

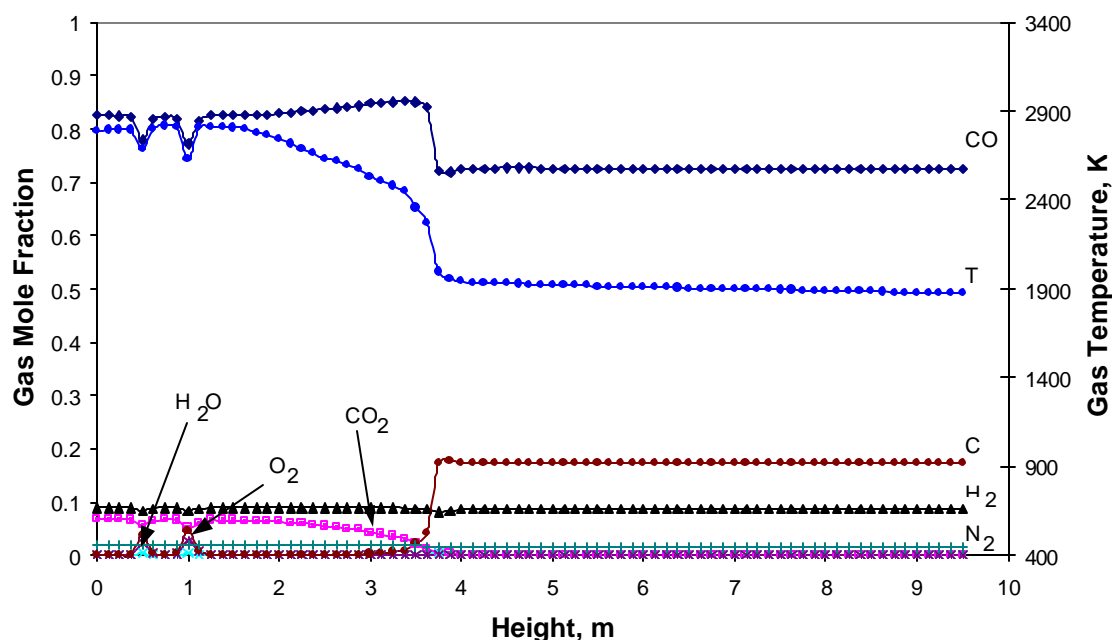


Figure 4.8 Mass-weighted average gas temperature and mole fraction along the gasifier height for oxygen-blown gasifier with coal powder fuel and wall cooling (Case 3).

#### 4.4 Effects of Coal Distribution (Cases 4 and 8)

The coal in the baseline case was distributed such that 75% was injected in the first stage, and 25% was injected in the second stage. A simulation under conditions specified as Case 4 in Table 4.1 was performed to investigate the effects of coal distribution. In Case 4, 50% of the coal slurry was injected into the first stage; the other 50% was injected into the second stage. Figure 4.9 illustrates a very high percentage of  $\text{CO}_2$  and a low percentage of  $\text{CO}$  in the combustor region. As the gas flows up into the second stage and the remaining coal slurry is injected, some of the  $\text{CO}_2$  reacts with the carbon to produce  $\text{CO}$ . This is indicated by a significant decrease in the  $\text{CO}_2$  fraction and an increase in the  $\text{CO}$  fraction. The  $\text{H}_2$  fraction also increases slightly in the reductor.

The CO<sub>2</sub> mole number in the exit gas is much higher than in the baseline case, i.e. 0.55 kmoles compared to 0.29 kmoles, which is not a good sign. Even though the CO<sub>2</sub> mole number significantly reduces after the coal injection at the second stage, the final CO<sub>2</sub> content is about twice as much as the 75%-25% coal distribution case. Using less coal in stage 1 seems to deprive the opportunity for CO<sub>2</sub> to find coal and undertake the gasification process (R1.2) at high temperatures, as can be seen by the slow increase of CO in Figure 4.9. The subsequent gasification in stage 2 with 50% more fresh coal does not provide effective gasification as in stage 1. The overall production of CO is less efficient than in the baseline simulation; however, the H<sub>2</sub> production is slightly higher. The final product of the CO + H<sub>2</sub> is 0.27 kmoles less (or 11% reduction) than Case 1 with 0.37 kmoles reduction of CO and a slight increase of H<sub>2</sub> from 1.07 kmoles to 1.17 kmoles. The carbon fuel conversion efficiency in Case 4 is 65%, and the fuel conversion efficiency is 67%.

Since comparison of Case 1 and Case 2 indicates that injecting plenty of coal into stage 1 can provide better opportunity for the gasification process, a one-stage gasification was simulated in Case 8 by setting 100% of the coal slurry and oxygen injected into the first stage. The mass-weighted gas temperature and composition averages are shown in Figure 4.10. In Figure 4.10, the gas temperature and composition are pretty much uniform inside the vessel. This low gas temperature at about 750 K and the uniform composition suggest that all the reactions R1.1 to R1.5 occur as soon as the coal slurry and the oxygen are injected into the gasifier.

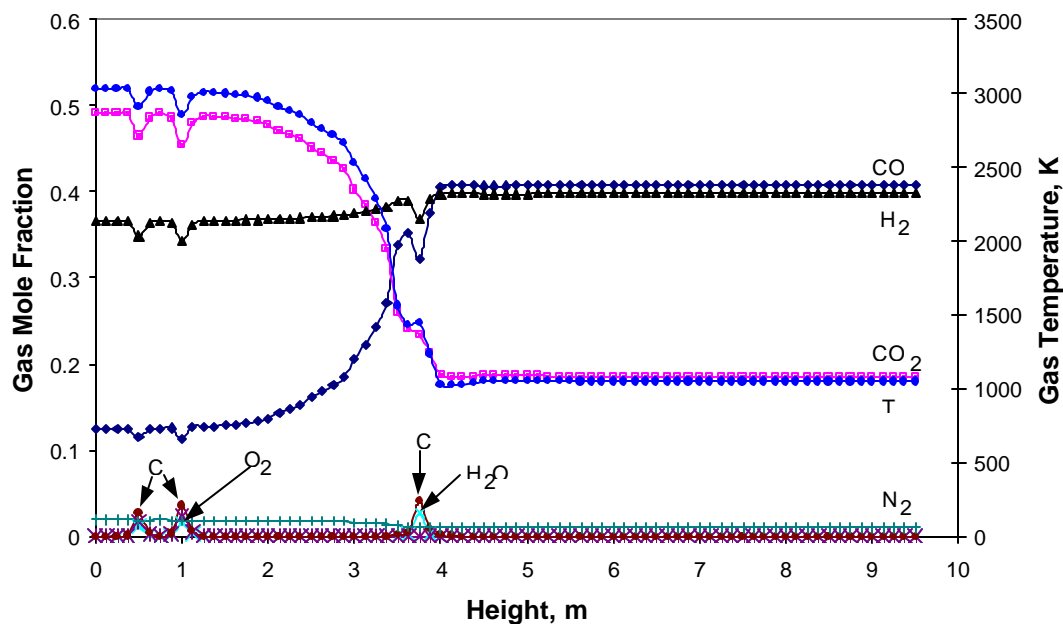


Figure 4.9 Mass-weighted average gas temperature and mole fraction along the gasifier height for Case 4 with 50-50 equal coal distribution between two stages (Case 4).

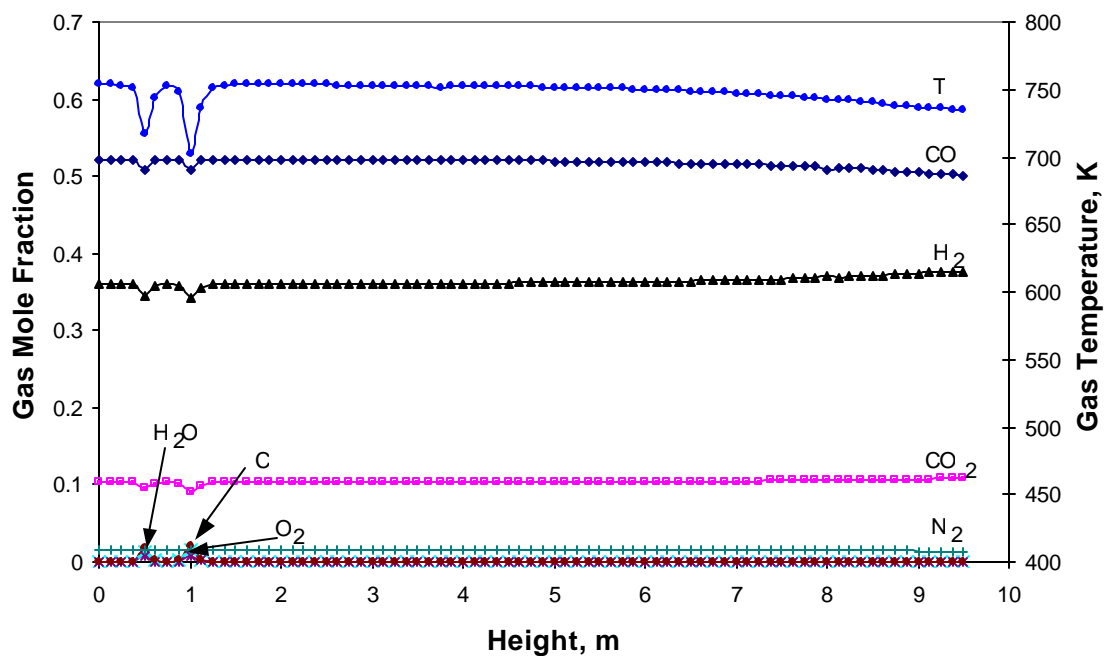


Figure 4.10 Mass-weighted average gas temperature and mole fraction along the gasifier height for gasifier with one-stage coal injection (Case 8).

As Table 4.2 indicates, the temperature and composition of the exit gas in the one-stage case are quite similar to the two-stage baseline case, although the carbon fuel conversion efficiency reduces to 82% or 4 percentage points lower than in the two-stage case. The fuel conversion efficiency is 76% or 3 percentage points lower than the two-stage case. This indicates that the two-stage design allows more flexibility for adjusting the operating parameters to achieve better carbon fuel conversion efficiency than the one-stage design. However, the one-stage gasifier requires less capital cost and offers a simpler control and operation.

#### **4.5 Effects of Oxidant (Air-blown, Case 5)**

Gasifiers can be operated as oxygen-blown or air-blown. An air-blown gasifier has the advantage of not needing an Air Separation Unit (ASU) to supply the oxygen. ASU is an intensive energy consumption device that reduces overall plant efficiency. Case 5 simulates a gasifier operating as an air-blown gasifier. The oxidant is air with composition of 21% O<sub>2</sub> and 79% N<sub>2</sub> by weight. Similar to previous cases, the overall mole ratio of O<sub>2</sub>:C is 0.3 with the total mass flow rate at the inlets of 60 kg/s. Figure 4.11 illustrates the mass-weighted-average gas temperature and gas composition for Case 5. As expected, the temperature in the combustor is lower than that of the oxygen-blown (Case 1) due to the abundance of N<sub>2</sub> to absorb and the energy released by the reactions.

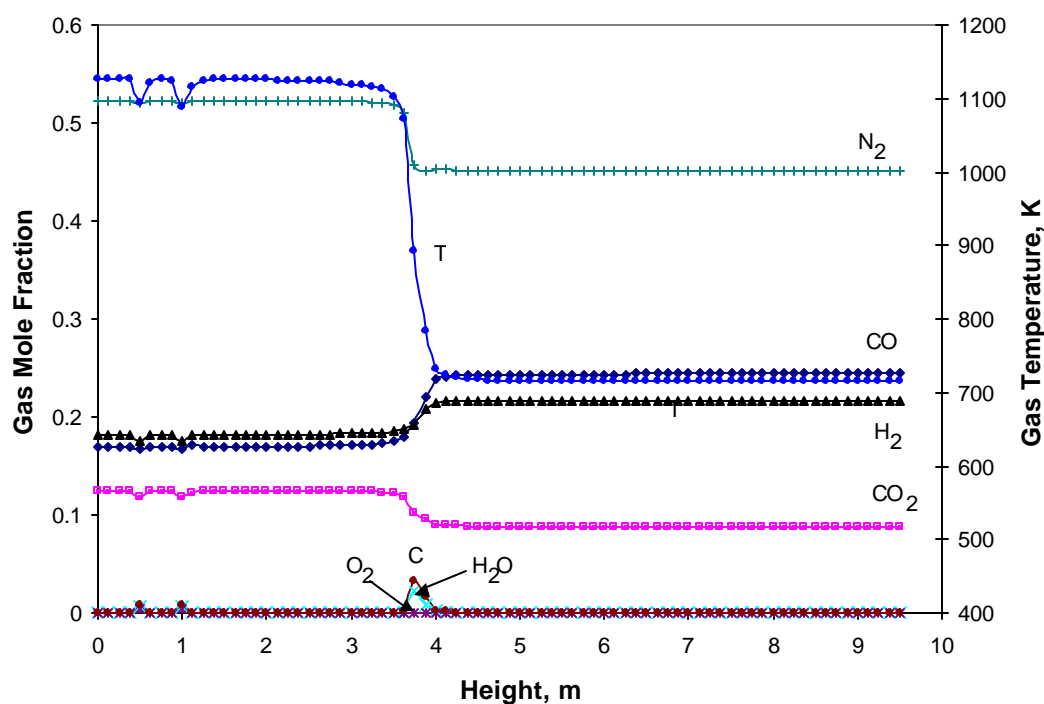


Figure 4.11 Mass-weighted average gas temperature and mole fraction along the gasifier height for air-blown gasifier (Case 5).

The overall CO concentration distribution is qualitatively similar to the oxygen-blown -- a fairly high concentration at the combustor stage followed by a slight increase in the reductor zone. The exit gas of the air-blown gasifier has a higher mole number of CO<sub>2</sub> and a lower mole number of CO than the oxygen-blown gasifier. As shown in Table 4.2, the carbon fuel conversion efficiency of the oxygen-blown gasifier (Case 1) is 86%, which is 38 percentage points higher than the air-blown 48% (Case 5). The fuel conversion efficiency of the air-blown gasifier is 46% compared to 79% of the oxygen-blown case. Speculation leads to the lower temperature in Case 5 favoring the watershift process (R1.5) and deterring the endothermic gasification reaction (R1.3), so CO is further converted to CO<sub>2</sub> and H<sub>2</sub>. This speculation is derived from examining the two CO<sub>2</sub>

producing process (R1.4 and R1.5). The conclusion is R1.4 is restricted by the limited  $O_2$  supply and only R1.5 can produce more  $CO_2$  without more  $O_2$ .

The syngas heating value in the air-blown gasifier is 5.3 MJ/kg and is the lowest among the cases discussed so far. Of course, this is expected due to the less carbon input, dilution by  $N_2$ , and the poor fuel conversion efficiency in air-blown gasifier compared to the oxygen-blown.

#### **4.6 Effects of Injector Angle (Cases 6 and 7)**

Flow structure is an important factor that affects carbon conversion efficiency. To investigate the effect of the injection direction on the gasification process, the injector angles of the first stage have been modified as shown in Figure 4.12. Figure 4.12(a) pictures the first stage portion of the gasifier where all eight injectors have been tilted  $30^\circ$  downward; Figure 4.12(b) shows the first stage portion of the gasifier with all eight injectors tilted  $30^\circ$  upward. Cases 6 and 7 ran using the inlet configurations illustrated in Figures 4.12 (a) and (b), respectively, with the same inlet conditions as in the horizontally positioned injectors case (Case 1).

Figure 4.13 shows the velocity vectors on the midplane in the combustor and diffuser regions and on the horizontal planes on the injector levels in Case 1. The velocity vectors on the horizontal planes show that the velocity in the center region of the combustor is very slow compared to the velocity in the region near the wall. This is due to the injectors' location being almost tangential. The plot on the vertical midplane shows that the vertical gas velocity in the combustor is very small. This may cause some of the gas to be trapped in the combustor and will never flow to the second stage and exit

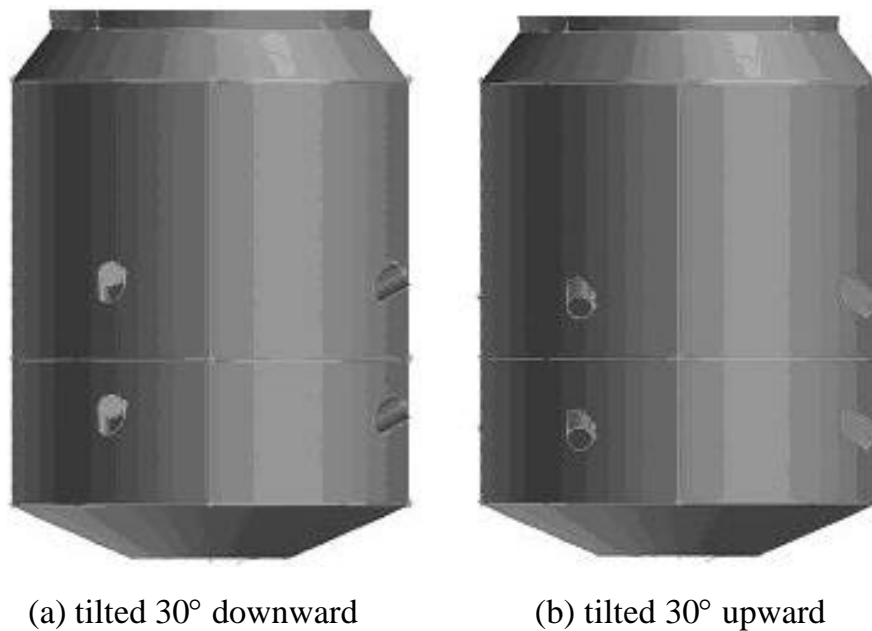


Figure 4.12 Lower injector configurations of (a) Case 6 and (b) Case 7.

the vessel. A strong upward flow near the wall and a slow downward flow in the center region are observed in the diffuser.

Figure 4.14 illustrates the velocity vectors on the gasifier midplane and on the horizontal planes on the injector levels in Case 6, where the first stage injectors are tilted 30 degrees downward. The downward flow from the first level downward injectors is observed in the lower bottom corners of the combustor on the vertical plane plot. The gas then turns upward when it hits the bottom wall. The gas from the second level downward injectors has turned upward before the gas reaches the vertical midplane because it is pushed upward by the flow from the first level injectors. A core of slow downward flow is observed in the center region of the combustor. The gas on the outside of the core flows up to the second stage.

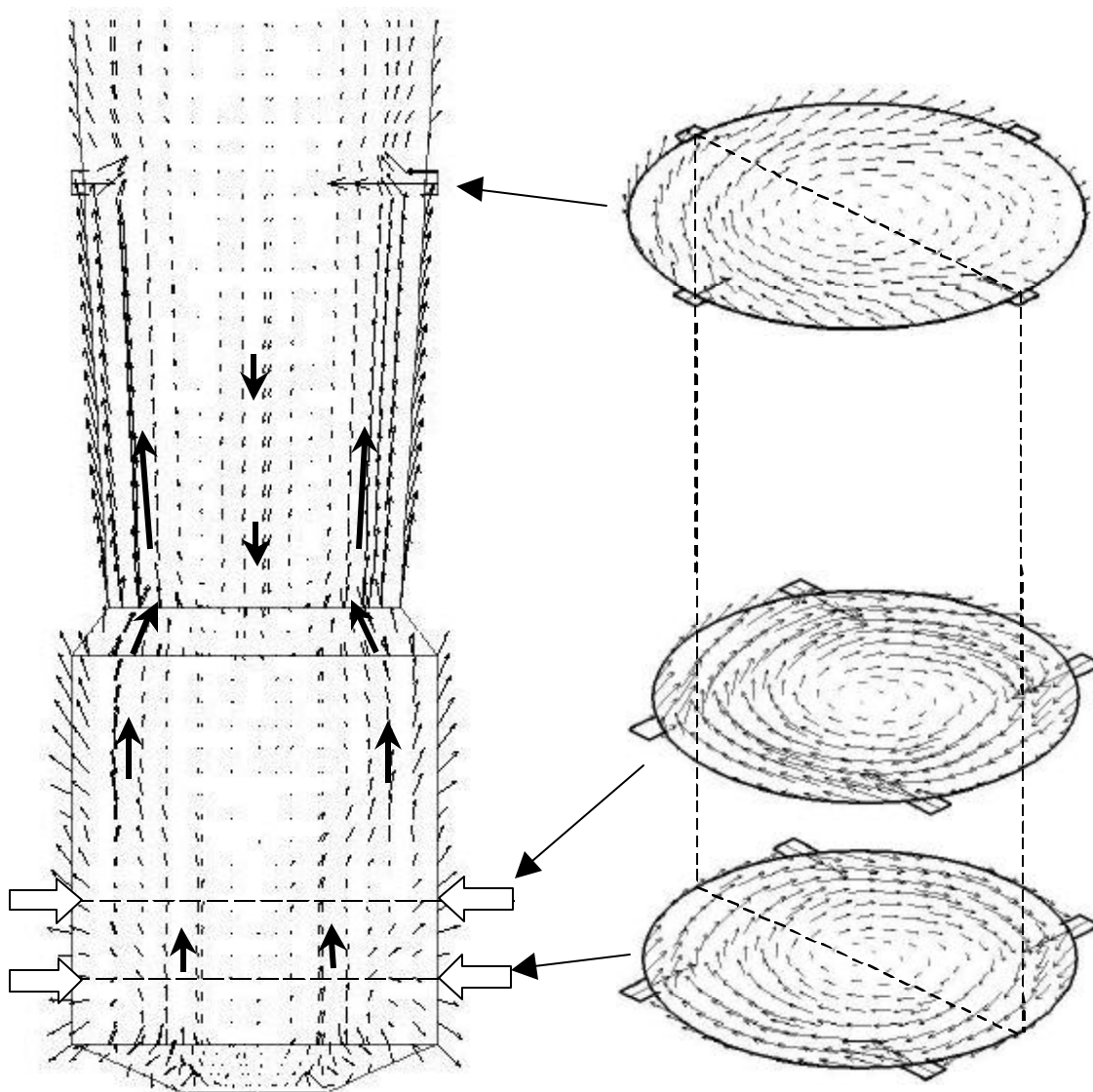


Figure 4.13 Velocity vectors on the center vertical plane for gasifier with the first stage injectors position horizontally (Case 1).

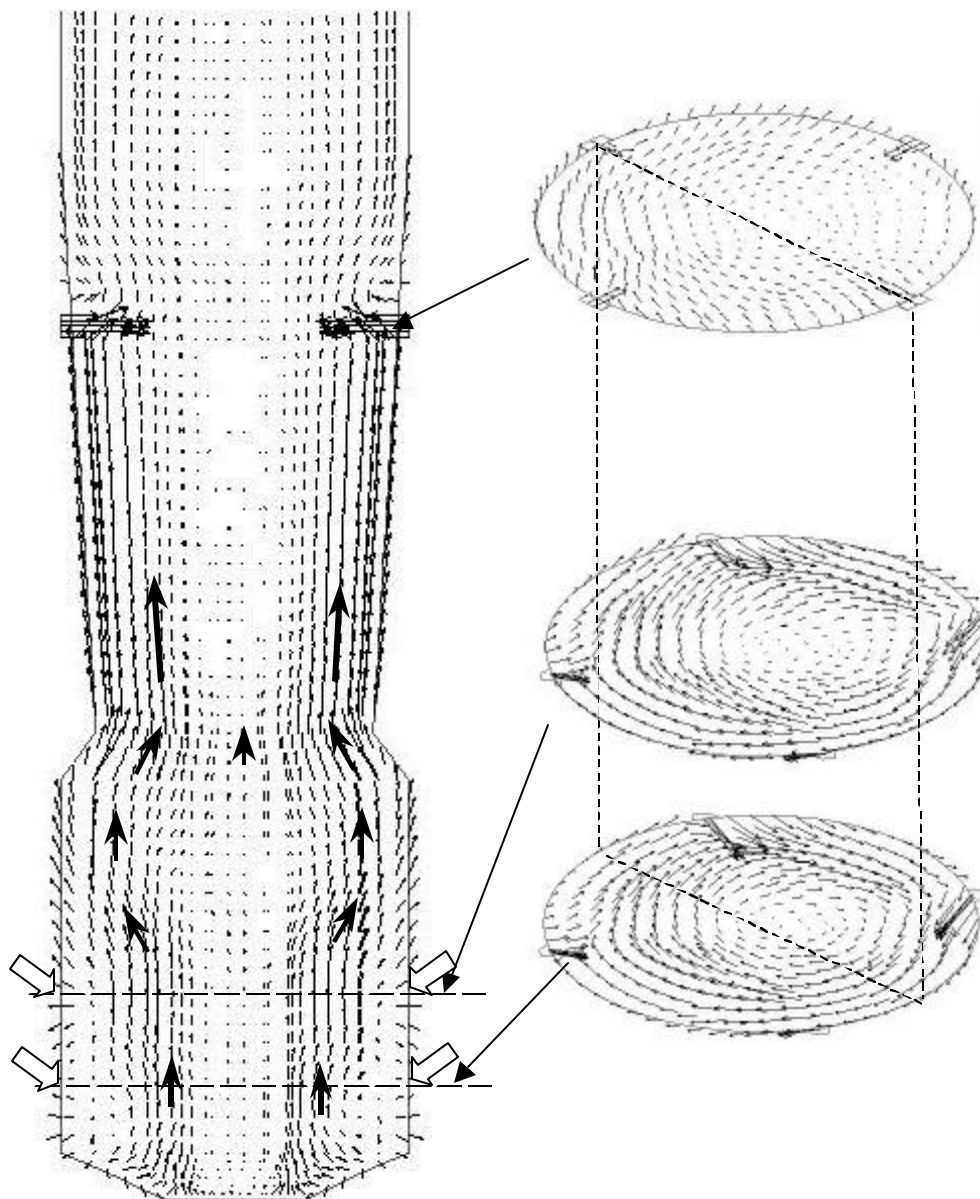


Figure 4.14 Velocity vectors on the center vertical plane for gasifier with the first stage injectors tilted  $30^\circ$  downward (Case 6).

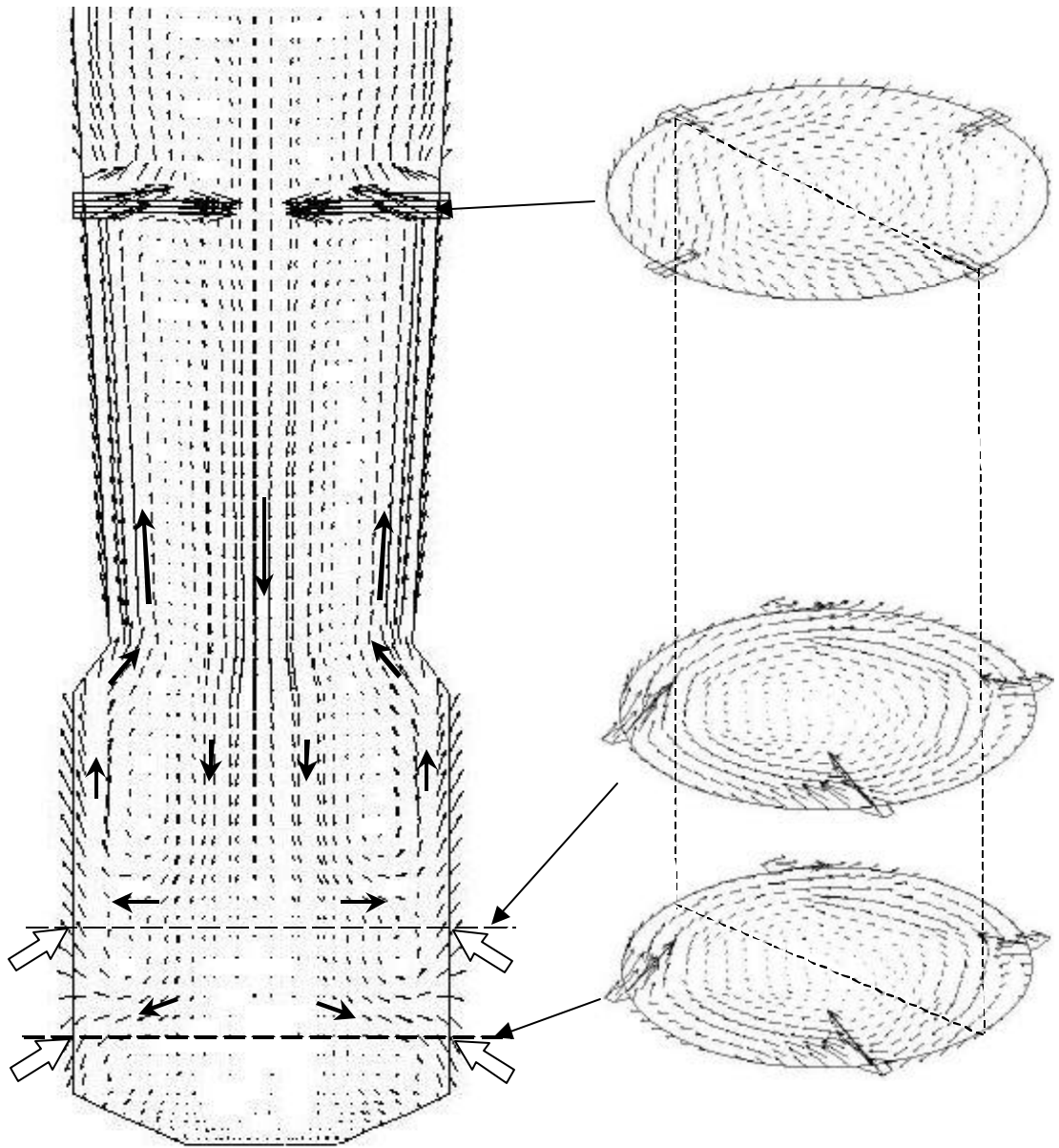


Figure 4.15 Velocity vectors on the center vertical plane for gasifier with the first stage injectors tilted 30° upward (Case 7).

The gas speeds up as it passes through the throat before entering the diffuser. In the diffuser, the gas with higher velocity exists near the wall and the gas with very low velocity in the center.

The velocity vectors for the gasifier with the first stage injectors are tilted 30 degrees upward (Case 7) are shown in Figure 4.15. A strong downward flow is observed in the center region of the diffuser. Flow with a very slow vertical velocity is seen at the bottom region of the combustor.

Figures 4.16 through 4.18 show the path line plots for Cases 1, 6, and 7. In Figure 4.16 the gas injected into the combustor through horizontal injectors does not flow quickly through the combustor and the reductor but flow around the combustor. The long circulation in the combustor increases the gas residence time, and some of the gas may be trapped in the combustor. On the other hand, the gas injected in the first stage through the 30-degree-upward injectors flows into the combustor quickly then flows from the combustor into the reductor as seen in Figure 4.18.

Illustrated in Figure 4.19 are the mass-weight gas temperature and composition averages for Case 6. A sudden jump of CO fraction right after the second stage injectors is observed. Similar to the previous cases, the jump is a result of the  $\text{CO}_2$  reaction with the char injected in the second stage to produce CO. This is suggested by the decrease of  $\text{CO}_2$  and the increase of CO. The carbon fuel conversion for Case 6 is 17 percentage points lower than in Case 1 (69% vs. 80%). It is interesting to observe that Case 6 produces more  $\text{H}_2$  than Case 1 (1.23 kmoles vs. 1.07 kmoles). The  $\text{H}_2/\text{CO}$  for Case 6 is higher than in Case 1, i.e. 0.98 compared to 0.68.

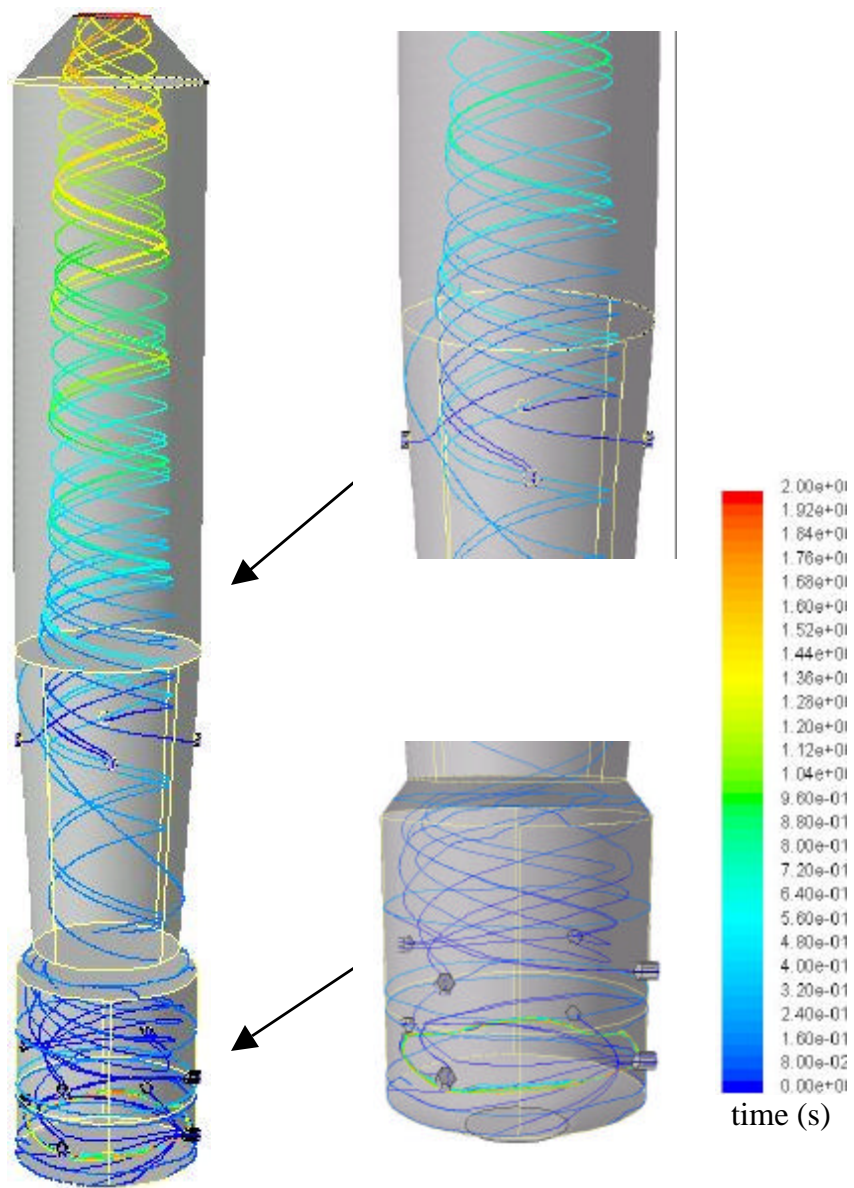


Figure 4.16 Flow path lines for gasifier with the first stage injectors horizontal (Case 1).

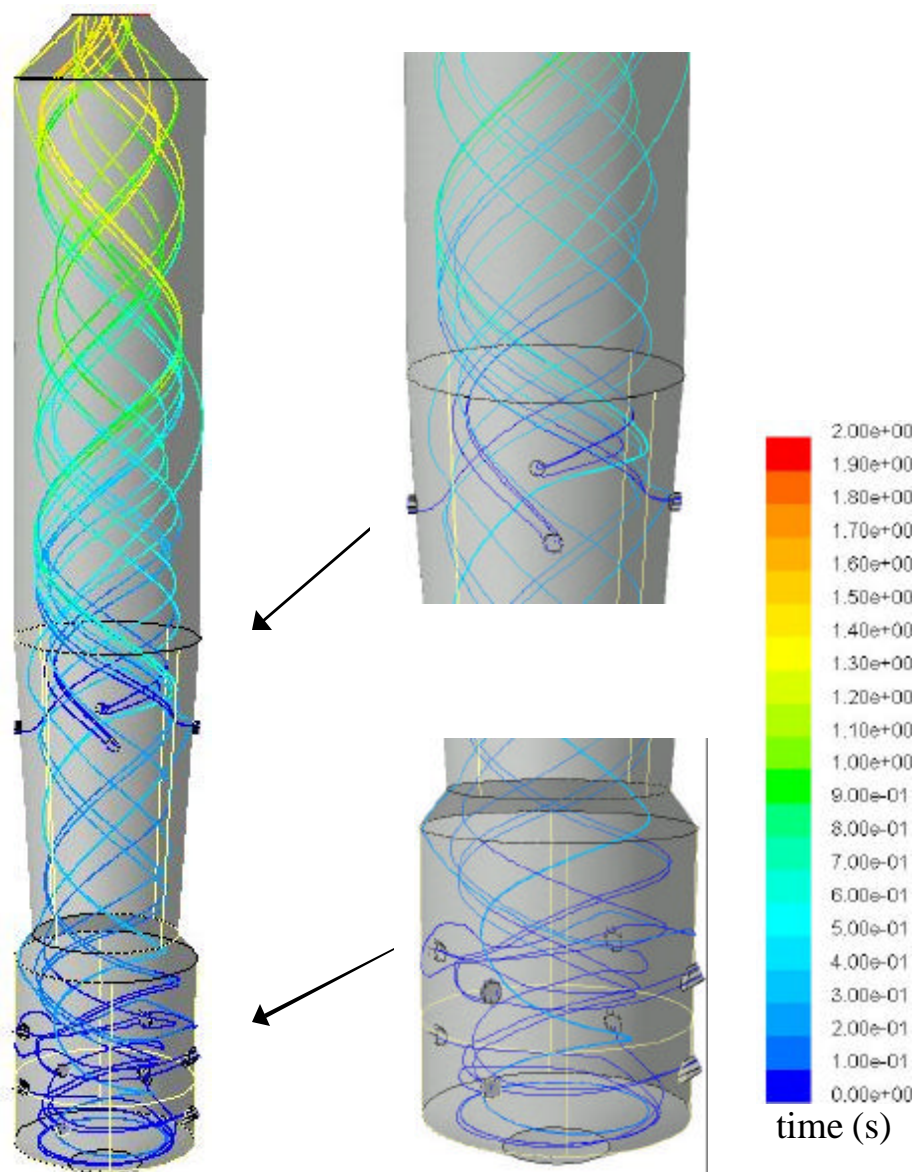


Figure 4.17 Flow path lines for gasifier with the first stage injectors tilted 30° downward (Case 6).

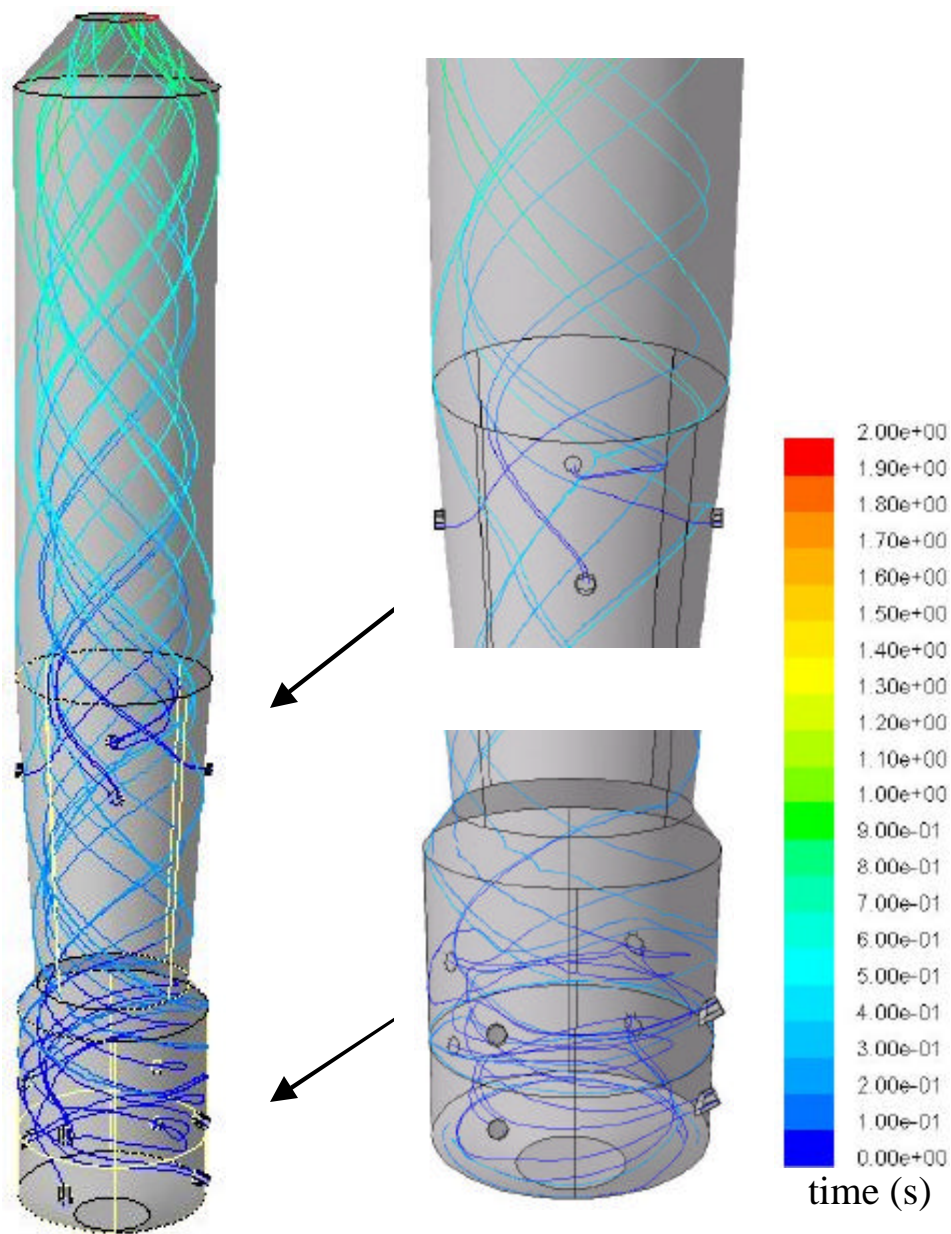


Figure 4.18 Flow path lines for gasifier with the first stage injectors tilted 30° upward (Case 7).

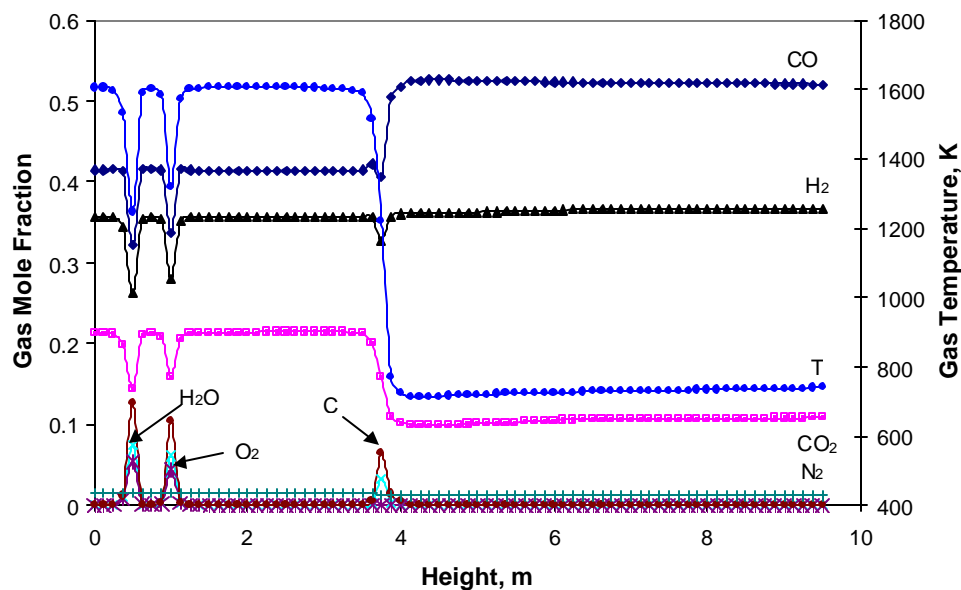


Figure 4.19 Mass-weighted average gas temperature and mole fraction along the gasifier height for gasifier with the first stage injectors tilted  $30^\circ$  downward (Case 6).

The gas temperature and composition for Case 7 is shown in Figure 4.20. The overall trend of the gas compositions is similar to Case 6. However, Case 7 produces more CO compared to Case 6. The carbon fuel conversion percentage for Case 7 is 79%, which is ten percentage points higher than in Case 6, and seven percentage points lower than in Case 1. In addition, at the later stage of stage 2, the  $\text{CO}_2$  and  $\text{H}_2$  increase while the CO,  $\text{H}_2\text{O}$ , and temperature decrease. This might suggest the occurrence of the watershift reaction. Comparison of Cases 1, 6, and 7 indicates that horizontal injections provide the best performance.

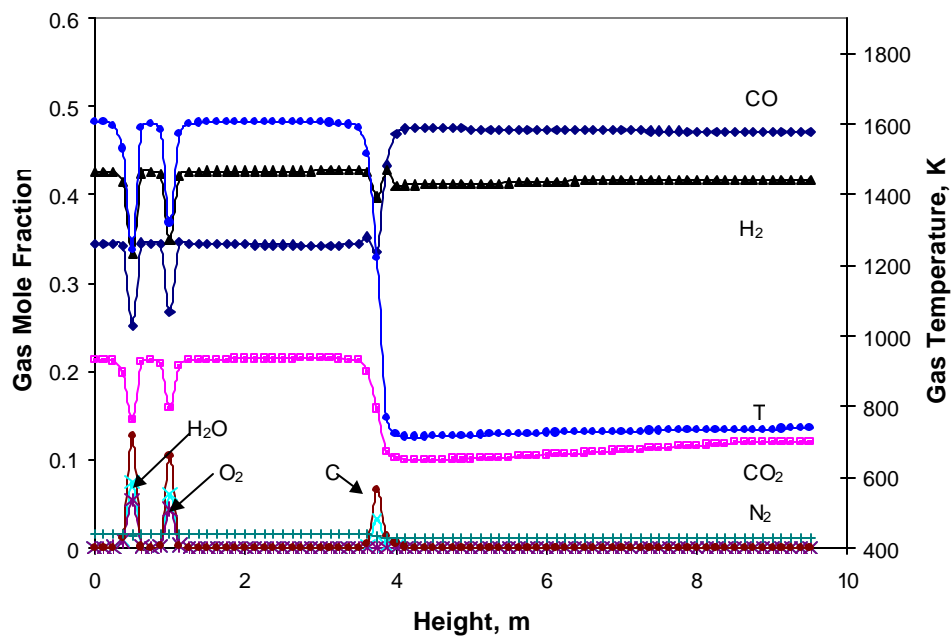


Figure 4.20 Mass-weighted average gas temperature and mole fraction along the gasifier height for gasifier with the first stage injectors tilted 30° upward (Case 7).

Table 3.1 Gas temperature and species fractions for three different grids.

	<i>Coarse Grid</i>	<i>Medium Grid</i>	<i>Fine Grid</i>
Exit gas temperature (K)	763	717	723
Mole fraction of CO	49.2%	53.0%	54.6%
Mole fraction of H <sub>2</sub>	33.5%	36.0%	34.9%
Mole fraction of CO <sub>2</sub>	16.1%	9.8%	9.3%
Mole fraction of H <sub>2</sub> O	0.0%	0.0%	0.0%
Mole fraction of N <sub>2</sub>	1.2%	1.2%	1.2%
Mole fraction of C	0.0%	0.0%	0.0%
Grid number	35,168	95,182	160,170
Convergence time (physical time)	4 hours	12 hours	17 hours

## CHAPTER FIVE

### CONCLUSIONS

In this study, the computational simulation of coal gasification and the thermal flow inside a two-stage entrained-flow gasifier has been conducted. The results show that the highest temperature, approximately 1600 K, for a two-stage gasifier with coal slurry feed occurs in stage 1 where the coal slurry is injected and reacts with O<sub>2</sub> through an incomplete combustion reaction leading to production of CO and with H<sub>2</sub>O through a gasification reaction to produce H<sub>2</sub>. A fraction of the CO reacts with O<sub>2</sub> and produces CO<sub>2</sub>. The conversion of coal to syngas is further boosted when the remaining coal is injected into the second stage. The mole fractions of CO and H<sub>2</sub> increase through the reactions  $C + CO_2 \rightarrow 2CO$  and  $C + H_2O \rightarrow CO + H_2$ , respectively. The carbon fuel conversion efficiency, which is defined as the percentage of total injected carbon that reacts to produce CO as the final product, is 86%. The term fuel conversion efficiency is defined as the ratio of the total mass of the useful syngas produced (H<sub>2</sub> and CO) to the total mass of the raw carbon, water, and oxygen injected into the process. The fuel conversion efficiency is 79%. The heating value of the syngas is 12.5 MJ/kg.

#### **Effects of Coal Mixture (Slurry vs. Powder)**

A coal powder feed produces more CO than coal slurry feed. However, the H<sub>2</sub> production of the gasifier with coal powder feed is only a quarter of the coal slurry feed

case (0.23 kmol/s vs. 1.01 kmol/s), due to the less amount of moisture in the coal powder feed. The carbon fuel conversion efficiency of the coal-power-fed gasifier (74%) is lower than the slurry-fed cases (86%), but the fuel conversion efficiency is higher in the powder-fed gasifier (91% vs. 79%). The syngas heating value is 10.1 MJ/kg, which is 20% less than the slurry-fed case.

### **Effects of Wall Cooling**

A gasifier with wall cooling is also studied. The results show that the overall gas temperature is lower than in the gasifier without wall cooling. However, the exit gas composition is only slightly different, suggesting that the wall cooling effect on the gas composition is insignificant.

### **Effects of Coal Distribution**

The study of coal distribution suggests that using less coal in stage 1 deprives the opportunity for  $\text{CO}_2$  to find the coal and undertake the gasification process ( $\text{C(s)} + \text{CO}_2 \rightarrow 2\text{CO}$ ) at high temperatures. The subsequent gasification in stage 2, which uses more coal, does not provide as effective gasification as in stage 1. Using less coal in stage 1 gives a less efficient overall production of CO, but a slightly higher  $\text{H}_2$  production. This indicates that the two-stage design allows more flexibility for adjusting the operating parameters and achieving better carbon conversion efficiency.

### **Effects of Oxidant**

As expected, due to the abundance of nitrogen, the overall temperature in the air-blown gasifier is lower than in the oxygen-blown. The syngas of the air-blown gasifier has a higher mole number of CO<sub>2</sub> and a lower mole number of CO than in the oxygen-blown gasifier. The fuel conversion of the air-blown gasifier (48%) is 38 percentage points lower than the oxygen-blown gasifier (86%). The fuel conversion efficiency of the air-blown gasifier is 46% compared to 79% of the oxygen-blown case. The syngas heating value in the air-blown operation is 5.3 MJ/kg, which is low due to less carbon input, dilution by N<sub>2</sub>, and poor fuel conversion efficiency. In a real application, the air-blown gasifier is easier to operate and requires approximately 30% less of capital and O&M costs by not using an air separation unit.

### **Effects of Injector Angle**

The injectors in the first stage have been modified to tilt 30 degrees downward and 30 degrees upward. The simulation results show that the carbon fuel conversion for the operation with 30 degrees upward injectors is 17 percentage points (79%) lower than the operation with horizontal injectors. The operation with the 30 degrees upward injections produces more H<sub>2</sub> than the operation with horizontal injectors (1.23 kmol vs. 1.07 kmol). The gas composition for the gasifier with injectors tilted 30 degrees upward does not vary much from the 30 degrees downward case. The carbon fuel conversion is 79%, which is 10 percentage points (14.5%) higher than the case with 30 degrees downward injection. The horizontal injection provides the best performance when comparison among the three different injection angle cases was made.

**Recommended Future Studies**

The following are the plan of future studies:

- a. Implement finite reaction rate for the reactions to obtain more accurate results.
- b. Add devolatilization model to simulate reaction of coal particles.
- c. Modify the injection angle of the second stage inlets to study its effects.

## REFERENCES

- Bockelie M.J, Denison K.K., Chen Z., Linjewile T., Senior C.L., Sarofim A.F., “CFD Modeling For Entrained Flow Gasifiers in Vision 21 Systems”, *Proceedings of the 19<sup>th</sup> Annual International Pittsburgh Coal Conference*, Pittsburgh, PA. Sept 24-26, 2002(a).
- Bockelie M.J, Denison K.K., Chen Z., Linjewile T., Senior C.L., Sarofim A.F., “CFD Modeling For Entrained Flow Gasifiers”, *Proceedings of the Gasification Technologies Conference 2002*, San Francisco, CA, Oct. 28-30, 2002(b).
- Chen, C.M., Miyoshi T., Kamiya H., Horio M., Kojima T., “On the Scaling-up of a Two-Stage Air Blown Entrained Flow Coal Gasifier”, *The Canadian Journal of Chemical Engineering*, **77**, 745-750, 1999.
- Chen C., Horio M., Kojima T., “Numerical Simulation of Entrained Flow Coal Gasifiers”, *Chemical Engineering Science*, **55**, 3861-3833, 2000.
- FLUENT 6.1 User’s Guide, February 2003.
- Patankar S.V., *Numerical Heat Transfer and Fluid Flow*, McGraw Hill, 1980.
- Smoot D.L., Smith P.J., *Coal Combustion and Gasification*, Plenum Press, 1985.
- Tomeczek J., *Coal Combustion*, Krieger Publishing Company, 1994.
- US Department of Energy/The Pinon Pine Power Project, Topical Report Number 8, December 1996.
- US Department of Energy/Tampa Electric Integrated Gasification Combine-Cycle Project, Topical Report Number 19, July 2000(a).
- US Department of Energy, “Gasification Markets and Technologies – Present and Future, July 2000(b).
- US Department of Energy/Wabash River Coal Gasification Repowering Project, Topical Report Number 20, September 2000(c).

## **APPENDICES**

## APPENDIX A

### Application of FLUENT Code

#### Step 1: Grid

1. Read the grid file

**File → Read → Case...**

After reading the grid file, **FLUENT** will report the number of fluid cells that have been read, along with numbers of boundary faces with different zone identifiers.

2. Check the grid

**Grid → Check**

The grid check lists the minimum and maximum x and y values from the grid, and reports on a number of other grid features that are checked. Any errors in the grid would be reported at this time.

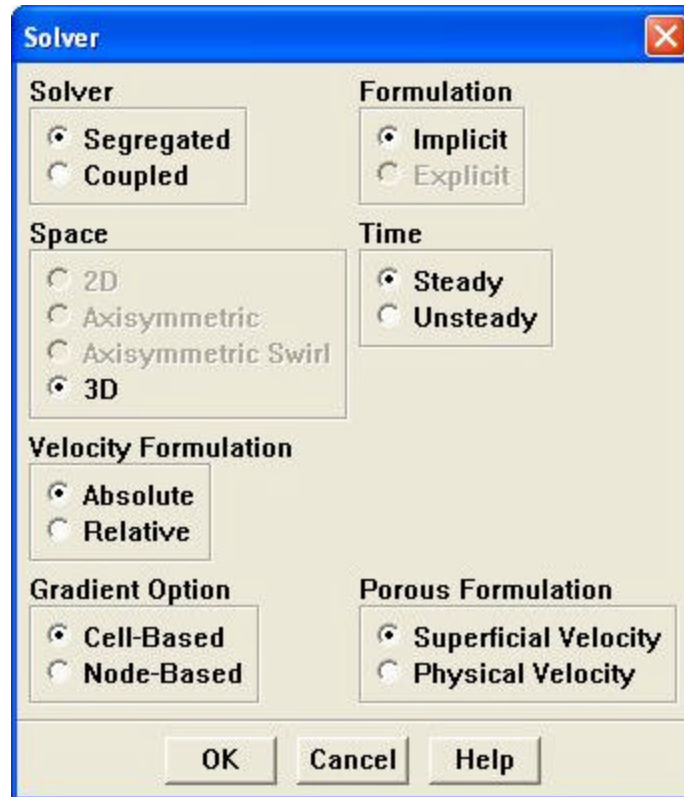
3. Display the grid.

**Display → Grid...**

**Step 2: Model**

1. Define the domain space as 3D, and choose segregated solver.

**Define → Models → Solver...**



2. Enable the  $k$ - $\epsilon$  turbulence model.

Define → Models → Viscous...

**Viscous Model**

**Model**

- Inviscid
- Laminar
- Spalart-Allmaras (1 eqn)
- $k$ - $\epsilon$  (2 eqn)
- $k$ - $\omega$  (2 eqn)
- Reynolds Stress (7 eqn)
- Large Eddy Simulation

**$k$ - $\epsilon$  Model**

- Standard
- RNG
- Realizable

**Near-Wall Treatment**

- Standard Wall Functions
- Non-Equilibrium Wall Functions
- Enhanced Wall Treatment

**Options**

- Viscous Heating
- Full Buoyancy Effects

**Model Constants**

Cmu: 0.09

C1-Epsilon: 1.44

C2-Epsilon: 1.92

TKE Prandtl Number: 1

**User-Defined Functions**

Turbulent Viscosity: none

**Prandtl Numbers**

TKE Prandtl Number: none

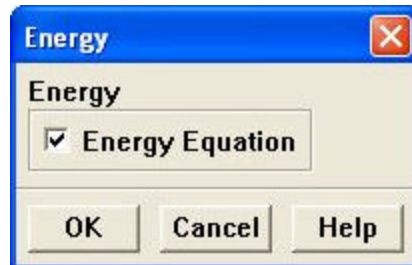
TDR Prandtl Number: none

Energy Prandtl Number: none

OK Cancel Help

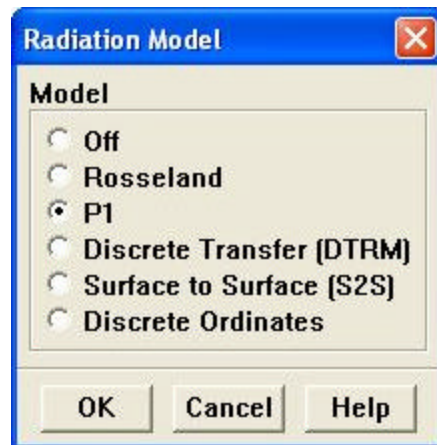
3. Enable heat transfer by activating the energy equation.

**Define** → **Models** → **Energy...**



4. Enable Radiation

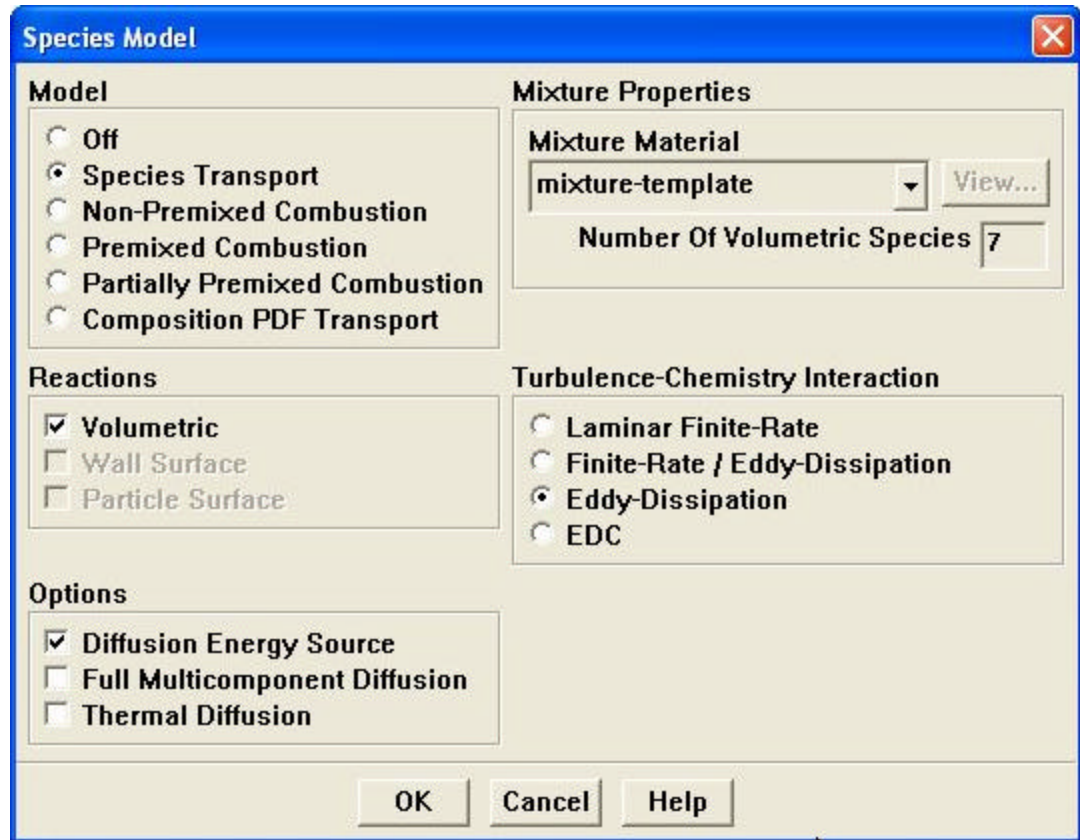
**Define** → **Models** → **Radiation...**



- a) Select P1 model as radiation model

5. Enable chemical species transport and reaction.

**Define** → **Models** → **Species...**



- (a) Select **Species Transport** under **Model**.
- (b) Select **Volumetric** under **Reactions**.
- (c) Select **Eddy-Dissipation** under **Turbulence-Chemistry Interaction**.

The eddy-dissipation model computes the rate of reaction under the assumption that chemical kinetics are fast compared to the rate at which reactants are mixed by turbulent fluctuations (eddies).

- (d) Click **OK**.

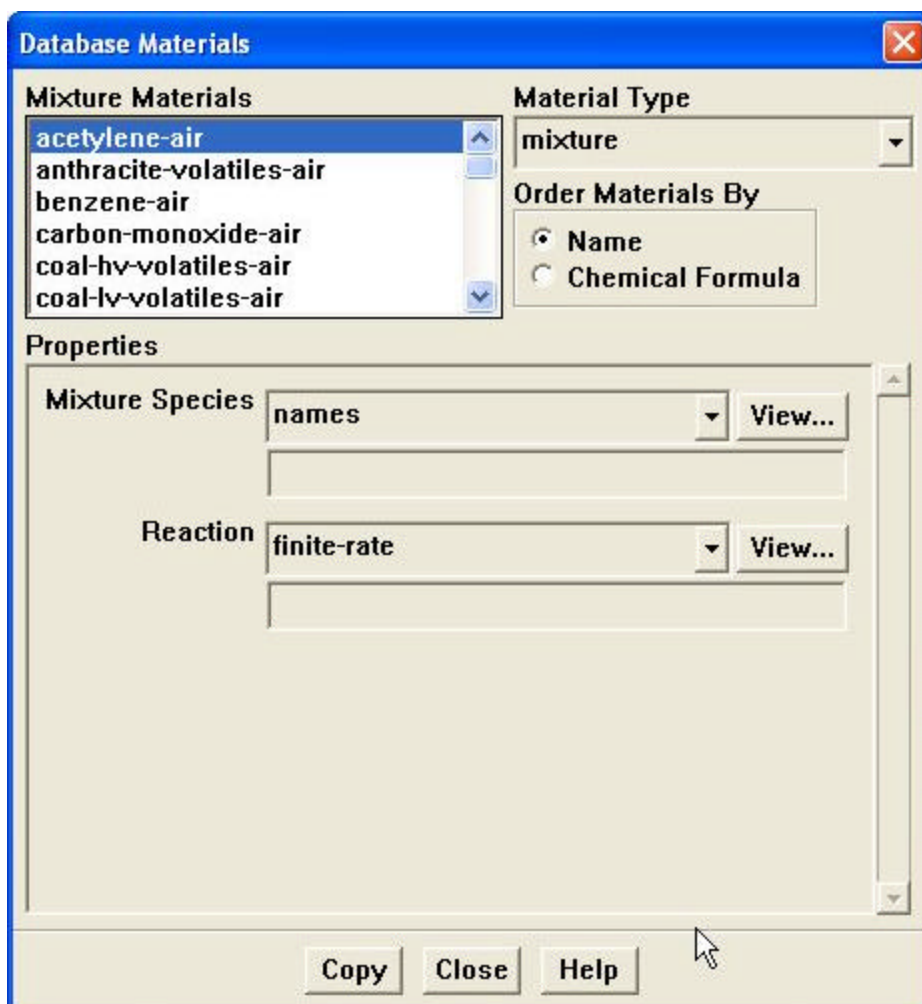
### Step 3: Materials

Define → Materials...

The screenshot shows the 'Materials' dialog box with the following configuration:

- Name:** mixture-template
- Material Type:** mixture
- Chemical Formula:** (empty)
- Mixture Materials:** mixture-template
- Mixture:** none
- Order Materials By:** Name (selected), Chemical Formula (unselected)
- Database...:** (button)
- Properties:**
  - Mixture Species:** names (dropdown), Edit... (button)
  - Reaction:** eddy-dissipation (dropdown), Edit... (button)
  - Mechanism:** reaction-mechs (dropdown), Edit... (button)
  - Density (kg/m3):** incompressible-ideal-gas (dropdown), Edit... (button)
- Buttons:** Change/Create, Delete, Close, Help

- The mixture **mixture-template** already consists of species oxygen (O<sub>2</sub>), water (H<sub>2</sub>O), and nitrogen (N<sub>2</sub>). The other species needed for the simulation but are not included in the mixture yet need to be added to the mixture. Copy the fluid materials from the database to the mixture.
  - Click the **Database...** button and the **Material Database** panel will open.



- (b) In the **Material Type** drop-down list, select **fluid**.
- (c) Select **carbon-dioxide (CO<sub>2</sub>)** under **Fluid Materials** and click **Copy**.
- (d) Repeat step (c) to copy **carbon-monoxide (CO)**, **carbon-solid (C<s>)**, and **hydrogen (H<sub>2</sub>)**.

**Database Materials**

**Fluid Materials**

- calcium-oxide [cao]
- calcium-sulfate [caso4]
- calcium-sulfide [cas]
- carbon-dioxide [co2]**
- carbon-disulfide-vapor [cs2]
- carbon-monoxide [co]

**Material Type**  
fluid

**Order Materials By**

Name  
 Chemical Formula

**Properties**

Density (kg/m<sup>3</sup>) constant View...  
1.7878

Cp (j/kg-k) constant View...  
840.37

Thermal Conductivity (w/m-k) constant View...  
0.0145

Viscosity (kg/m-s) constant View...  
1.37e-05

Copy Close Help

**Materials**

Name: carbon-monoxide

Material Type: fluid

Order Materials By:  Name  Chemical Formula

Chemical Formula: co

Fluid Materials: carbon-monoxide [co] Database...

Mixture: mixture-template

**Properties**

Cp (j/kg-k) piecewise-polynomial Edit...  
[ ]

Molecular Weight (kg/kgmol) constant Edit...  
28.01055

Standard State Enthalpy (j/kgmol) constant Edit...  
-1.105396e+08

Standard State Entropy (j/kgmol-k) constant Edit...  
197531.6

Change/Create Delete Close Help

**Materials**

Name: carbon-solid

Material Type: fluid

Order Materials By:  Name  Chemical Formula

Chemical Formula: c<s>

Fluid Materials: carbon-solid (c<s>)

Mixture: mixture-template

Database...

**Properties**

Cp (j/kg-k): piecewise-polynomial

Molecular Weight (kg/kgmol): constant   
12.01115

Standard State Enthalpy (j/kgmol): constant   
-101.268

Standard State Entropy (j/kgmol-k): constant   
5731.747

**Materials**

Name: hydrogen

Material Type: fluid

Order Materials By:  Name  Chemical Formula

Chemical Formula: h2

Fluid Materials: hydrogen (h2)

Mixture: mixture-template

Database...

**Properties**

Cp (j/kg-k): piecewise-polynomial

Molecular Weight (kg/kgmol): constant   
2.01594

Standard State Enthalpy (j/kgmol): constant   
0

Standard State Entropy (j/kgmol-k): constant   
130579.1

**Materials**

Name	nitrogen	Material Type	fluid	Order Materials By	<input checked="" type="radio"/> Name <input type="radio"/> Chemical Formula
Chemical Formula	n2	Fluid Materials	nitrogen [n2]	Database...	
		Mixture	mixture-template		

**Properties**

Cp (j/kg-k)	piecewise-polynomial	Edit...
Molecular Weight (kg/kgmol)	constant	Edit...
	28.0134	
Standard State Enthalpy (j/kgmol)	constant	Edit...
	0	
Standard State Entropy (j/kgmol-k)	constant	Edit...
	191494.8	

Change/Create Delete Close Help

**Materials**

Name	oxygen	Material Type	fluid	Order Materials By	<input checked="" type="radio"/> Name <input type="radio"/> Chemical Formula
Chemical Formula	o2	Fluid Materials	oxygen [o2]	Database...	
		Mixture	mixture-template		

**Properties**

Cp (j/kg-k)	piecewise-polynomial	Edit...
Molecular Weight (kg/kgmol)	constant	Edit...
	31.9988	
Standard State Enthalpy (j/kgmol)	constant	Edit...
	0	
Standard State Entropy (j/kgmol-k)	constant	Edit...
	205026.9	

Change/Create Delete Close Help

**Materials**

Name: water-vapor

Material Type: fluid

Order Materials By:  Name  Chemical Formula

Chemical Formula: h2o

Fluid Materials: water-vapor (h2o)

Mixture: mixture-template

Database...

**Properties**

Cp (j/kg-k): piecewise-polynomial [Edit...]

Molecular Weight (kg/kgmol): constant [Edit...]  
18.01534

Standard State Enthalpy (j/kgmol): constant [Edit...]  
-2.418379e+08

Standard State Entropy (j/kgmol-k): constant [Edit...]  
188696.4

Change/Create Delete Close Help

2. Enable temperature dependence of the specific heat for each species.

**Materials**

Name: carbon-dioxide

Material Type: fluid

Order Materials By:  Name  Chemical Formula

Chemical Formula: co2

Fluid Materials: carbon-dioxide [co2]

Database...

Mixture: mixture-template

**Properties**

Density (kg/m<sup>3</sup>): constant (Edit...)  
1.7878

Cp (j/kg-k): piecewise-polynomial (Edit...)

Molecular Weight (kg/kgmol): constant (Edit...)  
44.00995

Standard State Enthalpy (j/kgmol): constant (Edit...)  
-3.935324e+08

Change/Create Delete Close Help

(a) In the **Material Type** drop-down list, select **fluid**.

The **fluid** material type gives you access to each species in the mixture.

(b) Select **carbon-dioxide (CO<sub>2</sub>)** under **Fluid Materials**.

(c) In the drop-down list for **Cp**, select **piecewise-polynomial**.

This will open the **Piecewise Polynomial Profile** panel.

**Piecewise Polynomial Profile**

Define: Cp      In Terms Of: Temperature      Ranges: 2

Range: 1      Minimum: 300      Maximum: 1000      Coefficients: 5

Coefficients			
1	429.9289	2	1.874473
3	-0.001966485	4	1.297251e-06
5	-3.999956e-10	6	
7		8	

OK      Cancel      Help

(d)

- Click on OK to accept the coefficients describing the polynomial temperature variation of  $C_p$  for carbon dioxide.
- Click on **Change/Create** in the **Materials** panel to accept the change in the properties for carbon dioxide,  $\text{CO}_2$ .

3. Repeat steps (b), (c) and (d) above for the remaining species and click on **Change/Create** to accept change for each species.
4. In the **Material Type** drop-down list, select **fluid**.
5. Choose **incompressible-ideal-gas** in the **Density** drop-down list.

The Materials dialog box is shown with the following settings:

- Name: mixture-template
- Material Type: mixture
- Order Materials By: Name (selected), Chemical Formula
- Chemical Formula: (empty)
- Mixture Materials: mixture-template
- Database...: (button)
- Mixture: none
- Properties:
  - Reaction: eddy-dissipation
  - Mechanism: reaction-mechs
  - Density (kg/m<sup>3</sup>): incompressible-ideal-gas
  - Cp (j/kg-k): mixing-law

Buttons at the bottom: Change/Create, Delete, Close, Help.

6. Enable composition dependence of the specific heat.

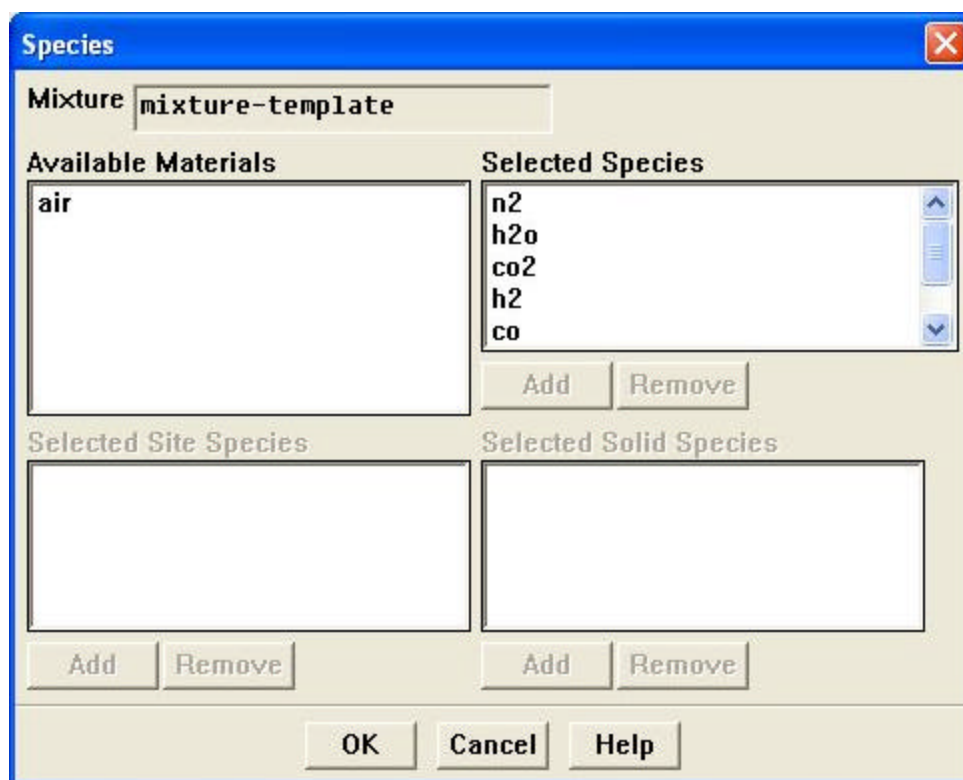
**Define** → **Materials...**

The Materials dialog box is shown with the following settings:

- Name: mixture-template
- Material Type: mixture
- Order Materials By: Name (selected), Chemical Formula
- Chemical Formula: (empty)
- Mixture Materials: mixture-template
- Database...: (button)
- Mixture: none
- Properties:
  - Reaction: eddy-dissipation
  - Mechanism: reaction-mechs
  - Density (kg/m<sup>3</sup>): incompressible-ideal-gas
  - Cp (j/kg-k): mixing-law

Buttons at the bottom: Change/Create, Delete, Close, Help.

- (a) In the drop-down list next to **Cp**, select **mixing-law** as the specific heat method.
- (b) Click on the **Change/Create** button to render the mixture specific heat based on a local mass-fraction-weighted average of all the species.
7. Add the species to the mixture.
- (a) Click the **Edit...** button next to the right of the **Mixture Species**. The **Species** panel will open.



- (b) Add the species from the **Available Materials** to the **Selected Materials**.
- (c) Click **OK**.
8. Set the reaction equations.
- (a) In the **Material Panel**, click the **Edit...** button next to the right of the **Reaction**.  
The **Reactions** window will open.

Reactions ✕

Mixture  Total Number of Reactions

Reaction Name  ID  Reaction Type  
 Volumetric  Wall Surface  Particle Surface

Number of Reactants  Number of Products

Species	Stoich. Coefficient	Rate Exponent
<input type="text" value="c&lt;s&gt;"/>	<input type="text" value="1"/>	<input type="text" value="1"/>
<input type="text" value="o2"/>	<input type="text" value="0.5"/>	<input type="text" value="0.5"/>

Species	Stoich. Coefficient	Rate Exponent
<input type="text" value="co"/>	<input type="text" value="1"/>	<input type="text" value="0"/>

Arrhenius Rate

Pre-exponential Factor

Activation Energy (J/kgmol)

Temperature Exponent

Include Backward Reaction

Third Body Efficiencies

Pressure Dependent Reaction

Mixing Rate

A  B

Reactions

Mixture  Total Number of Reactions

Reaction Name  ID  Reaction Type  Volumetric  Wall Surface  Particle Surface

Number of Reactants  Number of Products

Species	Stoich. Coefficient	Rate Exponent
<input type="text" value="c&lt;s&gt;"/>	<input type="text" value="1"/>	<input type="text" value="1"/>
<input type="text" value="co2"/>	<input type="text" value="1"/>	<input type="text" value="1"/>

Species	Stoich. Coefficient	Rate Exponent
<input type="text" value="co"/>	<input type="text" value="2"/>	<input type="text" value="0"/>

Arrhenius Rate

Pre-exponential Factor

Activation Energy (j/kgmol)

Temperature Exponent

Include Backward Reaction

Third Body Efficiencies

Pressure Dependent Reaction

Mixing Rate

A  B

Reactions

Mixture  Total Number of Reactions

Reaction Name  ID  Reaction Type  Volumetric  Wall Surface  Particle Surface

Number of Reactants  Number of Products

Species	Stoich. Coefficient	Rate Exponent
<input type="text" value="c&lt;s&gt;"/>	<input type="text" value="1"/>	<input type="text" value="1"/>
<input type="text" value="h2o"/>	<input type="text" value="1"/>	<input type="text" value="1"/>

Species	Stoich. Coefficient	Rate Exponent
<input type="text" value="co"/>	<input type="text" value="1"/>	<input type="text" value="0"/>
<input type="text" value="h2"/>	<input type="text" value="1"/>	<input type="text" value="0"/>

Arrhenius Rate

Pre-exponential Factor

Activation Energy (j/kgmol)

Temperature Exponent

Include Backward Reaction

Third Body Efficiencies

Pressure Dependent Reaction

Mixing Rate

A  B

Reactions

Mixture  Total Number of Reactions

Reaction Name  ID  Reaction Type  Volumetric  Wall Surface  Particle Surface

Number of Reactants  Number of Products

Species	Stoich. Coefficient	Rate Exponent
<input type="text" value="co"/>	<input type="text" value="1"/>	<input type="text" value="1"/>
<input type="text" value="o2"/>	<input type="text" value="0.5"/>	<input type="text" value="0.5"/>

Species	Stoich. Coefficient	Rate Exponent
<input type="text" value="co2"/>	<input type="text" value="1"/>	<input type="text" value="0"/>

Arrhenius Rate

Pre-exponential Factor

Activation Energy (j/kgmol)

Temperature Exponent

Include Backward Reaction

Third Body Efficiencies

Pressure Dependent Reaction

Mixing Rate

A  B

Reactions

Mixture  Total Number of Reactions

Reaction Name  ID  Reaction Type  Volumetric  Wall Surface  Particle Surface

Number of Reactants  Number of Products

Species	Stoich. Coefficient	Rate Exponent
<input type="text" value="co"/>	<input type="text" value="1"/>	<input type="text" value="1"/>
<input type="text" value="h2o"/>	<input type="text" value="1"/>	<input type="text" value="1"/>

Species	Stoich. Coefficient	Rate Exponent
<input type="text" value="co2"/>	<input type="text" value="1"/>	<input type="text" value="0"/>
<input type="text" value="h2"/>	<input type="text" value="1"/>	<input type="text" value="0"/>

Arrhenius Rate

Pre-exponential Factor

Activation Energy (j/kgmol)

Temperature Exponent

Include Backward Reaction

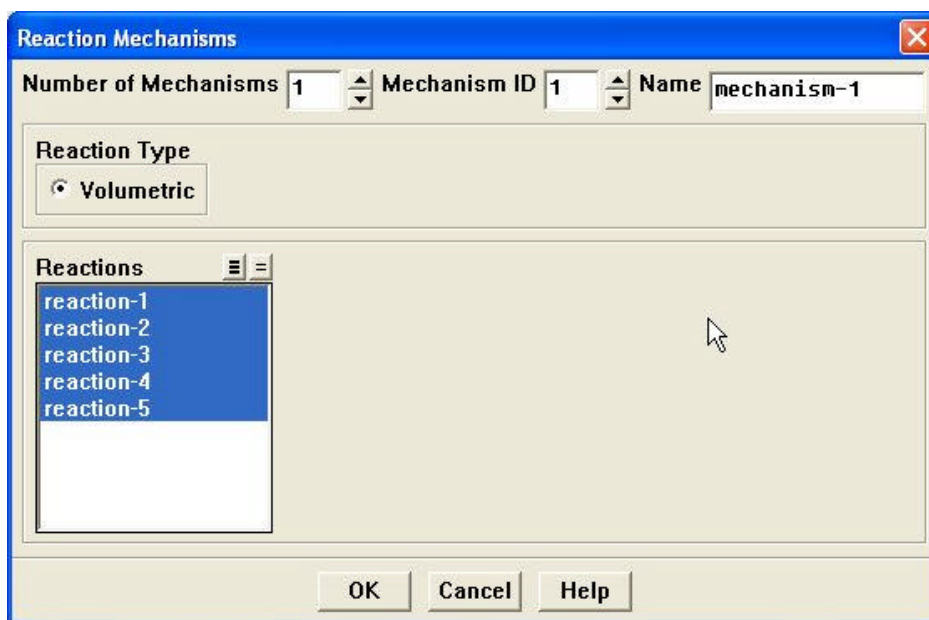
Third Body Efficiencies

Pressure Dependent Reaction

Mixing Rate

A  B

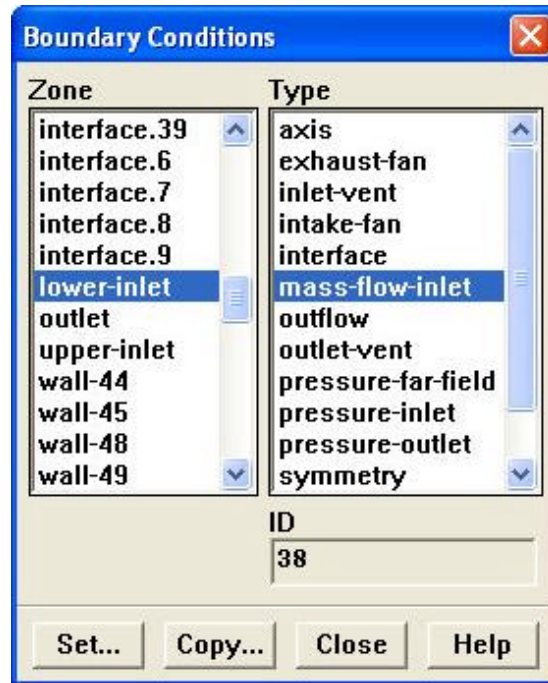
- (c) Set the **Total Number of Reactions** to **5**.
  - (d) For the reaction **ID 1**, set the **Number of Reactants** to **2** and **Number of Products** to **1**.
  - (e) Define the first reaction equation by picking the species from the **Species** pull-down window and typing the corresponding stoichiometric coefficient of each species into the **Stoich. Coefficient** window box.
  - (f) Retain the default **Mixing Rate** constants.
  - (g) Click the **ID** scroll-up button to go to the next equation.
  - (h) Repeat Steps (d) and (e) for the other four reaction equations.
  - (i) Click **OK** to accept all the reaction equations.
9. Turn on the reaction mechanism.
- (a) In the **Material Panel**, click **Edit...** button next to the right of **Mechanism**.
  - (b) Click all the 5 reactions listed in the **Reaction** window.



- (c) Click **OK**.

**Step 4: Boundary Conditions**

Define → Boundary Conditions...



1. Select lower-inlet (the first stage injectors) under the **Zone** window and mass-flow-inlet under the **Type** window. Click **Set...** to set its boundary condition.

Mass-Flow Inlet

Zone Name  
lower-inlet

Mass Flow Specification Method: Mass Flow Rate

Mass Flow-Rate (kg/s): 49.6

Total Temperature (k): 425 constant

Supersonic/Initial Gauge Pressure (pascal): 0 constant

Direction Specification Method: Normal to Boundary

Reference Frame: Absolute

Turbulence Specification Method: Intensity and Hydraulic Diameter

Turbulence Intensity (%): 5

Hydraulic Diameter (m): .2

Species Mass Fractions

n2	0.02	constant
h2o	0.29	constant
co2	0	constant
h2	0	constant

OK Cancel Help

2. Select upper-inlet (the second stage injectors) under the **Zone** window and mass-flow-inlet under the **Type** window. Click **Set...** to set its boundary condition.

Mass-Flow Inlet

Zone Name  
upper-inlet

Mass Flow Specification Method: Mass Flow Rate

Mass Flow-Rate (kg/s): 10.4

Total Temperature (k): 425 constant

Supersonic/Initial Gauge Pressure (pascal): 0 constant

Direction Specification Method: Normal to Boundary

Reference Frame: Absolute

Turbulence Specification Method: Intensity and Hydraulic Diameter

Turbulence Intensity (%): 5

Hydraulic Diameter (m): .2

Species Mass Fractions

n2	0	constant
h2o	0.47	constant
co2	0	constant
h2	0	constant

OK Cancel Help

3. Select outlet under the **Zone** window and pressure-outlet under the **Type** window.  
Click **Set...** to set its boundary condition.

Pressure Outlet

Zone Name  
outlet

Gauge Pressure (pascal) 0 constant

Radial Equilibrium Pressure Distribution

Backflow Total Temperature (k) 425 constant

Backflow Direction Specification Method Normal to Boundary

Turbulence Specification Method Intensity and Hydraulic Diameter

Backflow Turbulence Intensity (%) 5

Backflow Hydraulic Diameter (m) .5

Species Mass Fractions

n2	0.79	constant
h2o	0	constant
co2	0	constant
h2	0	constant

OK Cancel Help

4. Select wall.1 under the **Zone** window and wall under the **Type** window. Click **Set...** to set its boundary condition

Wall

Zone Name  
wall.1

Adjacent Cell Zone  
Fluid

Thermal | DPM | Momentum | Species | Radiation | UDS

Thermal Conditions

Heat Flux  
 Temperature  
 Convection  
 Radiation  
 Mixed

Heat Flux (w/m2) 0 constant

Internal Emissivity .7 constant

Wall Thickness (m) 0

Heat Generation Rate (w/m3) 0 constant

Material Name  
aluminum Edit...

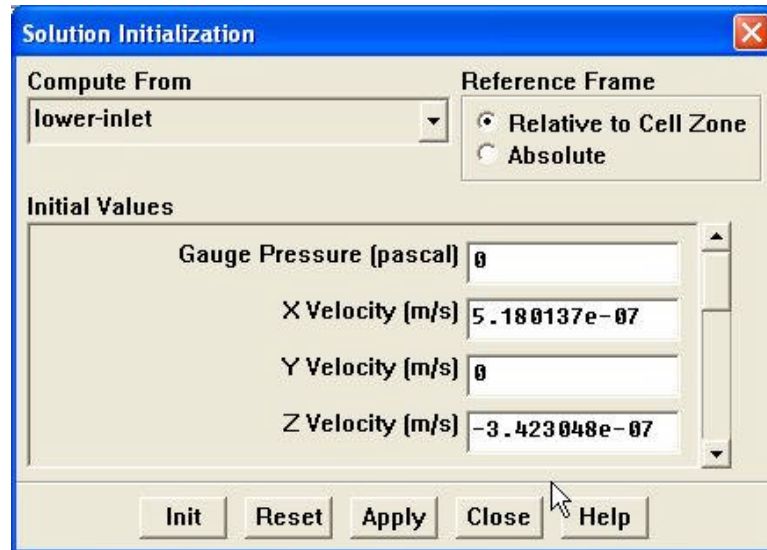
Shell Conduction

OK Cancel Help

### Step 5: Solution Initialization

1. Initialize the field variables.\

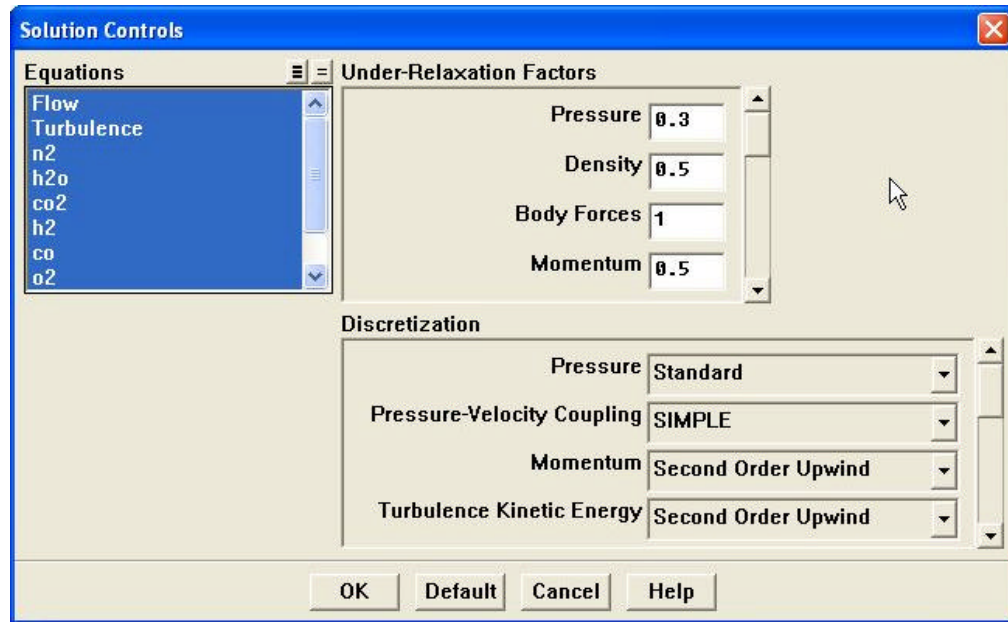
**Solve** → **Initialize** → **Initialize...**



- (a) Select **all-zones** in the **Compute From** drop-down list.
  - (b) Adjust the **Initial Values** for **Temperature** to 2000
  - (c) Click **Init** to initialize the variables, and then close the panel.
2. Set the under-relaxation factors.

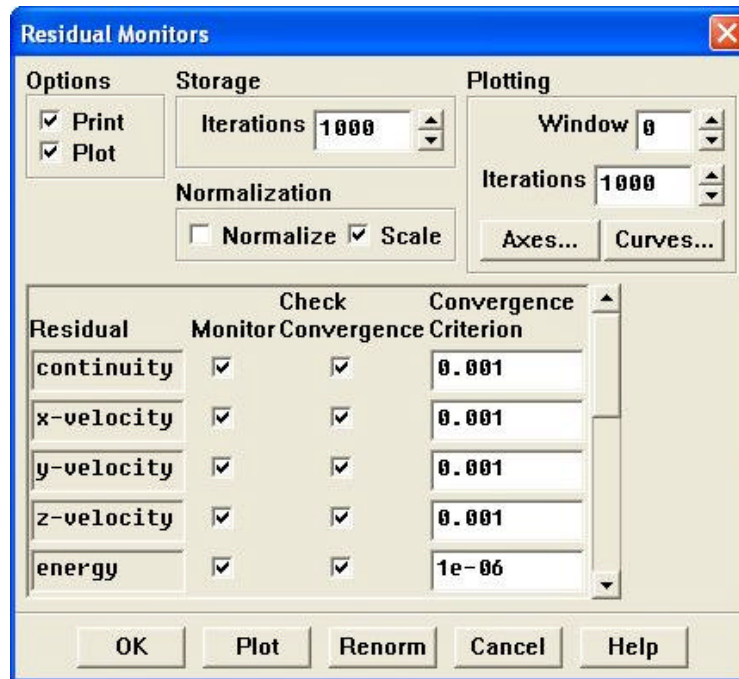
**Solve** → **Controls** → **Solution...**

- (a) Set the under-relaxation for the density, momentum, and energy to 0.5
- (b) Set the under-relaxation for all species to 0.6.
- (c) Keep the default under-relaxation factors for the rest.
- (d) Click **OK**.



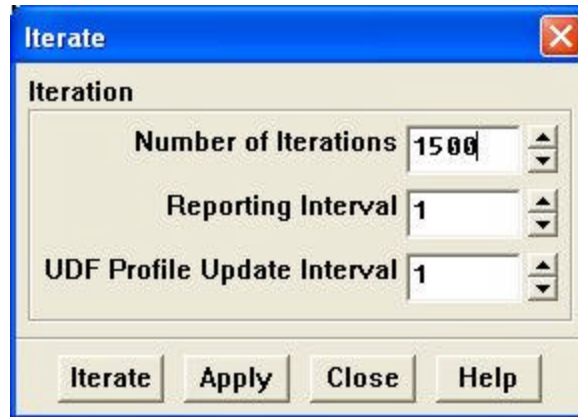
3. Turn on residual plotting during calculation

**Solve → Monitors → Residual...**



4. Start the calculation by requesting 1500 iterations

**Solve → Iterate...**



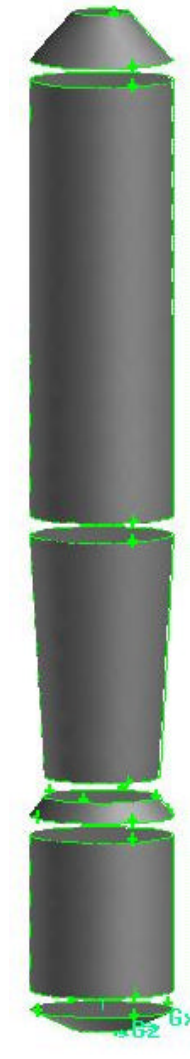
### **Step 6: Post-processing**

Review the solution by examining graphical displays of the results and performing surface integrations.

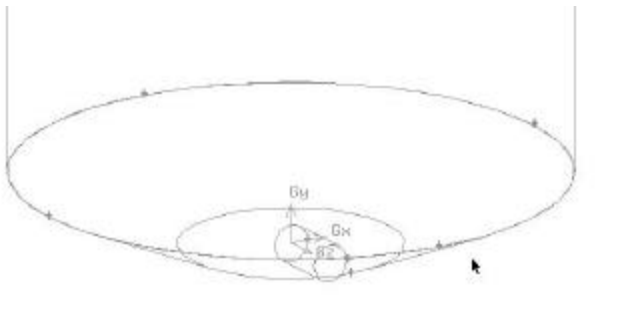
## APPENDIX B

### Geometry Generation and Meshing

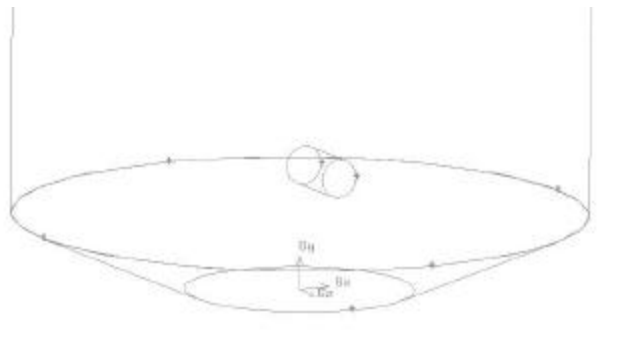
The geometry generation and meshing in this study was done in GAMBIT. The picture below shows the main parts of the gasifier. The gasifier is basically made up of two cylinders and three frustums.



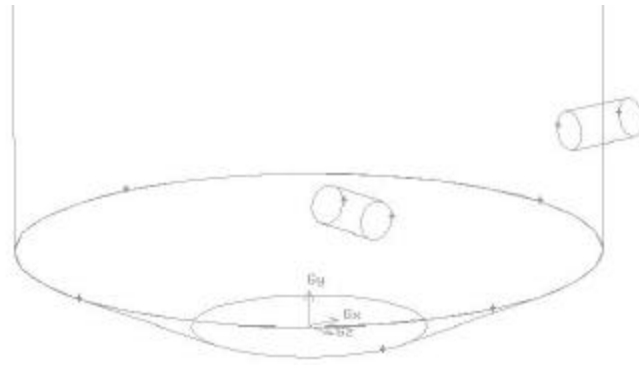
1. Create each cylinder and frustum one by one and move it on top of one another, and then UNITE all the parts together.
2. Create a horizontal circle with size bigger than the diameter of the gasifier.
3. Use this circle to SPLIT the united volume at the location where the parts meet.  
Be sure to select **Connected** and **Bidirectional** in the **Split Volume** window.  
This allows separate meshing of each volume.
4. Create a small cylinder for the tangential first stage injectors at the origin.



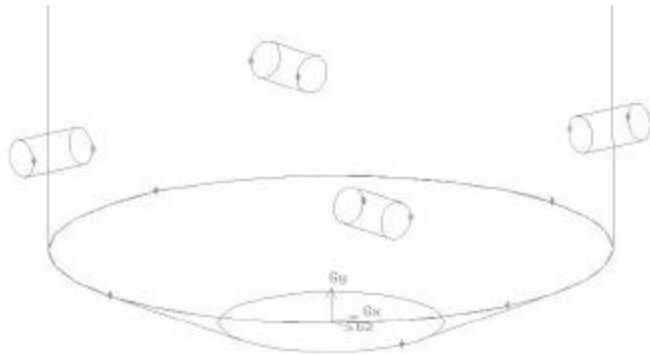
5. Move the cylinder to the location of the injector.



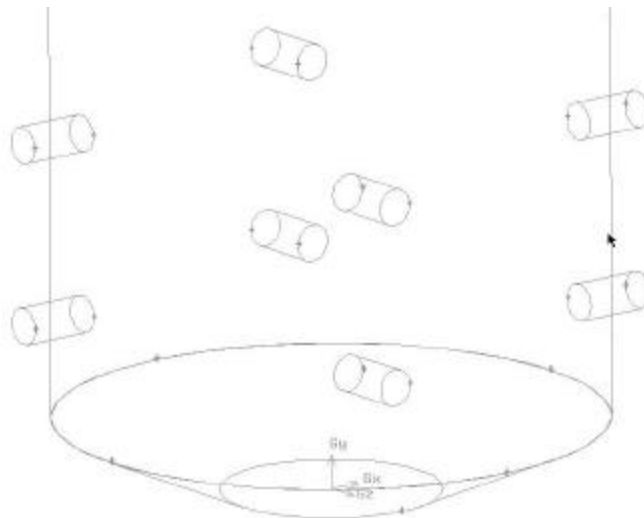
6. Copy the cylinder 90 degrees around the Y-axis.



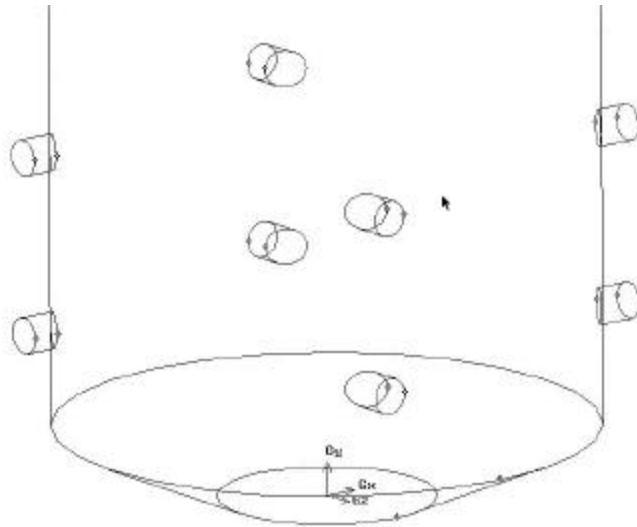
7. Repeat Step 4 but increase the rotation by 90 degrees each time until we have 4 cylinders.



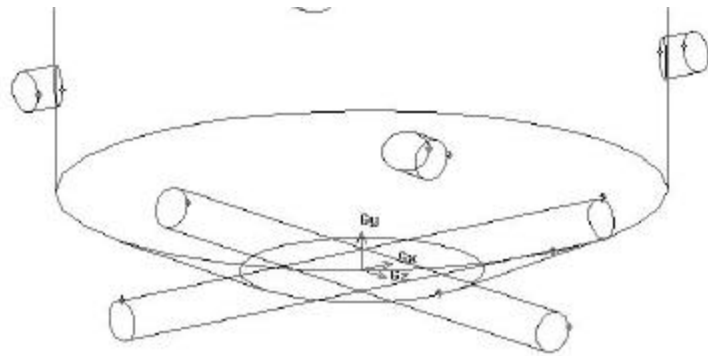
8. Copy all four cylinders upwards to get the injectors at the next level.



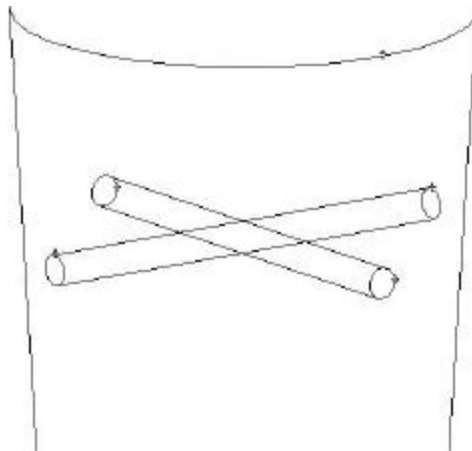
9. UNITE all the small cylinders with the big vertical cylinders.



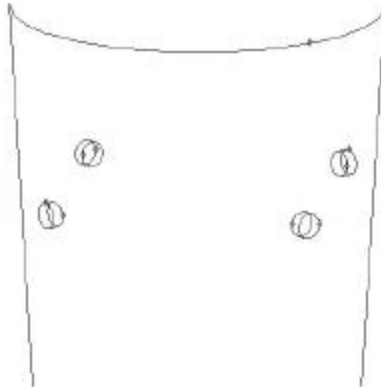
10. Create two long cylinders for the second stage injectors at the origin.



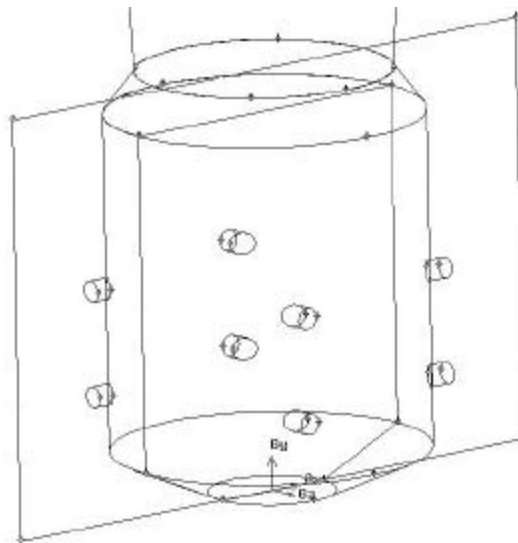
11. Move the cylinders up to the location of second stage injection.



12. Unite the cylinders with the frustum.

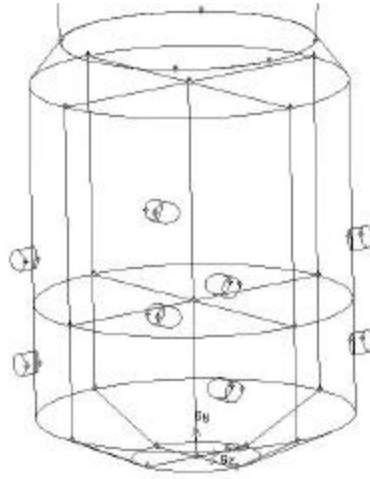


13. We now need to divide the combustion chamber cylinder into four volumes with one inlet each. Create a vertical rectangular face and use it to split the combustion cylinder. Be sure to select **Connected** and **Bidirectional** in the **Split Volume** window. This process is necessary because each inlet must be connected to only one surface so it can be meshed. Two or more inlets can not be connected to the same one surface because meshing can not be performed.

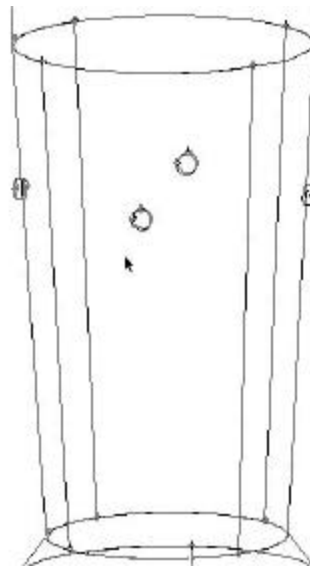


14. Rotate the rectangular face 90 degrees and use it to split the combustion cylinder once again.

15. Create a horizontal circular plane and use it to split the combustion cylinder.



16. Repeat Steps 13 and 14 for the diffuser frustum.



17. Mesh the top surface of the top frustum using the **Quad Pave** scheme.

18. Mesh the frustum using the **Hex/Wedge Cooper** scheme with the meshed top surface as the source face.

19. Next mesh the reductor cylinder using the **Hex/Wedge Cooper** scheme.

20. Repeat step 19 for the throat, the combustion cylinder, and the base bottom frustum.

21. Mesh all the inlet cylinders also using **Hex/Wedge Cooper** scheme.
22. Define the boundary types. Specify the faces where the inlet cylinders meet with the gasifier wall as **interfaces**.
23. Specify the inlet surface as **mass\_flow\_inlet** and the exit surface as **pressure\_outlet**.
24. Export the mesh.

## VITA

Armin Silaen was born in Cairns, Australia, in 1979. He graduated from Rice Memorial High School in Burlington, Vermont, in 1998. He enrolled in the University of New Orleans and received a Bachelor of Science degree in Mechanical Engineering in 2002. He then joined the Graduate Program in the Department of Mechanical Engineering at the University of New Orleans.